Computational Simulation of Bone grafts for Impaction bone grafting

By

Ashwin Jeyakar Dhanasekaran

Thesis submitted to Flinders University for the degree of

Doctor of Philosophy

College of Science and Engineering
Flinders University
1284 South Road, Tonsley, SA 5042

August 2021

Table of Contents

Abstract

Revision arthroplasty with impaction bone grafting is an attractive method with the potential to restore bone stock in the tibia/femur when there is bone loss caused by the removal of failed primary replacement implants. However, the surgery is complex and problematic implant subsidence is often reported as a root cause of failure in these procedures. The mechanism that causes this subsidence is not well understood due to a lack of knowledge on the material characteristics of the bone grafts or a universal standard procedure to achieve a stable impaction. As the bone loss pattern in each patient is unique, revision replacement systems consist of a variety of stems and sleeves that augment to fill bone defects, restore alignment, and ensure adequate fixation to the remaining bone. The array of components in a revision replacement system provides challenges for both the manufacturer and the surgeon.

The primary objective of this thesis was to understand the mechanical properties of bone grafts and capture them using numerical modelling. The secondary objective was to validate the numerical model and analyse the data captured from the numerical model to explain the characteristics of bone grafts that cannot be explained from experimental testing methods. The study demonstrated that mechanical properties of bone grafts are highly variable and can be captured by performing a repeatability test and performing statistical analysis on the results to estimate uncertainty. Finite element models can better understand the mechanical characteristics that cannot observe traditional experimental testing. The results from the model demonstrated that when bone grafts are impacted in a single layer, the impaction stresses were only concentrated in the proximal end of the impaction site and not evenly distributed across to the distal end of the graft bed. Single-layer impactions produced a lower graft stiffness and shear strength, with the bone grafts at the proximal side exhibiting a high magnitude of plastic deformation with high impaction stress levels. The model also demonstrated that most stress consolidation occurs in the

first 20 impaction cycles with impact stresses 3.0MPa – 5.0 MPa. The study demonstrated that impacting bone grafts at stresses between 3.0 MPa – 5.0 MPa for 10 to 20 impactions cycles is adequate to achieve a stable impacted bone graft in revision tibias. Impacting the bone grafts in evenly distributed layers can help increase the graft stiffness by equally distributing the impaction forces across the bone grafts and achieving a densely packed bone graft.

Declaration

I certify that this thesis does not incorporate without acknowledgement any material previously submitted for a degree or diploma in any university and that to the best of my knowledge and to the best of my knowledge and belief, does not contain any material previously published or written by another person except where due reference is made in the text

Signed: ……...

Date:

Dedicated to the memory of my father,

Dhanasekaran Raja Mani

Acknowledgements

Undertaking this thesis far from home has been an incredible challenge that I would not have been able to overcome without the support of many people. Firstly, I would like to thank my supervisors Prof. Mark Taylor and Assoc. Prof. Saulo Martelli, for their guidance throughout my candidature. To Mark, thank you for always having your door open to me for your practical advice, particularly on mechanical engineering topics, which I found invaluable. Since the first day I arrived in Adelaide, your enthusiasm, patience, and seemingly endless knowledge have inspired me to achieve my best. I have learnt a tremendous amount as your student. Thank you to Saulo for coaching me through all my conference abstract submissions and all the MDRI and Flinders University staff for their assistance. Thank you to all my colleagues at MDRI, including Maged, Hamed, Dermot, Rami, Robbie, Anand, Sophie, and Michael, for making every day at Tonsley hugely enjoyable. I am also very grateful to Sitansu from Redarc for helping me with MATLAB programming; I wouldn't have finished my PhD in time if it wasn't for your programming skills. A very special thank you to Angeline, who has most recently lived the thesis as much as I have. Above everyone, you have been the most supportive, caring and understanding person throughout this process. Thank you for assuring me I had the grit to see this through when I needed it the most. Finally, my biggest thank you goes to Mum, Dad and Teny for all their love and support, not just in this but in everything I do. This is for you.

List of Figures

List of Tables

This page is intentionally left blank.,

Chapter 1 :

Introduction

Around 2.2 million people in Australia suffer from a wide range of knee disorders, though osteoarthritis is the most common affecting as a gross figure 12% of females and 6.8% of males in 2018 – 19 (AOA 2019). Total Knee Arthroplasty (TKA) is a common treatment for osteoarthritis and is one of Australia's most effective major surgical procedures. Total Knee replacement surgery helps to relieve pain, restores function, and improves the quality of life for patients suffering from severe knee arthritis.

The Australian Orthopaedic Association National Joint Replacement Registry reported that in 2017-2018 54,102 knee replacements were performed, out of which 2134 of those were revision knee replacements. Revision knee replacement surgery accounts for 8% of all knee joint replacement operations in Australia (AOA 2019). Revision surgery imposes a significant financial burden on Australia's health care system, with an estimated cost of $120M per annum for the surgery alone (AOA 2019). In comparison with standard knee replacements, revision surgery is complex due to significant bone loss and soft tissue damage leading to instability of the knee. Failure of revision knee replacement surgery is 14.2% at 5 years (AOANJRR 2016), which is more than three times the standard knee replacement failure rate.

It is necessary to have good management of bone loss for the tibia and femur. The severity and location of the defects help decide the best type of reconstruction, as each patient's bone loss pattern is unique and often multifactorial. There are currently several ways available for reconstruction, namely cement, cement with screws, using modular metal augments such as stems, wedges, cones or metaphyseal sleeves, cancellous or structural bone grafts (Huff & Sculco, 2007).

Impaction bone grafting is one of those methods used to treat bone loss in revision knee and hip replacements with compacted bone grafts to achieve a stable implant and help restore the living stock bone by promoting bone regrowth. However, these bone grafts are not very well understood. It has been established that the mechanical properties of bone grafts are highly variable, and most of the research that has been done on impaction bone grafting has been on hip replacements. Although similar methods are used in knee replacements, no standard processes or efficient procedures used universally on impaction bone grafting. A detailed study is necessary to understand the mechanical characteristics, stability, and limitations.

This can be done using either mechanical testing or using numerical modelling. Mechanical testing is widely used to determine the performance of an implant. There is no shortage of papers and published material using mechanical testing to understand the mechanical properties of bone grafts. However, the literature only captures gross differences and instantaneous material properties of the bone grafts and does not calculate the idealised material properties for the bone grafts.

On the other hand, finite element analysis has been extensively used to assess the performance of standard and revision knee replacements by evaluating the initial mechanical environment through the simulation of time dependent processes, including bone remodelling and wear. Finite element analysis has the potential to provide valuable information to guide in treating these defects. However, only a few studies based on FEA have been attempted to study revision knee replacements and their defects. The current literature on finite element modelling is based on reference models, and in most cases, only simulates the impaction end point and not the impaction process. The practical limitations in physical testing create a need to move beyond the current suite of pre-clinical mechanical tests to test new designs to, the use of computational models as a viable solution.

1.1. Research Aims

The overall aim of the research presented in this thesis is to understand better, address, and assess impaction bone grafting. This will be undertaken by attempting to computationally model the impaction bone-grafts process to minimise the time and achieve a normal morphological condition of bone grafts after impaction in the most efficient way possible.

Aim I Explore the mechanical variables involved in impaction bone grafting and develop an experimental method to acquire the basic material properties required to model bone grafts.

Aim II: Develop a robust method capable of modelling bone grafts and replicate the experiment using a numerical model.

Aim III: Explore the material properties of bone grafts and determine which variables have the greatest influence.

Aim IV: Analyse the variables in impaction bone grafting using the numerical model to explain the characteristics of bone grafts that cannot be explained from experimental testing.

1.2. Thesis Outline:

To achieve the research aims, this thesis is organised into the following chapters:

Chapter 1: Provides an extensive review of the literature. The chapter explores the reasons for revision knee replacements, the various techniques involved in revision surgeries, a study of current literature in impaction bone grafting, the mechanical variables involved, an overview of numerical models on bone grafts, and a summary of the limitations to provide a basis for the research in this thesis.

Chapter 2: Discuss how the bone grafts are prepared for the experiment, the experimental test apparatus, the test procedure, and the process involved in the experimental tests and their results. The stress-strain relationship, stiffness and strain energy of graft material is also discussed in detail. This is achieved by cyclic loading of morselized bone grafts in a thick-walled stainless-steel cylinder through a custom 3-axis testing rig.

Chapter 3: Explore the various computational modelling techniques. This includes Finite element analysis and discrete element analysis, the methods of computational models which have failed, the reasons for their failure and the computational modelling technique best suited to model bone grafts. The chapter replicates the experimental test simulating morselized bone grafts in a thick-walled cylinder identical to the experimental test subjected to the same loading conditions. The results from the computational model are discussed and compared with the existing experimental results.

Chapter 4: Investigate the differences between the numerical and experimental models. A sensitivity study is carried out designed using a design of experimental approach Box Behnken design. The interactions between young's modulus, yield strain and friction are studied. A 3-way ANOVA is used to determine the best combination of the three variable parameters needed to match the experimental results.

Chapter 5: This chapter analyses the data recorded from the numerical model to investigate the influence of impaction stress, number of impactions and the influence of layered impaction technique on the fill ratio, the bulk modulus, and the accumulated permanent strain.

Chapter 6: Summarizes the findings and discusses work that could be carried out in the future.

Chapter 2 :

Literature Review

2.1. Overview of Knee problems

Knee problems are quite common, they occur in people of all ages caused due to disease or injury. The main diseases that affect the knee are osteoarthritis, rheumatoid arthritis, haemophilia, avascular necrosis and bone dysplasia. (Mittleman et al 2016).

Osteoarthritis occurs because of cartilage wear on the gliding surface of the knee, causing stiffness and pain. Bones rub directly against each other when the cartilage wears away completely causing decreased mobility and chronic pain (Mittleman et al. 2016). This type of arthritis is more common with 97.38% diagnosed as the reason for failure in people 50 years and older. They can also occur in those who have a lifestyle causing high stress on joints such as labourers and athletes (Barabara et al 2016). Rheumatoid arthritis is a type of autoimmune disease where the body's immune system attacks the synovial membrane causing inflammation and excessive production of synovial fluid. This is chronic and inflammation can damage the cartilage leading to cartilage loss, stiffness and pain. Rheumatoid arthritis accounts for 3.8% of all failures of Total knee replacements (TKR)

Knee injuries are also caused as a result of a direct blow or sudden movements resulting in a straining beyond the knee's normal range of motion. Traumatic arthritis occurs as a result of a serious knee injury like a fracture, ligament damage or meniscus tear. The impact of the accident also can result in the development of osteoarthritis, causing knee pain and stiffness. If the knee is severely damaged and non-surgical treatments like medications and walking support fail, a total knee replacement is a largely safe and effective procedure to relieve pain, correct the leg deformity and help the patient resume normal activities.

This image has been removed due to copyright restriction. Available online from "(Foran et al 2020)"

Figure 2.1: Types of components used in total knee replacement surgeries (Foran et al 2020)

There are various treatments that can be used to treat knee arthritis. Amongst the surgical options, Arthroscopic surgery, a minimally invasive surgery to repair an injury or clean out debris. Osteotomy is performed to reshape the bone to relieve the pressure off injured parts and correct the alignment of the bones. Total knee replacement surgery is TKR is the last resort in the treatment of Arthritis and the most essential factors to consider in a knee replacement is the type of replacement prosthesis and the type fixation option. There is no single "best prosthesis". The types of primary knee operations are classified based on the constraint, bearing type and fixation method. Fixed bearing implants are most commonly used, in which the polyethene component of the tibial tray is firmly fixed to the metal base platform (Huang et al 2007). The primary difference between a mobile and fixed bearing is that mobile bearings have a polyethene insert that rotates inside the tibial tray and allows for a better degree of rotation than fixed-bearing knees on the medial and lateral sides of the knee. (Ranawat et al. 2012)

The other classification types of knee replacements are related to fixation namely, cemented and cement less/un-cemented. In cemented TKR's, poly-methyl-methacrylate (PMMA) is used to hold the components of the artificial joint in place. According to Robertsson (Robertsson et al 2019) in Sweden, the most common method for fixing components in knee arthroplasty is the use of bone cement. Similarly in the British Orthopaedic registry records cementation of the prosthesis as the most common choice among surgeons (NJR England & Wales 2016). Cemented total knee replacement are either constrained or unconstrained. If they are constrained, they can be either a constrained condylar or mono block polyethene tibia. Unconstrained replacements can be fixed unconstrained and mobile unconstrained; fixed posterior-stabilised, and mobile posterior stabilised. Cement less implants can have either a textured finish or coated with hydroxyapatite

and with or without a porous coating to promote bone growth into the surface of the implant. Un-cemented/hybrids include unconstrained, fixed, mobile and posterior stabilised fixed type of implants. Uni-compartmental knee replacements are either fixed or mobile. Uni-compartmental knee implants are used when the disease is on either medial or lateral compartmental side. The report (AOANJRR 2019; Robertsson et al 2019) also suggests that figuratively bone cement has been used in a majority of arthroplasties however, the use of un-cemented implants has increased slightly in the past few years.

2.2. Failure of Total knee replacement:

Total knee arthroplasty is extremely successful, cost-efficient and increases longevity causing their demand likely to increase (Haddad et al 2016). The 10 years survivorship of TKA is considered to be 90% – 98% at the same time 15 to 20-year survival rate have been reported to be as high as 96% in some studies (Heysey et al 2014; Keeney et al 2011; Vessely et al 2006). Australian arthroplasty register was analysed, and the failure rate was high in patients who were less than 55 years of age and these high failure rates in younger patients can be associated with functional demands, a high level of activities and even higher remaining life expectancy. There is also a higher rate of obesity in young patients (Julin et al 2010). Survivorship of total Knee arthroplasty is dependent on factors like the surgical technique, type of implant and the demographics of the patient. Like all biomedical devices, knee replacements can fail over time. In a study conducted by Ostendorf (Ostendorf et al., 2002) the most common factors leading to revision are aseptic loosening, infection, polyethene wear, instability, aseptic necrosis, periprosthetic fracture & arthrofibrosis (Austin et al 2004).

Infection, aseptic loosening and overloading due to mal-alignment causes most TKA failures (Bisschop et al 2010). Revision Knee replacement is a complex procedure that requires specialized implants, tools and extensive planning. The surgeries take longer than the original knee

replacement and required mastery of difficult surgical techniques. The table below (Table 2.1) states the reasons for revision surgery in the year 2018, these surgeries can be single stage where the prosthesis exchange occurs in one single surgery or two stages where two surgeries/hospitalizations occur at an interim period of 2 – 3 months between surgeries. Two stage surgeries impair the quality of life of the patients with impair health and functional status. The table shows that aseptic loosening accounts for over $2/5^{th}$ of single-stage revision operations and pain being $1/5^{th}$ of single stage revision operations. In the case of two-stage revision operations, infection is recorded as the prominent reason for revision surgery with over 75% of both stage one and stage two.

Reason for revision	Percentage of all revision joint operations of each stage type with the stated reason for revision		
	Single Stage (n-53,150)	Stage one of two-stage (n=7,108)	Stage two of two-stage (n=7,886)
Aseptic Loosening	38.7	11.5	12.0
Other Indication	21.1	4.1	5.9
Pain	16.9	4.9	4.8
Instability	17.6	4.4	4.4
Implant wear	14.4	3.5	2.5
Lysis	9.6	10.0	6.5
Malalignment	7.9	1.4	1.6
Infection	5.8	84.2	77.1
Dislocation/subluxation	4.2	1.6	1.2

Peri-prosthetic Fracture	4.0	1.5	1.4
Implant Fracture	1.3	0.2	0.3
Stiffness	5.9 (n=53,150)	2.6 (n=7,108)	1.8 (n=7,881)

Table 2.1: Reasons for revision knee replacements from England and Wales Orthopaedic Registry (UKR 2018) All revision knee procedures of each stage type with indicated reason for revision have been listed in percentage.

The Australian orthopaedic association national joint replacement registry also reports that the most common reasons for performing a revision knee replacement are: infection (16.4%), loosening/lysis (37.1%), pain (14.4%), and instability (11.7%). (AOA 2019)

A study by Kurtz et al (Kurtz, Ong, Lau, Mowat, & Halpern, 2007) predicts that the number of total knee arthroplasties performed annually is estimated to grow by 174% between 2005 - 2030, the burden posed by revision TKA is expected to increase. The costs of revision TKA is significantly more as a result of increased surgical time, prolonged hospital stays, custom implants, greater blood loss and medication. The knee to be revised have several risks for complications, reconstructive problems, suboptimal comfort or functions, and amputation. (Garino, 2002). To have a successful revision the implants require a stable foundation for component placement, an accurate mechanical alignment, proper fixation, and ultimately must be infection-free. Achieving a well-balanced, mobile and painless knee while managing bone loss in revision surgeries is challenging.

2.3. Effect of failure in Knee replacements

Failures in knee replacements lead to removal of knee replacements which in turn leads to bone loss or bone destruction leaving significant defects in the bone. Bone defects in revision TKA are commonly encountered and this affects implant alignment and the bone-implant interface. Bone defects can be caused because of shielding stress, infection osteolysis and micro-motion of a loose implant. These defects can be either contained or uncontained. In a contained defect the peripheral

cortical rim which surrounds the area of bone is intact which allows treatment with a morselized bone graft or cement and screws which depends on the size of the defect. The uncontained defect can be treated with impaction bone grafting if used in conjunction with cages or requires reconstruction with bulk structural allograft or metal augments or metaphyseal sleeves or cone as the peripheral cortical rim in the tibia/femur is absent. (Daines et al 2013; Vasso, Beaufils, Cerciello, & Panni, 2014) The size, shape and position of the defects influence the approach needed to reconstruct the knee.

2.4. Bone classifications:

Clinical assessment is performed on the failed replacement usually in the form of a radiograph to assess the quality of the bone defect. This assessment allows the surgeons to plan on the surgery in terms of the size of the stem, amount of graft required and the need for other accessories.

Bone defects have several classifications in revision total knee arthroplasty. Each classification considers the degree of cancellous bone loss, cortical bone loss and if the defect is contained or uncontained. The following are some of the most commonly used bone defect classifications.

2.4.1. ENDO (Engelbrecht) Classification:

This is one of the most commonly used classifications which is based on radiographic and intraoperative findings. With regards to knee prosthesis, the increasing loss of bone stock is classified from type - 1 to type - 4. Type - 1 defects are minor bone defects with thin radiolucent lines but no subsidence of components; type - 2 involves moderate bone loss with a wider radiolucent line around the implant and signs of implant subsidence; type - 3 defects are those with a severe bone loss with severe condylar defects and widening of the distal femur or proximal tibia; type – 4 defects are massive representing a total or severe loss of bone stock with more than half

of the femur defective or the proximal parts weakened by severe cortical thinning or severe osteoporosis. Figure *2.2* shoes the ENDO classification with all 4 types.

This image has been removed due to copyright restriction. Available online from

"(Kluber et al 1996)"

Figure 2.2: ENDO classification of failed knee replacement with increasing loss of bone stock from type 1 to type 4(Kluber et al 1996)

2.4.2. Anderson Orthopaedic Research Institute classification:

This is the second most widely used classification. It categorizes femoral and tibial defects separately into types I, type II, and Type III. Type 1 (Figure 2.3. a) defects have their metaphyseal bone intact with only minor bone defects which does not compromise component stability. Type 2 defects have considerably more metaphyseal bone loss and are further subdivided with type 2A (Figure 2.3 b) Defects with only one femoral condyle or tibial plateau and type 2B (Figure 2.3. c) Defects with both femoral condyles and tibial plateau. Type 2 defects generally require metal augments and reconstruction using morselized or structural allograft. Type 3 (Figure 2.3. d) Defects where the bone loss is severe with a major portion of the femoral condyle or tibial plateau deficient and may even occasionally affect ligaments or tendon insertions. This classification considers the location of the defect and stability of the implants to provide a guideline on preoperative planning and treating of these defects (Engh et al 1999).

This image has been removed due to copyright restrictions. Can be viewed online at "(Engh et al 1999)"

Figure 2.3 Anderson Orthopaedic research institute classification of bone defects (Engh et al 1999)

2.4.3. Soloff and De Wall Malefijit Classification:

This classification classifies contained bone defects that are repaired by impaction bone grafting. The size of the defect is defined as small moderate or large. Mostly used as an intra-operative description and does not have a guide for preoperative planning. (De Waal et al 1995)

2.5. Introduction to revision knee surgery

2.5.1. Approaches to revision surgery:

Revision surgery involves the removal of the failed primary implants and the insertion of new components. The main challenges in revision surgery for a failed tibial and distal femoral stem is the extensive loss of bone stock in the distal femur and the proximal tibia. There are several methods to fill the defects, including stems, cement, screws, cones, sleeves, augments, autografts, xenografts, allografts and a wide range of synthetic materials such as tantalum, titanium, iron or magnesium, polymers such a polylactides, polyglycolides, polyurethanes, polycaprolactones and ceramics such as silicate-based glasses, calcium sulphate hemihydrate. Among all the above-stated bone loss compensation techniques allografts, autografts, xenografts and impaction bone grafting are the only techniques that help compensate for bone loss and reconstruct the original shape of the bone without replacing them with augments or sleeves which are made of metal and can never be replaced by the body. Autografts cannot be used for large defects as they are sourced from the patient and xenografts are grafts typically sourced from bovine bones and extensively tested to eliminate antigenicity. Synthetic graft materials are used as graft extenders rather than on their own as they are not resorbed by the body but acts as scaffold for new bone cells to ingrown.

2.5.1.1. Allograft

The two most common types of bone grafts are bulk grafts and morselised bone grafts

2.5.1.2. Morselized allograft:

Impaction bone grafting was first introduced in total hip arthroplasty. Schreurs et al (Schreurs et al 1998) used impaction grafting for the first time in revision hip surgery in Europe. For the knee, this technique has been modified to restore bone stock in younger patients who are more likely to require multiple revision surgeries (Suárez et al 2002). This philosophy has been adopted in revision knee arthroplasty to augment moderate-to-significant bone loss using an impacted allograft. Impaction grafting of morselized allograft requires a careful resection of the defect with a high-speed burr to define the lesion. The contained defects can be treated immediately whereas uncontained defects need a wire mesh augmentation (Suárez et al 2002). Morselized bone grafts are typically used to fill small defects and in conjunction with other techniques described above. The bone is impacted at the base of the defect while progressing towards the joint. While treating uncontained defects the proximal portion of the tibia or distal portion of the femur is exposed to secure wire mesh to host bone for cortical reconstitution.

2.5.1.3. Bulk Structural Allograft:

Structural pieces of femoral heads or distal femoral bone segments are used to fill the defect. This type of allografts can accommodate different types of shape and sizes of bone defects. They provide good initial support of the prosthesis and have the potential to restore bone stock with graft incorporation. A femoral head allograft sourced from surgery and cadavers is used for contained and uncontained defects and it's the most commonly used allograft (Engh et al 1999). The bone is first cleared of any fibrous tissues and membranes and the cartilage and cortical bone

are removed from the allograft leaving only the exposed cancellous bone. The marrow elements are removed from the trabecular bone. The host bone is prepared using an acetabular reamer to receive the femoral head graft until a solid base for the allograft is attained. The graft is positioned and fixed with Kirschner wires and screws to hold it in place provisionally. Once stabilized an oscillating saw is used to roughly remove the protruding part of the graft. The final implants are then positioned over the graft after any additional alterations if required to accommodate stems and devices. (Engh et al 2007)

This image has been removed due to copyright restriction. Available online from "(Hooten, Engh, Heekin, & Vinh, 1996)"

Figure 2.4: Structural bulk allografts used in acetabular reconstruction (Hooten, Engh, Heekin, & Vinh, 1996)

Though these techniques are successful, they are not perfect and have their compromises. There are alternatives to using impaction bone grafting like the use of Stems in revision TKA give the ability to bypass deficient metaphyseal bone and fix the stem within the diaphysis (Nelson et al 2015). This implant can be cemented, non-cemented and hybrid which involves the proximal part of the tray cemented leaving the stem un-cemented. Cemented stems provide immediate fixation; but, may increase stress shielding of the metaphyseal bone and can be challenging to remove (Nelson et al 2015). Fixation of the hybrid stem is dependent on the placement of cement at the metaphyseal bone-impaction interface where the tibial base is cemented but the stem is left uncemented. Non cemented stems press-fit fit and not aimed to become Osseo integrated. An Osseo integrated stem would accentuate stress shielding and would be very difficult to remove if another revision is required. Offset stems can be used with either a cemented or cement less base plate which accommodates the position of the canal about the position of the tibial tray. Cement is typically used in defects at <5mm and can also be used in conjunction with cancellous screws for defects ranging from 5 to 10mm (Pagnano et al 2006). This enhances the load transfer from

the prosthesis to the underlying bone. Cement is inserted as pillars to support the implant. However, there are risks of infection and cement being an inert substance do not help in osseointegration.

Cones and Sleeves are used to fill large defects and provide biologic fixation. They provide immediate structural support and remove the concerns regarding disease transmission with the allograft, graft resorption and graft fracture. Being modular the design of cones allows for the management of defects of various sizes and shapes. However, the drawbacks of using cones are the lack of bone stock restoration and the need to remove additional native bone to accommodate the cone. Also, in case of a failure in the replacement and the implant needs to be removed for a revision procedure, the removal of these implants can be challenging as a result of biologic fixation. (Meneghini et al., 2007). Metaphyseal sleeves and cones provide good fixation at the metaphysis and results have shown that they can be used to manage even severe bone loss (Mneghini et al 2009). Cones and Sleeves are typically cement less device and have a porous coating to enhance osseointegration. The tibial baseplate is cemented into the cone and in some cases the sleeves to the flat resected surface of the tibial surface.

Metal Augments are used in the reconstruction of tibial and femoral defects which are uncontained measuring 5 to 10mm. Augments are either block-shaped or wedge-shaped and cover the Hemi plateau or the entire plateau. Wedge augments result in greater shear force at the implant-bone and are susceptible to mechanical failure(Vasso et al 2014). Block augment on the other hand may require additional resection of the host bone for proper sizing but exhibit better load transfer to the underlying bone (Backstein et al 2006). They also provide immediate support without the need for consolidation or maturation, a shorter surgery time and immunity to resorption. However, they require additional bone removal, do not have any bone stock restoration, the bone underneath the augments can resorb if not loaded and are costly.

2.5.2. Introduction to Impaction bone grafting:

Impaction bone grafting is a technique to treat bone loss where morselised bone graft (MCB) is impacted into the bone cavity to compensate for bone loss and reconstruct the original shape of the bone. The first use of bone grafts to restore bone stock dates back to 1984 in revision total hip arthroplasty with cement (Slooff, Huiskes, van Horn, & Lemmens, 1984). This technique was then modified by Gie et al(Gie et al., 1993a) for reconstruction of the medullary canal by impacting MCB grafts. Impaction bone grafting reduces the defect the implant is required to fill allowing for the use of standard size implant and replacement of bone stock with the graft. In revision knee replacement the first usage of impaction bone rafting was recorded in late 1992 (Whiteside et al 1993) to reconstruct a proximal tibia, this was followed by the use of bone grafts in another surgery in 1994. The primary objective of impaction bone grafting is to provide a stable bed for the implant during revision total knee replacement. This process also provides a mechanical and biological scaffold for the regeneration of the bone. In revision knee replacements impaction bone grafting is used to treat contained and uncontained defects. Reconstruction of the knee involves occlusion of the canal and compaction of MCB grafts over a guidewire to produce a stable foundation into which an implant can be implanted using cement.

Some studies in revision knee replacements have recorded promising results (Aglietti et al 1991; Chandler, 1992; Elia et al 1991; Haas, Insall, Montgomery, & Windsor, 2009; Whiteside et al 1993; Lindstrand, Hansson, Toksvig-Larsen, & Ryd, 1999) using bone grafting techniques including structural, block allografts and MCB allografts. More specifically the later technique, the subject of this current thesis, has been reported previously, (Samuelson et al 1988; Whiteside et al 1993; Ullmark & Hovelius, 1996) achieved good short term- stability. A follow-up study performed by Whittaker et al (Whittaker et al 2008) concluded that impaction bone grafting in the tibia did not provide sufficient initial stability resulting in poor incorporation of the graft as there are numerous techniques for bone grafting and an ideal method of restoring bone stock at the knee has not yet

been achieved. They suggested that there must be initial mechanical stability of the construct and no subsequent migration attaining which is questionable given that there is no ideal technique achieved for bone grafting. Alternatively, a two year follow up study by Toms et al (Toms et al 2013) concluded that the results of using impaction bone grafting in the tibia are satisfactory with no fractures, metal work failure, loosening or malalignment of implants negating the need of revision surgeries. They reported a 14% complication rate which was caused due to infection (5%), periprosthetic fracture (2%) and 5.2% in the form of neuropathic pain. They claimed that the data was not sufficient to establish a criterion to impaction bone grafting technique. This is because the nature of impaction grafting is a highly complex surgical process. The success of impaction bone grafting depends both on biological and mechanical issues. However, this process is highly recommended in hip replacement where several manufacturers have already developed instruments and smooth broaches to assist in the impaction and trialling process, impaction on the knee is lagging in this area. One advantage is that many of the tools and instruments used for hip impactions can be used to help perform the procedure on the knee. (Roids et al 2014). Table 2.2 shows the advantages and disadvantages of impaction bone grafting

Advantages	**Disadvantages**
Allows the use of short size stem	Availability of donor bone stock
Restoration of bone stock	Variable impaction techniques
Potential integration between the graft and host bone	Variability of bone quality
The procedure is highly recommended and successful in hip replacements	Mechanical properties are not very well understood

Table 2.2 Summary of the advantages and disadvantages of impaction bone grafting

2.5.2.1. Impaction bone grafting techniques

2.5.2.1.1. Exeter Impaction technique

This technique started its use in revision hip surgery invented at the Princess Elizabeth Orthopaedic Hospital in Exeter, England (Gie et al., 1993a; Schimmel, Buma, Versleyen, Huiskes, & Slooff, 1998). An adapted version of this technique for knee replacement uses bone chips with sizes 2-4mm for the distal end of the defect, 5-10mm for the proximal end. A study by Willem et al (Schreurs et al 1994) recommended 3-4mm and 8-10mm for distal and proximal ends of the defect respectively.

This image has been removed due to copyright restriction. Available online from "(Naim & Toms, 2013)"

Figure 2.5*: Exeter technique in impaction bone grafting at Exeter knee reconstruction unit with a short, cemented stem* (Naim & Toms, 2013)

2.5.2.1.2. Radial Impaction technique

This impaction technique was developed by Stulberg (Stulberg et al 2000; Stulberg et al 2002) for hip replacements who believed that the Exeter technique created complications as the technique required the used implants with limited sizes and had many un resolved issues such as unknown optimal implant surface treatment, fixation, graft type size, preparation or delivery system or graft impaction technique. Stulberg proposed a surgical technique based on the Exeter technique which composed of 80% cancellous bone and 20% cortical bone instead of 100% cancellous bone as used by the Exeter team. He also used tapered, polished impactors (instead of flat end distal impactors). Stulberg suggested that adding a small proportion of cortical bone into the cancellous bone improved the supportive structure and as a result increase initial stability. However, there is not much literature or research to demonstrate the short- or long-term effect of mixing cortical

bone with cancellous bone in bone grafts. This technique used a polyethylene plug attached to a guide wire longer than the stem length inserted to the canal, allografts were filled in the femoral canal and impacted longitudinally with canal fillers placed over a guide wire. The stability of the final impacted graft was tested by connecting a torque wrench to the guide wire and twisting the guide wire. However, a standard torque value was not defined.

2.5.2.1.3. Modified Exeter technique:

This technique was proposed by Thomasson (Thomasson et al 2005), which suggested the use of fresh frozen femoral allograft harvested from primary total hip arthroplasties. The graft was morselized using an acetabular reamer without consideration to the size of the resulting bone grafts. This technique uses cementing of the distal stem to the host bone but doesn't allow for remodelling and the bone grafts are only impacted proximally. This technique was used between 1996 and 2002 but was only used in hip replacements.

2.6. Complications in revision surgery

Infection, loosening of implants and periprosthetic fracture are the major three complications with impaction bone grafting (Boettner, Bechler, Springer, Faschingbauer, & Jungwirth-Weinberger, 2020). Implant subsidence of either the femoral or tibial component can compromise implant stability and result in loosening and pain. Fractures can occur either intra-operatively or post-operatively. Intra-operative fractures occur when the stress of impaction exceeds the strength of the bone during impaction bone grafting. Post-operative fractures occur due to overloading. Peri-prosthetic infection can be caused by a bacterial or fungal infection which can occur either immediately post-operative or in the first 6 months post-operation.

Impaction grafting requires the bone grafts to be firmly impacted to achieve initial stability. This is achieved by compacting the bone grafts initially to secure fixation before introducing the implant. In the process of impaction, the bone graft is compressed in both the distal and radial direction. This results in transient stresses around the cortical bone. An intra-operative tibial fracture occurs when the stress applied exceeds the strength of the surrounding bone. Fractures usually occur during the impaction process when reconstructing the medullary canal. During the process of impaction bone grafting a large amount of energy is delivered to the bone graft and is transmitted to the surrounding structures. However, the risk is necessary to deliver sufficient impaction force so that the bone grafts consolidate and provide a stable bed for the implant. Lee et al (Lee et al., 2017) summarised their 10-year follow-up study of revision total knee arthroplasty between 1996 to 2006 with records of 225 revision cases of which 36 (16%) cases experienced a periprosthetic fracture.

Implant subsidence or component migration can be caused due to either inadequate or loss of fixation which gives a potential for failure of the procedure. This can occur due to one of two reasons, the subsidence of the revision components or as a result of resorption and lack of incorporation of the bone graft. A 10 year follow up study by Hilgen et al (Hilgen et al., 2013) on 29 revision knee arthroplasties with impaction bone grafting found that 12 knees were treated with revision surgery after the first revision as a result of mechanical failure and aseptic loosening of the component where the surgeons reported a lack of incorporation with bone graft resorption as the reason for the failed cases.

Infection is the number one complication observed in revision knee arthroplasty post impaction. Lee et al (Lee et al., 2017) reported that out of 225 cases 120 (58.2%) patients suffered complications due to infection, The main pathogens of infection were staphylococcus aureus (25.7%). Staphylococcus epidermis (13.3%) and streptococcus (13.3%). Lotke et al (Lotke et al 2006) reported 5% of their 48 patients suffered from infection due to staphylococcus epidermis.

Hilgen et al (Hilgen et al., 2013) reported 2 cases suffered from Staphylococcus aureus one-month post-surgery. Boettner et al (Boettner et al., 2020) reported one of their 3 cases suffered from infection due to post-operative wound drainage. However, none reported failure of the prosthesis as a result of infection, the majority of the complications were resolved without additional surgical procedures.

2.6.1. Mechanical Variables in Impaction bone grafting

It has been established that the mechanical properties of bone grafts are highly variable. The variability of the grafts in this thesis is classified into three types based on the mechanical properties, the preparation technique and the graft technique of bone (Albert et al 2008b).

Type 1: Variables based on preparation techniques. This type describes all variables in the preparation of grafts like the size of the graft, the uniformity of the bone graft, sterilization etc. This variable generally remains constant, and these variables are not affected by the impaction technique. These are variables that can be controlled and have a known value.

Type 2: Variables based on mechanical properties. These are the mechanical properties of the host graft material namely apparent young's modulus & yield strength. There is a reasonable understanding of the bulk properties of cancellous bone which explains that low level of irradiation, large particle size, better grading, defatting and the removal of cartilage and soft tissue help improve the mechanical properties of the bone grafts. There is reasonable amount in the literature about these properties which are discussed further in this chapter. This variable generally remains constant, and the variables are not affected by the impaction technique.

Type 3: Variables based on the impaction technique. These variables are hard to control as they do not have a specific value. These variables include impaction force or stress and the number of impactions.

Over the past years since the introduction of impaction bone grafting numerous studies have been performed (Bavadekar et al., 2001; Brewster et al 1999; Brewster et al 2016; Brodt et al 1998; Cornu et al., 2004; Speirs, Hotz, Oxland, Häusler, & Nolte, 1999; Van Der Donk, Buma, Verdonschot, & Schreurs, 2002; Voor, Nawab, Malkani, & Ullrich, 2000a; Voor, White, Grieshaber, Malkani, & Ullrich, 2004) to determine the optimal preparation technique for bone grafts (type 1 variables), however, a standardised method has not yet been developed. In addition to this no not much research has been carried out to find the best impaction method (type 3 variables) except for a few studies by Heiner et al & Voor et al (L. Fosse, Rønningen, Lund-Larsen, Benum, & Grande, 2004; Heiner et al 2005; Voor et al., 2004). A good understanding of the type 1 & type 3 parameters is essential to achieve better mechanical properties of bone grafts and higher implant stability. Both of these variables will be studied and explored in this thesis.

2.6.1.1. Sterilization techniques

Bone grafts used in impaction bone grafting have been prepared as fresh frozen allografts (Gie et al., 1993a; Schimmel et al., 1998), freeze-drying allografts (lyophilisation) (Cornu et al., 2003b, 2003a), irradiated (Pelker et al 1987), autoclaved (Allogo et al 1995; Wangerin, Ewers, Wottge, & Randzio, 1986), or acid and alkaline treated allografts (Hotz et al., 1999; Speirs et al., 1999). Gie et al & Schimmel et al (Gie et al., 1993a; Schimmel et al., 1998) suggests the use of fresh frozen femoral heads instead of freeze-dried femoral heads as they compact faster than fresh frozen femoral heads. Cornu et al (Cornu et al., 2003b) demonstrated that fresh frozen femoral heads compacted faster than freeze-dried/ cryopreserved bone grafts with the fresh frozen bone graft compacting up to half of its initial height whilst freeze dried bone grafts compacted only one thirds its initial height for a similar set of 15 impactions. Cadaveric experiments conducted by (Pelker et al 1987) showed that fresh frozen bone grafts produce stiffer bone grafts when subjected to large torsional loads. Irradiation of allografts is frequently used as a sterilisation technique to minimise

the risk of disease transmission. It can be accomplished on any type of allografts using X-rays, gamma rays, or high energy electrons which are used to minimise viral and other pathological contamination using the ionisation process (Hernigou, 2000). Zhang (Yongxing Zhang et al., 1994)reported that there were no significant differences in material properties or mechanical properties on fresh frozen and freeze-dried bone grafts as long as the radiation dosage was in the range of 20 – 25kGy. However, Fideler et al (Fideler, Vangsness, Bin lu, Orlando, & Moore, 1995) performed irradiation of bones from patellar grafts and suggested that a dosage of 20kGy can reduce the biomechanical strength of fresh frozen bone grafts by up to 15%. Anderson et al (Anderson et al 1992) on the other hand studied cancellous bone grafts and found that there was a significant difference in the normalised elastic modulus when the bones had been irradiated with a radiation dosage of 60kGy. (Hernigou, 2000) suggested that high dose radiation can be harmful to the tissues and osteogenic potential while (Fideler et al., 1995) suggested that 30kGy of gamma radiation is necessary for the sterilization of fresh frozen allograft. An alternate method to sterilize the bones was autoclave sterilization. This is a heat treatment method that is accomplished by exposing bone grafts under high pressure to heat or pressurised steam. The method is performed at a temperature of 132° C for 60 minutes (Speirs et al., 1999). In some cases, autoclaving is also combined with treatments such as alkaline or acidic sterilization. Combining autoclave with alkaline or acidic sterilization has also been reported to reduce the strength and elastic modulus on auditory ossicles as reported by Hotz et al (Hotz et al., 1999). A study conducted by Speirs (Speirs et al., 1999) noted that the process of autoclaving bones reduces the yield strength in compressive tests of allografts produced from auditory ossicles. It is assumed that the process would have a similar effect on bone allograft graft material.

In summary, fresh frozen allografts provide better mechanical behaviour in compression and torsion testing than freeze dried allografts. Irradiation at low to medium doses does not alter the integrity of the structural properties of the bone grafts. However, there is still no gold standard for bone graft sterilization.

2.6.1.2. Size and grading

The behaviour of the bone grafts is a function of particle size and layering. However, there are no standard size or distribution which is followed by surgeons. Brewster et al (Brewster et al 1999) proposed that for grafts to have superior mechanical characteristics, well-graded aggregates composed of a mixture of materials are necessary. Brewster et al reported that a well-graded aggregate would yield a higher strength than aggregates using uniform particle size due to the presence of interparticle contacts resulting in a higher load per contact than a uniform aggregate of particles (Brewster et al 2016). A study conducted by Bolder et al (Bolder et al., 2003) recommended the use of large bones grafts (average 9mm) firmly impacted by hammering to achieve optimal stability of the acetabular cup. A similar study conducted by Ullmark (Ullmark, 2000) reported the use of large sizes (6 – 8mm) of bone graft chips to results in better stability of the implant than using smaller sizes. Furthermore, there have been experimental results (Dunlop et al., 2003; Fetzer et al., 2001) showing that well-graded small size bone grafts (average 2mm) used in short stem cones and sleeves and well-graded large bone grafts for long stem implants would provide the best implant stability. However, the study done by Dunlop et al (Dunlop et al., 2003) involved using the small size bone grafts (average 2mm) that were not washed and the design of the experiment allowed for fast extrusion resulting in a greater release of fat. Similarly, Stroet et al (Stroet et al 2014) studied a 4 year follow up study of 26 cemented femoral revisions where a variety of short stems (13) and long stems (13) were used. The results showed that the use of bone grafts with cement produced good implant stability with no reported cases of revisions performed in the first 4 years of follow up.

2.6.1.3. Defatting

MCB's consist of small particles of cancellous bones and marrow, which can be made up of a combination of water, fat, and complex biological substances. Studies on bone graft material have has reported that the moisture content influences the density of the compacted bone where less water/fat content produced lower strain results than bone grafts where the water/fat content were higher (Voor, Nawab, Malkani, & Ullrich, 2000b). There has been various studies and methods used to de-fat the graft namely, washing by pulsed lavage with a warm 0.9% saline solution heated to 48 degrees (Dunlop et al., 2003), soaking the graft material in chloroform (Heiner & Brown, 2001), bone grafts soaked in detergent solution heated to approximately 80 degrees (Voor et al., 2004), bone grafts pre-soaked in acetone for up to 48 hours (Giesen et al., 1999) and washing the bone grafts in high-pressure saline. Dunlop et al (Dunlop et al., 2003) studied the effect of the particle size and washing of bone grafts. The study discovered that the particle size distribution does not change between the washed and pre-washes state of the bone grafts. They recorded that washing the bone grafts increase the shear resistance of the bone graft and suggested that the fat and marrow in the bone graft acted as an interparticle lubricant which can absorb the impaction energy. As a result, removing this lubricant like surface can help achieve higher compaction as a result of increased shear strength.

A similar study conducted by Brodt et al (Brodt et al 1998) also found that removing the fat content in the bone graft does not have any effect on the particle size. Their study also demonstrated that removing the fat content of the particles produced a higher average modulus before the yield strain and beyond the yield strain of the bone. Voor et al (Voor et al., 2000a) in their study demonstrated that the water content of the particle has an influence on the properties of the particles and reducing the fat content improved the mechanical behaviour of the particles both in static and dynamic testing. In summary, the lack of standard process indicates bone grafts are not industrially produced but are made at individual hospitals/clinics according to need. Additionally, there is still

no standard washing technique for bone graft material, however, from an engineering point of view, washing bone grafts can provide a better mechanical environment as the defatting process produces consistent material removing the influence of fat and water during the impaction process.

2.6.1.4. Mechanical Properties

Compared to the literature about cancellous bone, there is very little information is available about the mechanical behaviour of impaction bone grafts. The basic material properties have been defined in literature where numerous studies (Brewster et al 1999; Brodt et al 1998; Hanspeter et al 2004; Hanspeter et al 2005; Giesen et al., 1999; Malkani, Voor, Fee, & Bates, 1996; Voor et al., 2000a) have been carried out to quantify the mechanical properties of MCB graft materials. The relationship between the force applied and the deformation of the bone grafts are represented in the form of stress-strain (σ - ε) graphs. Stress (σ) can be defined as the ratio of load (F) applied perpendicular to the material cross-section by the cross-sectional area (A). Strain (ε) can be defined as the ratio of compression (Δl) or elongation from its initial length or height (l). A compressive modulus of elasticity (Young's modulus, E) is calculated by the slope of the stress-strain curve before the material starts yielding. It can be deduced by the change in stress by strain (σ /ε), slope ($\Delta\sigma/\Delta\varepsilon$). Figure 2.6 shows the comparison between a typical engineering stress-strain curve compared to that of a bone graft material where the bone graft material is seen to exhibit non-linear elastic behaviour. Mechanical properties of bone grafts are characterised as apparent values to replicate the mechanical behaviour during impaction.

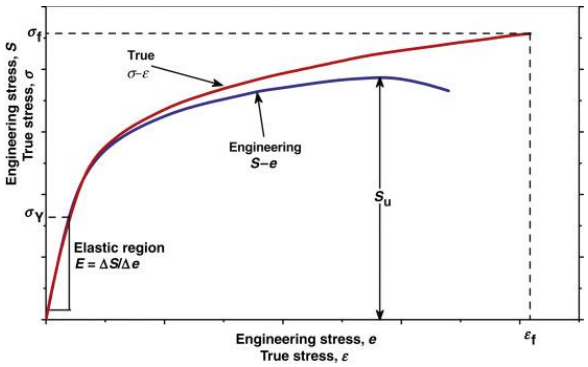

This image has been removed due to copyright restiction. Available online from "(Dooley, 2021)"

Figure 2.6 a) A comparison of typical tensile engineering stress-strain and true stress-strain curve (McKeen, 2016) *(Reproduced with permissions from Elsevier.), b) A schematic relationship between stress strain to see how elastic material strains while under loading* (Dooley, 2021).

The mechanical properties of bone grafts can be explained using a simple non-linear elastic model as seen from Figure 2.6 which explains function of the elasticity captured by the Youngs modulus, the post-yield behaviour explained by the yield strain and the frictional contact between the particles. Young's modulus explains the response of bone grafts under the impaction process and post-operative cycling loading during regular physical activities like walking. Mechanical properties of MCB grafts are measured by mechanical testing in compressive and shear tests. Achieving a high mechanical strength can help reduce subsidence in implants. A wide range of research has been conducted to capture the mechanical characteristics of bone grafts. These mechanical properties can be determined by a few different methods namely, Uni-axial compression (Giesen et al., 1999), triaxial compression (Brodt et al 1998), drop weight testing (Bavadekar et al., 2001), cycling compression (Grimm et al 2001) or shear testing. Each of these tests is used to measure the influence of modulus and shear strength and consequence of content and size however, they do not assess the behaviour of the bone grafts.

2.6.1.5. Elastic Parameters

One of the main ways to characterise the mechanical strength of bone grafts is to understand the bone grafts resistance deformation in response to an applied force. Giesen et al. (1999) studied impaction bone grafting to investigate the modulus of bone grafts. They used 16 ovine bone grafts created from bone mills and subjected them to a uni-axial compressive and creep test with a stress range of 2.75MPa for 24 cycles followed by a relaxation phase and a creep period of 900s at 1.81MPa. They estimated the apparent modulus of the bone grafts to be in the range of 32.5- 42.2 MPa. The bone grafts were not graded or washed to remove fat from the particles, as such the graft material exhibited visco-elastoplastic property. A similar study by Voor et al. (2000b) performed a one-dimensional consolidation test on bovine bone grafts hand-milled through bone mills. The use of one-dimensional compression allowed for the fat and water content in the particles to be extruded out during the compression. The applied stress values estimated for their test were in the range of 1.09 MPa resulting in an average apparent modulus of 7.32 MPa for 10 compression cycles at axial stress of 1.09MPa which is very low compared to (Giesen et al., 1999) who reported the average modulus of 38.7 MPa under axial stress of 1.18 MPa. A recent study done by McNamara et al. (2014) used a combination of MCB graft and hydroxyapatite in uniaxial compression and creep test. They used human femoral heads which were milled into bone grafts in the size of 2-5mm and then mixed with porous hydroxyapatite in the ratio of 2:1, 1:1 and 1:2 combinations. The bone grafts were subjected to 60 loading cycles at 5.5MPa followed by a stress relaxation phase and a creep phase for 12 hours at 3.0MPa. The reported modulus values were in the range of 300 to 450MPa for human bone grafts mixed with porous and non-porous hydroxyapatite.

Additionally, another form of capturing the material properties of bone grafts is through drop tower testing/hammer impaction testing which simulate the actual impaction process. Fosse et al (Fosse et al., 2004) conducted a slap hammer impaction test on bone grafts and characterised into

different modulus of elasticity namely, impact constrained modulus of elasticity (ICME), consolidated contained modulus of elasticity (CCME) and total constrained modulus of elasticity (TCME). They used bovine femoral heads, which were ground in a bone mill to sizes ranging from 2-3.2mm. The slap hammer was dropped from six different levels, ten times at each height, simulating peak stress at the highest point of 1.4MPa. The modulus captured at each level of impaction were reported. Consolidated constrained elastic modulus described the modulus of the bone grafts at the initial period of the load. Total constrained modulus of elasticity explained the change in modulus during the load step with a creep period of 120minutes. Impact constrained modulus of elasticity provides information on the apparent modulus, which correlates with the peak stresses in engineering stress equations. The values reported (ICME) from these tests were in the range of 3.0 to 97.4MPa. Studies by (Xu et al., 2011) & (Heiner et al., 2005) used a similar type of testing using human bone grafts with the former using two type sizes of bone grafts (7 - 10 mm large & small slurry 3 - 4mm) and reported instantaneous modulus in the range of 29.12 MPa for the slurry and 49.64 - 68.06 MPa for the larger bone grafts. The latter (Heiner et al., 2005) created a cavitary defect model in similar dimensions to an over-reamed femoral canal, filling them up with cancellous human bone grafts cut using a hand saw into 4-5mm cubes and impacting them using a surgical impulse force hammer. The study reported a compressive modulus in the range of 39 – 56 MPa.

The modulus of bone grafts is highly variable and depends on the bone graft's condition and the testing technique. An in-vitro study by Bavadekar et al. (2001) explains that high pre-compaction energy produces higher apparent modulus. A cycling compressive test by Phillips et al. (2006) also suggested and demonstrated that the stiffness of MCB graft is dependent on the prior loading. This is because the modulus of bone grafts saturates to a steady value after cumulative series of

impactions where the bone graft's orientation, increasing the bone graft's capacity to carry the load. Table 2.3 shows the reported modulus values for bone grafts from existing research.

Citation	Type of Test	Type of material used	Size and shape of the material	Loading range in MPa	Impaction numbers	Modulus reported in MPa
(Brodt et al., 1998)	Triaxial Compression testing	Human femoral heads	1.7 – 3.7 mm	0.276 to 0.552	5	100
(Giesen et al., 1999)	Uniaxial compressive loading	Ovine femoral heads	2 - 4 mm	2.75	36	32.5-42.2
(Voor et al., 2000a)	Uni-axial compression testing	Bovine Femoral heads	0.42 – 2 mm	1.09	10	8
(Bavadekar et al., 2001)	Drop tower testing	Human femoral heads	3.3 +/- 1 mm	0.5	150	Pure cancellous – 42 to 48, cortico-cancellous – 26
(Grimm et al., 2001)	Cycling compressive loading	Ovine femoral heads	1 - 2 mm, 2 - 4 mm, 4 - 6.3 mm	0.73	5000	3.65
(Verdonschot et al., 2001)	Confined compression testing	Human femoral heads	3 - 5 mm & 6-8 mm	2.68	98	85
(Fosse et al., 2004)	Drop tower testing	Bovine femoral heads	2 – 3.2 mm	1.4	15 & 30	ICME – 97.4 CCME – 69.4 TCME – 3.0
(Heiner et al., 2005)	Hammer impaction	Human femoral heads	4-5mm cubes	1.25	98	39 - 56
(Phillips et al., 2006)	Cycling compressive loading	bovine femoral heads	3 – 6 mm	3.0	60	75 – 110
(Fosse et al., 2006 a)	Drop tower testing	Human femoral heads	2 – 3 mm, 3 – 4 mm, 4 – 5 mm	1.4	10	24.2 – 50.9

(Fosse et al., 2006 b)	Drop tower testing	Bovine femoral heads	~ 2 mm	1.4	10	ICME – 21 to 53, CCME – 37 – 212, TCME – 8 – 17
(Albert et al., 2008b)	Cycling compressive loading	Human femoral heads	2.4 – 8 mm	1.1	20	70.8 – 87
(Cornu et al., 2009)	Confined compression testing	Human femoral heads	2 – 8 mm	0.5	150	30 - 65
(Xu et al., 2011)	Drop tower testing	Human femoral heads	2 mm & 7 – 10 mm	0.11	50	29.12 – 2mm bone grafts & 49.64 – 68.06 7 – 10 mm bone grafts
(Ayers et al., 2014)	Cycling compressive loading	Polyurethane foam from sawbones	1 – 6 mm	3.0	750	6.76
(McNamara et al., 2014)	Uni – axial compression testing	Human femoral heads plus hydroxyapatite	2 – 5 mm	6.8	60	300 - 450
(Putzer et al., 2017)	Uni – axial compression followed by Drop tower testing	Human femoral heads	5 – 10 mm	n/a	10	0.09 - 0.12

Table 2.3 Reported elastic parameters in terms of stiffness with the type of testing and the materials tested

2.6.1.6. Strength

The strength of a material is the ability to withstand the load applied before breaking down or subjecting to permanent deformation. Studies by Brodt et al. (1998) used a tri-axial compressive testing method to evaluate the mechanical behaviour of human MCB grafts. The study calculated the axial strain in pressure ranges of 0.276 – 0.522 MPa. Fresh frozen Human bone grafts removed of any soft tissue or cortical bone was morselised in a bone mill but was not defatted or cleaned

for the tests. The results reported where in terms of pre-crush phase modulus ranging from 51.67 – 152.4 MPa crush phase modulus ranging from 3.62 – 5.84 MPa, transition stress (0.17 – 0.27 MPa), transition strain (0.18 – 0.41%) and finally, the effective Poisson's ratio (0.14 – 0.25). The shear stiffness provides information on the bone graft's resistiveness when it is subjected to shear stress.

Studies by Brewster et al. (1999a) and Dunlop et al. (2003) shear tested bone grafts in two types (fresh graft & washed graft) to a max compressive stress of 350KPa. They reported that the mechanical properties of the bone grafts increased with normal load and the mechanical strength of the bone grafts with increasing compaction energy. The fresh grafts reported a shear strength of 244KPa, while washed grafts recorded an average shear strength of 280 KPa. A study by Voor et al. (2004) studied the effects of defatting and synthetic augmentation on the mechanical strength through a one-dimensional consolidation testing of human MCB and hydroxyapatite in separately and in various combinations. They demonstrated that 100% human MCB saturated with fat and water and resulted in a higher initial strain of 35.3% and a maximum constrained modulus of 8.23 MPa, whilst a 100% Hydroxyapatite recorded only an initial strain of 10.7% and a constrained modulus of 30.6 MPa over a load of 1.09 MPa. As a result, they concluded that a higher initial density with a lower strain and a higher initial modulus helps achieve higher strength. On the contrary, Bavadekar et al. (2001) suggested that the actual elastic modulus of the bone grafts will differ during impaction as undamaged bone grafts tend to reach a higher elastic modulus than structurally damaged cancellous bone grafts. Apart from these studies (Brodt et al., 1998; Brewster et al., 1999b; Dunlop et al., 2003; Bavadekar et al., 2001; Voor et al., 2004), there has been little research which have studied the strength of bone grafts.

2.6.1.7. Poisson ratio

Poisson's ratio defines the ratio of lateral and axial strain, which in the case of isotropic material like bones should be approximately 0.25 (William et al., 2001). Poisson's ratio helps recognise how the graft behaves under impactions conditions. A study conducted by Bavadekar et al. (2001) demonstrated that an apparent Poisson ratio could be estimated as higher density aggregate grafts behave similarly to a solid substance. Brodt et al. (1998) performed a tri-axial compressive testing of human bone grafts and predicted that bone grafts demonstrate anisotropic behaviour and total constrained apparent Poisson's ratio in the range of 0.12 – 0.25.

2.6.1.8. Impaction Stress

Impaction force (type 3 variable) is the measure of the stress applied to the test specimen. In impaction bone grafting, it has been established that higher the impaction heights (drop tower testing) (Bavadekar et al., 2001) or the higher impaction stress (cyclic compression tests) (Grimm et al., 2002) results in a higher consolidated stiffness and apparent mass density leading to higher stability (Fosse et al., 2004). A higher impaction stress helps achieve denser packed bone grafts and a lower amount of porosity. A huge range of impact stress has been used in literature, which ranges from 0.5MPa to 3.0MPa, which can be seen from Table 2.3 Reported elastic parameters in terms of stiffness with the type of testing and the materials tested. However, there is no standard or minimum stress specified by literature for distal femur's or proximal tibias. A better understanding of the impaction stress is necessary to achieve better mechanical stiffness.

2.6.1.9. Number of Impactions

The degree of compaction is influenced by the number of impaction cycles. A study by Bavadekar et al. (2001) investigated the effect of the number of impactions to the bone grafts and found that

the apparent stiffness increases with the number of impactions on a logarithmic scale. The study suggested that grafts gradually reach a steady value after 40 impactions. However, the study doesn't explore the effects of impaction stress beyond 0.5 MPa and its influence on the number of impactions.

2.6.1.10. Summary

Conclusively, most of the research conducted in impaction bone grafts has been on hip replacement from the existing literature on impaction bone grafting. There has been very little research undertaken in the impaction bone grafting in the knee with a few that have used similar methods as used in hip replacements and translated it into knee replacements. However, there is no clear definition of one efficient and standard process used universally on impaction bone grafting.

2.7. Numerical Modelling

Numerical modelling is widely used to investigate the biomechanics of the knee joint from the cell to the tissue level to the organ level. Finite element analysis is used for structural analysis that has evolved into an invaluable tool for biomechanical researchers to study the structural behaviour of all kinds of human tissues over the past forty years. Computational models have been used across a wide range of spectrum of orthopaedic devices. The push to perform computational analysis on orthopaedic devices is to study the bone-implant system's fundamental behaviour or study a specific device. It is also used to aid in the design and pre-clinical testing of new implants and to compare their performance with existing designs. This will be helpful to understand and learn about the stability of these implants.

2.7.1. Finite element analysis

This is an advanced computer technique developed in engineering mechanics that reconstruct stress, strain, and deformation in structures. This method was introduced to orthopaedic biomechanics in 1972 to evaluate stresses in human bones by predicting how the product reacts to real-world forces and other physical effects (Brekelmans et al., 1972). In orthopaedic biomechanics, the structures to be analysed are of biological origin. Hence, they do not have exactly defined angles, curves, and distances. They are patient-specific and highly inhomogeneous, which changes over a lifetime and depend on physiological load, health, age, and nutrition. A German orthopaedic surgeon Julius Wolff discovered that bone could adapt to mechanical loads. This plays an important role in hip and Knee Arthroplasty. The distribution of forces in and around the joint has to be reconstructed properly. If the design is improper, it can cause stress shielding, or if the implant mainly transfers the force, the adjacent bones are minimally loaded and subsequently degraded. This stress shielding cannot be completely avoided but can be minimised using finite element analysis and analysing the strain between the metalling implants and the bone interface.

2.7.2. Overview of FEA based research on bone grafts

Since the introduction of impaction bone grafting and the use of numerical modelling on orthopaedic biomechanical structures, there have been two popular approaches to simulate the behaviour of impaction bone graft. The first approach is to assign a simple non-linear elastic material properties model with an appropriate modulus. The second approach is to conduct an experimental test, and the result is used to define an appropriate constitutive material model. They model a scenario like micromotion of the implant post impaction or cement penetration profile or the mechanical response of the graft during activities such as walking or sitting or standing.-The following finite element studies use the second approach to simulate bone grafts in their model.

Hanspeter et al. (2006) (Figure 2.7) studied the cement penetration into impacted bones in hip replacements using a finite element analysis. They created a 3-Dimensional finite element model obtained from a cadaveric femur model on which the impaction bone grafting procedure was performed. The model consisted of a medullary canal filled with bone cement surrounded by an impacted allograft layer. Hanspeter et al. (2006) modelled the cement penetration profile within the medullary canal with the impacted bone graft as a constitutive model with partial saturated flow capabilities. The model was a solid elastic model constructed as an 8-node porous pressure brick element. To demonstrate fluid penetration in the model, the porous medium was attached to a finite element mesh and assumed that two fluids existed (wetting and non-wetting) at the same point, so that non-wetting fluid could diffuse through the medium and across the boundary so that its pressure is small enough to be neglected. A constitutive model describes the response of a material to different mechanical and loading conditions. The data obtained from experimental tests are used to feed and define the constitutive model. They proved the stress-strain relations formulate the governing equations, including the laws of conservation and kinematic relations. The finite element model predicted cement penetration into the impacted constitutive bone graft model accurately. However, the model failed to explain the effect of cement penetration against the strength of the bone graft or the stability of the bone graft.

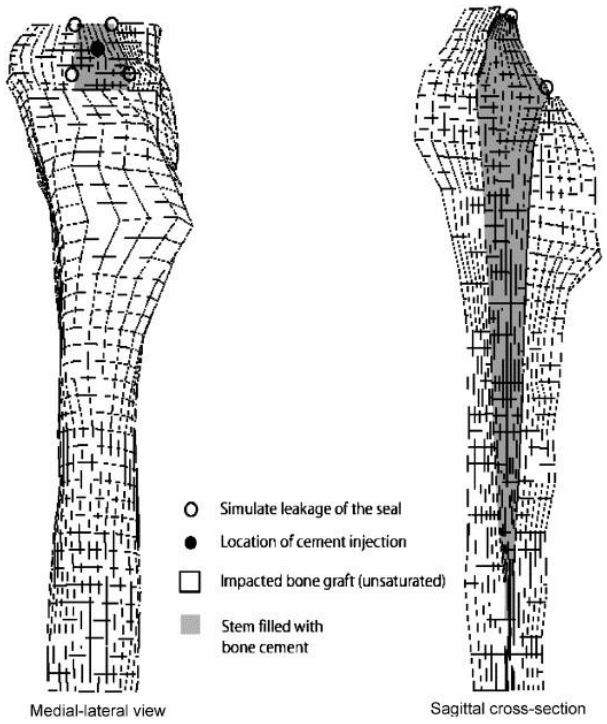

Figure 2.7 Finite element model indicating the site of cement injection in the medial-lateral view and sagittal cross-section view (Hanspeter et al., 2006) (Reproduced with permission from Eslevier.)

Phillips et al. (2006a) investigated the short term behaviour of acetabular construct after revision hip arthroplasty using a 3D finite element analysis. They created a constitutive elastoplastic material model, as seen from Figure 2.8, using a single element to describe the behaviour of morselised cortico-cancellous bone graft. The bone grafts were modelled as non-linear elastic and Drucker Prager Cap (DPC) plasticity based on previous studies conducted by the authors (Phillips et al., 2006b). They studied the displacement of the acetabular cup over walking cycles and reported that bone grafts are subjected to compressive and shear plastic strains following surgery. The study showed unique patterns of migration and rotation of the implant based on the activities (sitting, walking, and standing), which were found to be similar to clinical observations. The study results showed that the bone graft bed suffers from compression and shear plastic strain following surgery. The model developed by the researcher can be used in the assessment of cup designs and fixation devices. However, they do not characterise the properties of bone graft before and after impaction as it was not studied in their study.

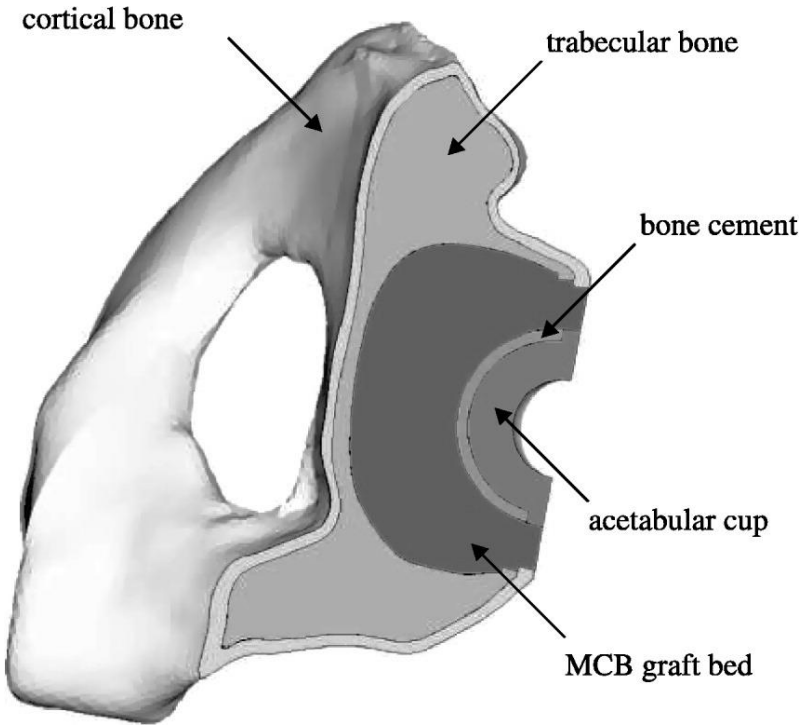

Figure 2.8 Transverse cross-section of the acetabulum with MCB graft bed embedded as a constitutive finite element model after impaction bone grafting (Phillips et al., 2006). (Reproduced with permission from Elsevier.)

A similar study investigated by Phillips et al. (2006a, 2006b) developed a constitutive model based on results of a similar experimental compressive test to describe viscoelastic and non-linear elastic behaviour of MCB graft. They conducted experimental tests as seen from Figure 2.9 on compressive testing of bone grafts to develop relationships describing the elastic, the viscoelastic and plastic behaviour of bone grafts which were then applied as input parameters to a constitutive model using finite element analysis to validate if the model can capture the behaviour of MCB grafts. The material properties used in the model were 18 GPa young's modulus and 0.3 Poisson ratio for cortical bone, 0.15 GPa and 0.2 for trabecular bone, 200 GPa and 0.3 for the metal component as a uniform confined modulus for each material. The study used a dynamic explicit model with load histories representative of normal walking, sitting, and standing up scenario to analyse plastic strain development in the bone graft bed. The results found from the study were consistent with the finding of Phillips et al. (2004). However, extended tests are required to quantify the visco elastoplastic behaviour.

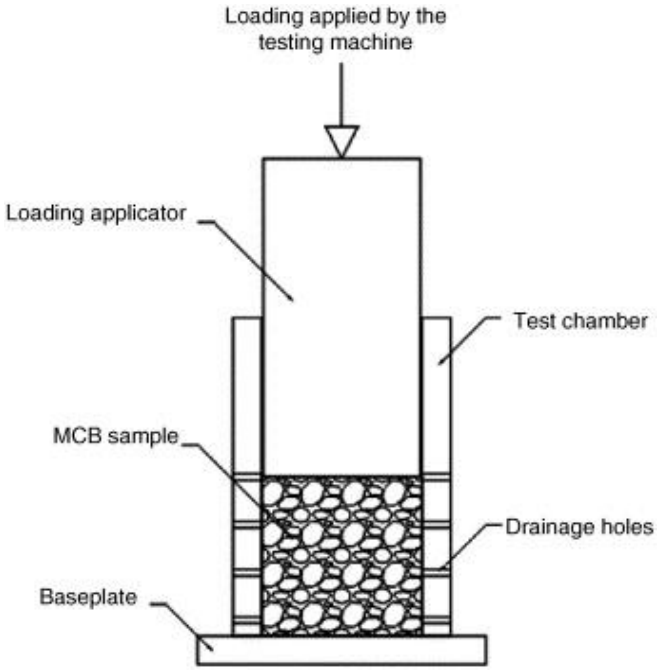

Figure 2.9 Mechanical test setup for impaction bone grafting of bovine bone grafts (*Phillips et al., 2006a*). *(Reproduced with permission from Taylor & Francis.)*

Albert et al. (2009) characterised mechanical properties of the graft bed in terms of impaction force, explored the relationship between subsidence and graft and bone cement regions after femoral impaction and alternatives in graft compaction methods. They created a finite element model to simulate the proximal femur after impaction allografting using a constitutive approach to assess cement penetration profiles and the graft density during cycling loading corresponding to a walking cycle. The finite element model assumed 20GPa for the cortical bone, with a Poisson ratio of 0.28 and 2GPa for the bone cement with a Poisson ratio of 0.37. The graft was modelled with elasto-plastic behaviour with three different densities and modulus 272mg/cm3 (low), 342 mg/cm3 (moderate), and 385 mg/cm3 (high). The young's modulus of the graft was set to 7.4 MPa (low), 12.2 MPa (moderate), 14.3 MPa (high), respectively. Mohr-coulomb cohesion and friction parameters were assumed constant for each graft density, and the Poisson's ratio was set to 0.2. The research demonstrated that increased density of the impacted bone grafts decreased the subsidence in the stem. However, there was no effect of change in subsidence in constructs with cement-endosteum contacts.

A study investigated by Totoribe et al. (2018) (Figure 2.10) assessed the micromotion of the tibial implant and the stresses between the tibial implant through a finite element study. They created a finite element model representing a linear elastic material with six variations of bone grafts to simulate a mechanical worst-case scenario. The tibia was fixed in all directions from the distal end; impaction was emulated using incremental force control with a maximum compressive force of 1800N. The interface between the bone and the tibial component was treated as a frictional contact set to 0.2. They simulated bone grafts with soft and hard bone grafts for small, medium, and large bone defects. The young's modulus was assigned to 17GPa for cortical bone, 0.4GPa for cancellous bone and a Poisson ratio of 0.3. The bone graft model was set to either 42 MPa for low strength bone graft to simulate a mechanical worst-case scenario and 150 MPa for high strength bone graft to simulate a tightly impacted morselized cancellous bone graft with a Poisson ratio of 0.2. All the models were analysed for micromotion beneath the stems. They recorded the most micromotion for the soft and large bone graft models and suggested using hard bone grafting to improve clinical outcomes. The numerical model was designed as a constitutive model and did not include the impaction process in the research. The model was assumed to be impacted, and the material properties were just assumed of cancellous bone and not of any compressive modulus recorded from literature.

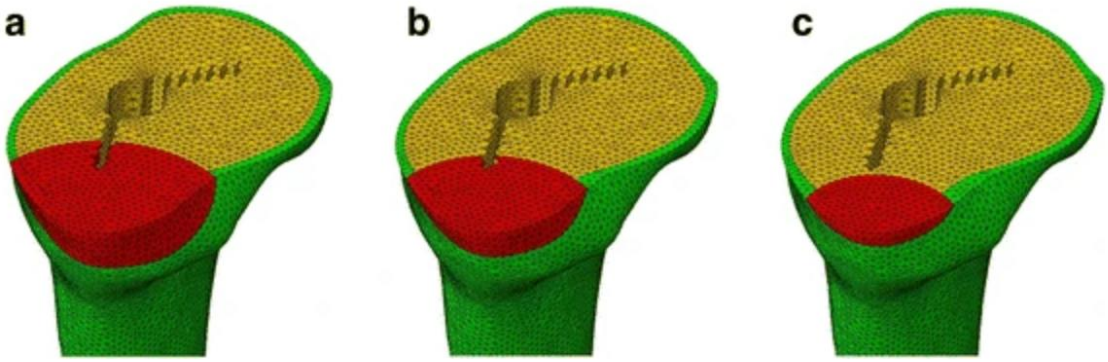

Figure 2.10 Finite element model created using constitutive laws for small (a), medium (b), and large (a) bone defects filled with bone grafts (Totoribe et al., 2018) (Reproduced under CC-BY License)

2.8. Conclusion

Impaction bone grafting is used to reconstruct the acetabular, proximal, and distal femoral and tibial defects in revision surgery and has been evolving for decades. It was initially proposed by Gie et al. (1993a, 1993b). This technique has been successful in hip replacements, however not so successful in knee replacements. Component subsidence and fractures are the two main issues resulting in complications and failure of impaction bone grafting.

Bone grafts are prepared using various techniques including fresh-frozen, freeze-dried, autoclaved, irradiated, alkaline treatment and acidic treatment. The preferred technique is the use of fresh frozen allograft material as they produce the best mechanical properties. MCB grafts are generally constrained to conduct experiments and are then characterised into apparent values to replicate the behaviour during impaction bone grafting. Current research suggests that the graft size, grading, and defatting have a significant effect on the graft's mechanical properties, such as compressive stiffness and shear resistance. The mechanical properties of bone grafts are quantified by mechanical strength such as Young's modulus, stress-strain behaviour, Poisson's ratio, elastic and plastic behaviour. However, to date, little research has been performed on investigating the post-yield behaviour of the bone graft.

Better graft preparation techniques combined with a good impaction technique is necessary to reach a stable bone graft bed. Hence the variables that influence bone graft behaviour have been classified into three variable types: preparation, mechanical properties, and impaction technique. The relationship between these parameters has not been well explored. Much of the published data are not comparable to the testing techniques used for them have been different. A wide range of values of Young's modulus has been measured (0.9 – 100 MPa). This is because there is a very wide range of materials to be tested, and there is no standard test or technique to quantify the mechanical properties of bone graft material. This is necessary to help understand the variables to allow a more accurate prediction of the results of impaction bone grafting and impaction technique to contribute to achieving better implant stability.

This is immensely valuable for studying and developing revision implants and procedures to help treat these conditions. They improve our understanding of the behaviour of bones, the relationship between load transfer & bone morphology and how to optimise tissue interaction with orthopaedic implants. (Poelert et al., 2013) However, there are certain limitations in the current research.

a) Experimental testing can be used to observe and capture the gross material properties. By building a numerical model that can capture the response of the experimental tests, which be used to better understand the properties of these bone grafts and their behaviour by complimenting the existing results and creating a new platform to explore these results in a much more versatile manner.
b) The finite element models created to date have either been based on reference models of tibia and femur created using constitutive modelling (Totoribe et al., 2018). The studies conducted so far only study bone grafts after impaction, their penetration properties, micromotion between the bone grafts and the stem interface. However, the literature only

simulates the impaction endpoint, and none focus on modelling the bone grafts for impaction or the impaction process. The only paper that studied the computational response of impaction bone grafting was done by Phillips et al. (2006). They only studied the bone grafts after the impaction process using a constitutive model that approximates the observed physical behaviour of a material under specific conditions. The use of a constitutive model approach in the numerical model means any change in parameters of the model or the structure has to be revalidated through experimental tests to derive a new finite element model. There is no robust technique to test, retest and explore mechanical properties of bone grafts with minimal changes. An effective technique to model the impaction using numerical modelling has not yet been attempted.

The main reason for this is that the mechanical properties and the behaviour of bone grafts are not properly understood, mainly due to a lack of experimental data. An important issue for FE models is the material properties such as elasticity (Young's modulus), Poisson ratio, shear properties, density, and bone mineral fraction differ. The second issue is the modelling of bone grafts are complex. A previous few experimental studies have been conducted by Xu et al. (2011) and Phillips et al. (2006a). They tried to estimate the instantaneous elastic modulus of the bone graft and calculate the apparent modulus of bone grafts. However, none of them has been used to replicate the same experiment on a computational model to validate the values calculated experimentally. It is a challenge to model bone grafts as the current modelling scenarios are crude and regular constitutive laws to model bone grafts are not well suited to represent the behaviour of bone grafts during impaction scenarios.

The objective of this PhD is to find a computational model which is not based on constitutive modelling, to try and explicitly account for the geometry and shape of the bone graft particles rather than a construct. The aim is to verify the computational model and tune the model to match the experimental result and then explore the type 3 variable, impaction technique and explore the

impaction force or stress and the number of impactions to try improve the impaction bone grafting process. To achieve this objective, the first step is to perform an experimental test based on existing literature to capture the material properties of the bone graft through impaction bone grafting. The results from the experimental study will be used as a base to create the computational model.

Chapter 3 :

Experimental testing

3.1. Introduction

The findings of the literature survey (Chapter 2) suggest that the mechanical characteristics of bone grafts vary depending on the size, shape, bone structure and density. Various studies have chosen to adopt different test methods, and throughout the literature, there has not been one standardised technique used to examine the behaviour of bone grafts. This study aimed to examine the core mechanical behaviour of bone grafts. Obtaining sufficient volumes of human material to characterise bone graft is difficult. Throughout literature, ovine and bovine bone grafts have been used to characterise bone grafts as they are readily available. In this study, bovine, ovine, and human bone grafts were used to assess if they capture the main features of the mechanical behaviour of bone grafts. In addition, it would provide data to verify and validate future computational models. Due to the reduced availability of human bone grafts, they were limited to a single test, whilst bovine and ovine bone grafts were subjected to repetitive tests. A confined compaction experimental setup like Phillips et al (2006a) was designed and used to test bone grafts created from bovine, ovine and human bone specimens separately. The primary objective of these experiments was to acquire precise material properties of bone grafts and to use this data to create a numerical model replicating the experiment and try to match the experimental data.

3.2. Materials and methods

3.2.1. Bone grafts

100 Frozen ovine knee and distal femoral joints from 6–8-month-old sheep; 15 bovine knee joints from 18month old cattle were sourced from butchers; and 12 human femoral heads sourced as cadaveric samples from 75-80-year-old women obtained from a dedicated body donation program was used. Ethics approval was not obtained as these specimens were previously used in testing fractures from previous experimental drop tower tests, which were granted ethics approval by the Social and behavioural Research Ethics Committee (SBREC) of flinders university (project # 6380). They were stored in freezers at an average temperature of -20^{0} C. Throughout literature the average size of bone graft used is in the range of 2.7mm – 5.2 mm emphasising the use of larger size bone grafts to provide better stability of the implant (Ullmark, 2000). As a result, 5mm size was chosen as the optimum size of the bone grafts as they are a representative of bone impaction graft material used in surgery. In most cases, bone mills are used to create bone graft material which often results in irregular shapes that increase the experiments variability. As the experimental study is used to acquire data to create a numerical model, to reduce variability between the tests the bone grafts shape was chosen to be cubes of 5mm sides like those used by Henier et al. (2005).

3.2.1.1. Preparation

The frozen knee and distal femoral joints were cut with a band saw along a quasi-transverse plane through the femoral epicondyles using a band saw (Figure *3.1*(a) & Figure *3.1*(b)).

Figure 3.1*: A representative sample of (a) frozen ovine distal femoral condyle before cutting (b) distal femoral condyle with the top soft tissue and cortical bone cut off*

The two halves were further cut through the transverse plane from the distal end of the femoral condyle and the frontal end of the tibial plateau to expose the cancellous bone at either end of the condyles (Figure 3.2 (a) & Figure 3.2 (b)). The same process was performed on the coronal and sagittal planes. The bone cortex, soft tissues, and cartilages were removed (Figure 3.3).

Figure 3.2 (a) Top view of distal femoral condyle showing cancellous bone, cartilage and ligaments (b) Side view of the sides cut from the distal femoral condyle

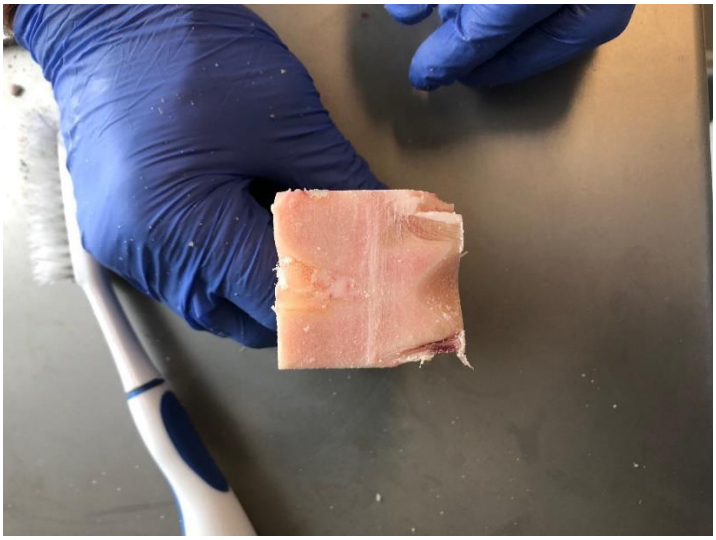

Figure 3.3 Final squared view of the distal femoral condyle before being sliced into slices

A backstop mechanism was fitted on the band saw table and aligned such that the outer end of the blade measured exactly 5mm from the backstop. The trimmed-down condyles were then placed on the band saw table with either the sagittal or coronal side facing the table (Figure 3.4).

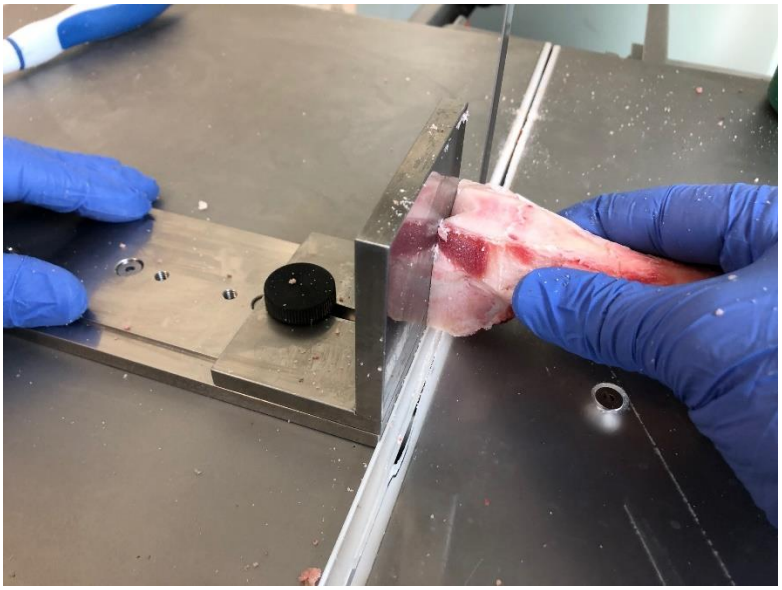

Figure 3.4 Distal femoral condyle pushed on the backstop to help in a clean-cut over the band saw

The condyles were sliced through the transverse place to yield 5 mm slices (Figure 3.5 (a) & Figure 3.5 (b)). The thickness of the slices was measured using a Vernier calliper to ensure a constant 5mm thickness (Figure 3.6).

Figure 3.5 (a) Sectional view of the sliced distal femoral condyle (b) Sliced distal femoral condyle

Figure 3.6 Sliced distal femoral condyle being measured for quality control

These slices were then trimmed off any remaining tendons and ligaments to give a clean cancellous bone slice (Figure 3.7 (a)), which were then cut into 5 mm fingers (Figure 3.7 (b)) and finally into 5mm cubes (Figure 3.8).

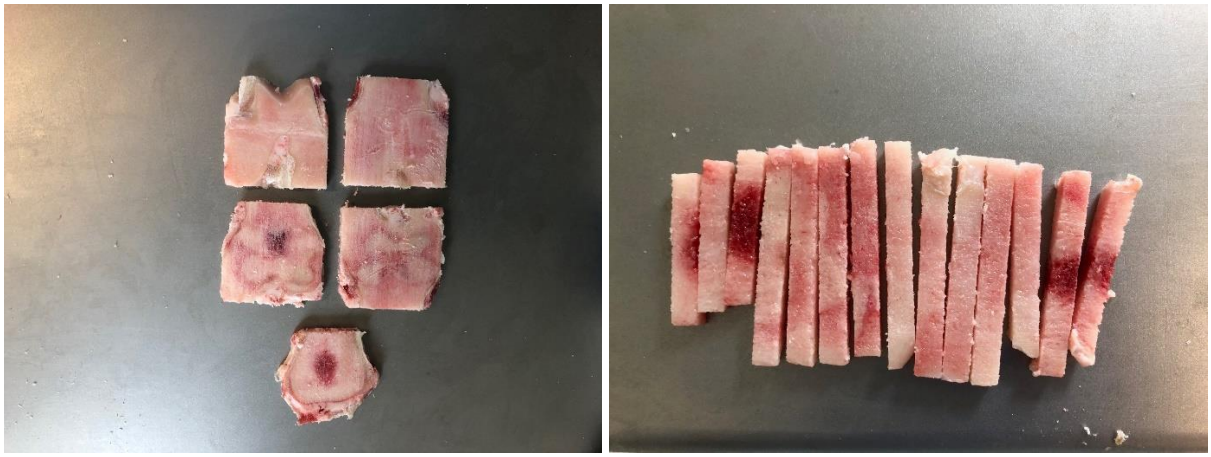

Figure 3.7 (a) Sliced distal femoral condyle before cutting into fingers (b) Distal femoral condyles after cutting into fingers

A random sample of 100 cubes was checked using a digital Vernier to ensure a constant size of the particles. The random sample of cubes had a mean edge size of 4.95mm with a standard deviation value of 0.04mm and a variance of 0.01mm.

Figure 3.8 Bone grafts cut into 5 mm cubes from the fingers

3.2.1.2. Cleaning and storage

In this study, the procedure used to clean the bone graft was adopted from the clinical practices used by orthopaedic surgeons from The Royal Adelaide Hospital, Adelaide, Australia. The bone graft cubes were agitated in a container with 2% saline heated to 48^0 C to remove blood tissues and fat. The process was repeated 5 to 10 times till the saline ran clear of any fat or blood tissues. The bone grafts produced from each specimen were then dried using paper towels, segregated in containers based on species. Each container with one specific species of bone grafts was mixed to ensure consistency between tests, then labelled with the species name date of preparation and quantity, stored at -20^0 C until required for testing. The bone grafts were thawed to room temperature before testing.

3.3. Experimental Device

As outlined in Table 2.3 Reported elastic parameters in terms of stiffness with the type of testing and the materials tested, several methods have been used to assess the mechanical behaviour of bone grafts. In this study, the experimental methodology developed by Phillips et al. (2006a) was found to be the best suited for both the experimental model and the computational simulation; hence, a custom apparatus with dimensions similar to Phillips's experiment (Phillips et al., 2006a) was created using stainless steel. A schematic diagram of the testing apparatus can be seen in Figure 3.9 Schematic diagram of the experimental test apparatus with dimensions – side view. The apparatus consists of a test chamber 100mm high. A set of 16, 2mm holes were drilled in the walls to help fluid exudation. The inner diameter of the tube was 50mm and a wall thickness of 10mm, which was machined from a single block of stainless steel. A solid cylindrical load applicator with a diameter of 49mm could telescope into the tube freely when driven by the actuator of the testing machine. A base plate was used to fix the test chamber to the rigid base of the testing equipment. Impaction was emulated using a Test Resources 800 series fatigue testing machine connected to a

load cell with a maximum calibrated loading rate of 10 kN. It had an actuator displacement resolution of 0.1 microns, connected to a data-logging computer to capture the displacement and the forces applied during the test.

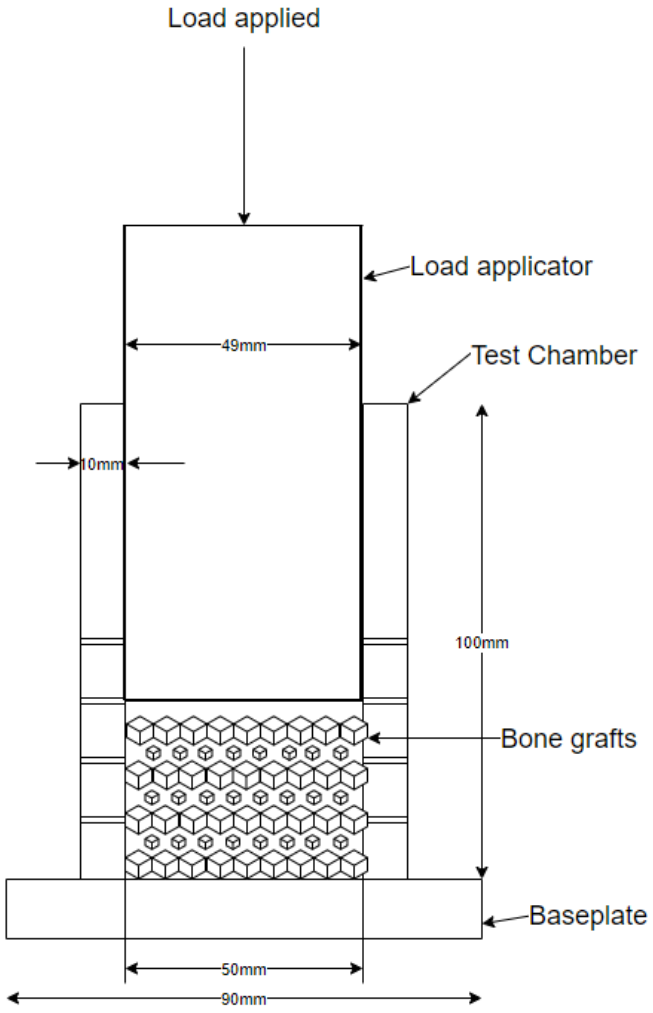

Figure 3.9 Schematic diagram of the experimental test apparatus with dimensions – side view

	Bovine Bone grafts	Ovine bone grafts	Human bone grafts
Source of specimen	36-month-old cows sourced from butchers	6 to 8-month-old sheep sourced from butchers	Femoral heads from donated cadavers, fractured from previous testing (ages 75 – 80).
Number of femoral and tibial heads used	15	100	13
Number of experiments	4	5	1

Table 3.1 Source, history and quantity of specimen used for experimental testing

3.3.1. Test Procedure

The bone grafts were poured into the test chamber as three layers of approximately equal height to simulate an irregular pattern. Each layer was preconditioned by placing the loaded applicator weighing 1.70 kg for 5 seconds. Following the final layer of preconditioning, the remaining cubes were packed to the brim of the test chamber till the bone grafts were level with the top of the chamber. Each test was conducted under similar conditions with loading profiles, as seen in Figure 3.10. A combination of force-controlled and displacement control was used for the test. Loading and unloading cycles were carried out under force control. The apparatus then switched to displacement control during the stress relaxation phase. Each test sample was subjected to a set of 60 loading and unloading cycles at 80 N of force at a speed of 0.1662mm/s, which was found to be on a similar scale as the literature (Cornu et al., 2003b; Fosse et al., 2004; Xu et al., 2011). A total of 6 stress levels were chosen, ranging from 0.5 MPa (942.85N) to 3.0 MPa (5671.1N) with ten loading and unloading cycles per stress level. The range of stress chosen for these tests was based on previous experimental testing conducted by Phillips et al. (2006a), and the values were similar to the stresses found in acetabulum during normal physiological activities (Dalstra & Huiskes, 1995). The bone graft cubes were allowed to relax for 900 seconds after the 10^{th} loading cycle for all six stress levels.

This Image has been removed due to copyright restriction. Available online from "(Phillips et al., 2006)"

Figure 3.10 Loading profile of experimental test with stress – time variations adapted from Phillips et al (Phillips et al., 2006)

3.3.2. Evaluation of instantaneous elastic modulus

The area of the applicator in contact with the bone graft particles and the corresponding applied force data were used to calculate the apparent stress acting on the bone graft particles using equation (3.1)

$$\sigma_a = \frac{F}{A} \tag{3.1}$$

Where, σ_a is the apparent stress, *F is the* force and *A is* the area of the impactor

The initial position of the loaded applicator was determined to be the point where the actuator measures a force of 10N upon contact with the bone grafts to account for the weight of the applicator and to reduce errors from the actuator. The displacement of the loaded applicator from this initial position was then used to calculate the apparent strain using equation (3.2)

$$\varepsilon_a = \frac{dl}{l_0} \tag{3.2}$$

Where, ε_a apparent strain, dl change in height, and l_0 initial height

The instantaneous elastic modulus was evaluated for all 60 loading and unloading cycles using equation (3.3)

$$Eic = \frac{(\sigma_a^L - \sigma_a^{UL})}{(\varepsilon_a^L - \varepsilon_a^{UL})} \tag{3.3}$$

Where the axial stress in the positive end of the loading phase is, σ_a^L and the axial stress at the end of the unloading phase σ_a^{UL}. The axial strain at the same positive end of the loading phase isε_a^L and the axial strain at the end of the unloading phase, ε_a^{UL}.

3.4. Results

It can be observed from Figure 3.11 that upon loading for the first time, the bone graft particles get compressed, and strain gets accumulated. A cyclic hysteresis is seen from the results on all three bone grafts. The largest jump in hysteresis was observed from human bone grafts at the end of the first loading cycle and stress level of 0.5 MPa, accumulating a strain of 0.42%, whilst bovine records 0.05% and ovine 0.03%. Beyond the first loading cycle on repetitive loading, the cyclic hysteresis continues; however, it decreases in magnitude at every stress level. At the end of the first stress level, 0.5 MPa, there is more strain accumulation in the ten loading cycles than any other stress level. The mean accumulated strain was 0.049% for ovine, 0.08% for bovine and 0.49% for the human specimen. As the applied stress level increases, the amount of permanent strain accumulated decreases. At the final stress level of 3.0 MPa, the mean accumulated strain was 0.21% in ovine, 0.25% in bovine and 0.7% in the human specimen.

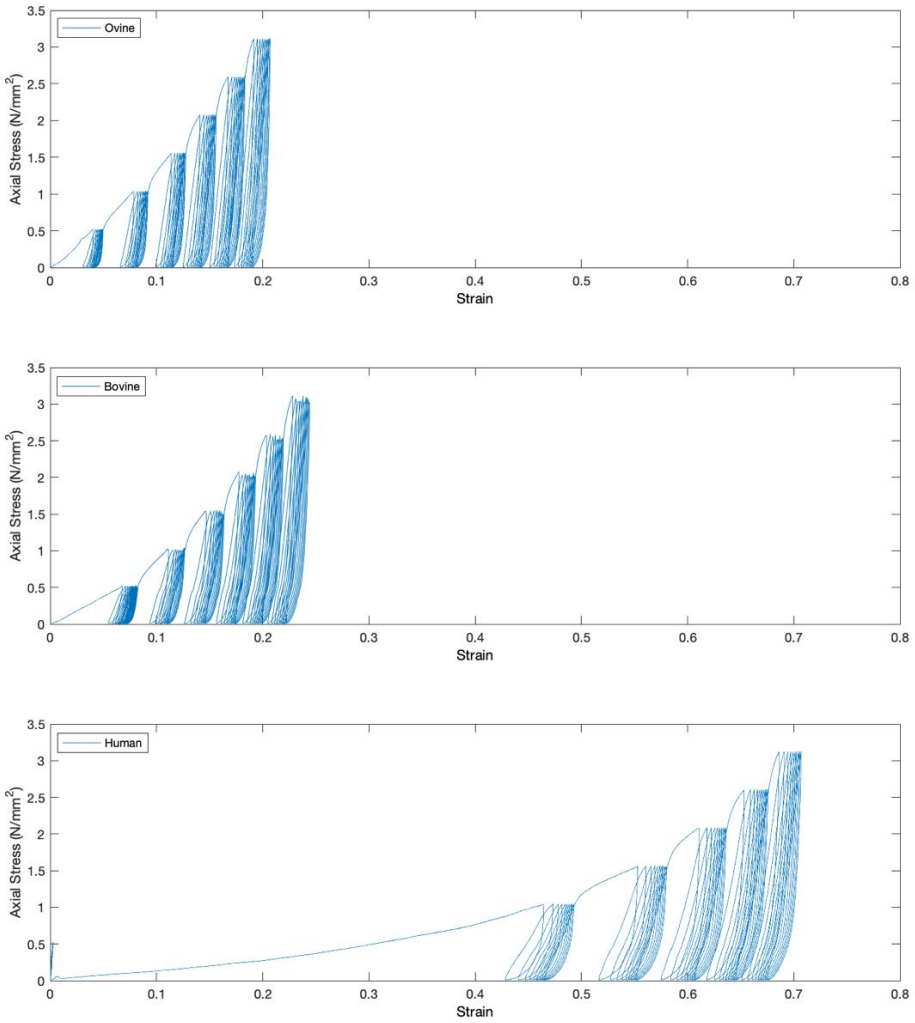

Figure 3.11 A representative graph of Stress vs strain relationship during loading and unloading for a total of 60 load cycles at 10 load cycles per stress level from 0.5MPa to 3.0MPa.

Test Number	Accumulated strain - Ovine bone grafts					
	0.5 MPa	**1.0 MPa**	**1.5 MPa**	**2.0 MPa**	**2.5 MPa**	**3.0 MPa**
1	0.04	0.09	0.12	0.155	0.18	0.20
2	0.08	0.12	0.16	0.19	0.22	0.25
3	0.05	0.10	0.14	0.17	0.20	0.23
4	0.07	0.12	0.17	0.20	0.24	0.27
5	0.07	0.12	0.16	0.19	0.22	0.25

(a)

Test Number	Accumulated strain - Bovine bone grafts					
	0.5 MPa	**1.0 MPa**	**1.5 MPa**	**2.0 MPa**	**2.5 MPa**	**3.0 MPa**
1	0.07	0.12	0.16	0.19	0.21	0.24
2	0.09	0.14	0.17	0.20	0.23	0.25
3	0.03	0.08	0.12	0.16	0.20	0.23
4	0.11	0.17	0.21	0.25	0.28	0.31

(b)

Accumulated strain - Human bone grafts					
0.5 MPa	**1.0 MPa**	**1.5 MPa**	**2.0 MPa**	**2.5 MPa**	**3.0 MPa**
0.01	0.49	0.58	0.63	0.67	0.70

(c)

Table 3.2 Accumulated strain values for all experimental tests using (a) Ovine bone grafts, (b) Bovine bone graft, (c) Human bone grafts, at the end of each stress level from 0.5 MPa to 3.0 MPa.

Table 3.2 (a) shows the accumulated strain for five experimental tests using ovine bone grafts at the end of the 10^{th} loading cycle. At the end of the first stress level of 0.5MPa, the average accumulated strain across all five tests range was between 0.04 to 0.07, which is a mean of 0.06 at the end of 10 loading cycles. The accumulated strain increases at each stress level as the stress is increased, with the final stress level of 3.0 MPa averaging at 0.24. Table 3.2 (b) shows the accumulated strain from bovine bone grafts, which follow the same general trend as the ovine bone grafts but accumulates slightly higher accumulated strain of 0.08 at the end of the first stress level 0.5 MPa. This increases as the stress level are increased and accumulate a final mean strain of 0.26 at the end of the final stress level of 3.0 MPa. Table 3.2 (c) shows the strain results from human bone grafts where the most accumulation of strain happens in the second stress level of

1.0 MPa, accumulating a permanent strain of 0.49 which accounts for more than 60% of the total strain accumulated overall stress levels during the test.

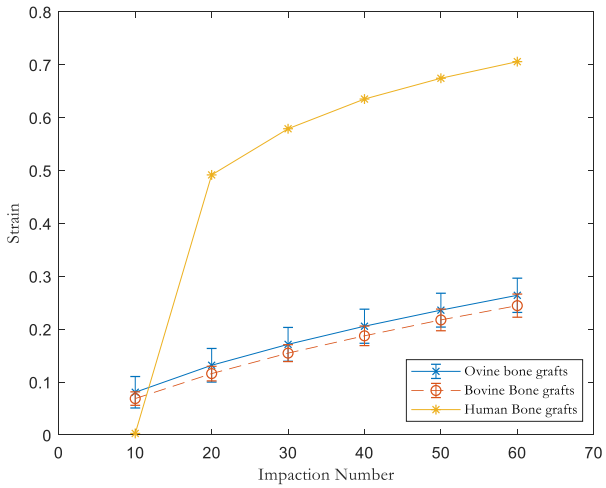

Figure 3.12 Change in strain during impaction for all tests between ovine and bovine bone grafts to show variations in strain across the experiments

Figure 3.12 shows that the increase in strain for both bovine and ovine bone grafts are at a similar rate throughout the loading and unloading cycles. Ovine bone grafts accumulated a strain of 0.06 to 0.024%, whereas bovine bone grafts measure between 0.08 to 0.26%. It can be deduced from the graft that the differences of strain between all 5 tests on ovine bone grafts have a variance of 0.01 at 0.5 MPa stress level increasing to a maximum of 0.021 at 3.0 MPa stress level. Bovine bone grafts on the other hand have a variance of 0.029 at 0.5 MPa stress level which increases to a maximum variance of 0.032 at 3.0 MPa stress level.

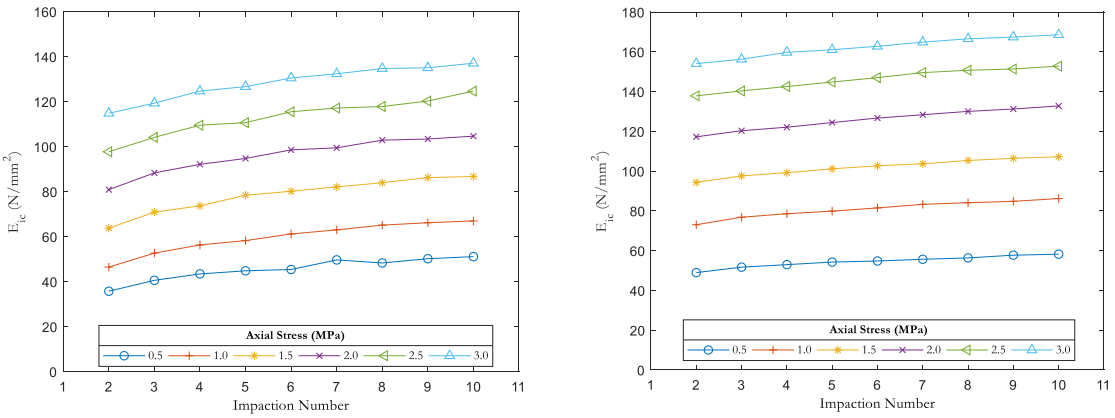

Figure 3.13 Mean instantaneous confined elastic modulus (E_{ic}) for 4 experiments using bovine (left -(a)) and 5 experiments using ovine (right – (b)) bone grafts.

The mean instantaneous confine elastic modulus (E_{ic}) for the bovine bone grafts (Figure 3.13 (a)) start at 28 MPa, increasing to 47 MPa, which is a 15% increase by the end of the loading cycle at 0.5 MPa stress level. At the end of the second (1.0 MPa) and third stress level (1.5 MPa), the average increase in E_{ic} is 22 MPa or 22%. E_{ic} Increases 27% by the end of the fourth and fifth stress level of 2.0 MPa and 2.5 MPa, further increasing by 23% at the final stress levels of 3.0 MPa to a final mean value of 137 MPa.

Similarly, looking at the mean results from ovine bone grafts in Figure 3.13 (b) the elastic modulus accumulated is 48 MPa increasing to 64 MPa, which is a 9% increase by the end of the loading cycle at the first stress level. At the end of the second (1.0 MPa) and third stress level (1.5 MPa), the average increase in E_{ic} is 19 MPa or 10%. E_{ic} Increases 12% by the end of the fourth (2.0 MPa) stress level and 9% by the end of the fifth stress level of 2.5 MPa. The final stress levels of 3.0 MPa E_{ic} increase by 9.4% with a mean final, E_{ic} value of 177 MPa.

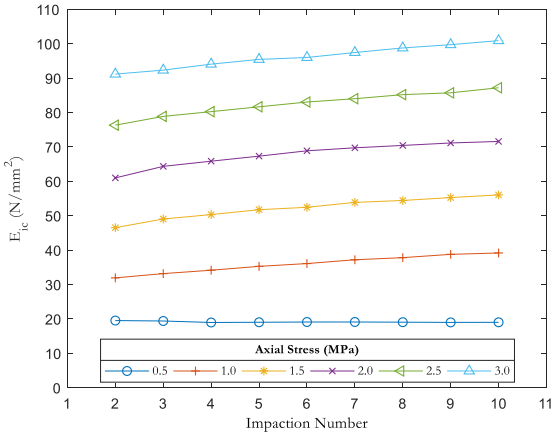

Figure 3.14 Instantaneous confined elastic modulus (E_{ic}) for the experiment using 5mm human bone grafts.

The instantaneous confined elastic modulus (E_{ic}) for the human bone graft, as seen from Figure 3.14, start at 19 MPa after the first loading cycle increasing to 19.7 MPa, which is around an average of 0.74% increase by the end of the 10th loading cycle at first (0.5 MPa) stress level. At the end of the second (1.0 MPa) the elastic modulus increases 10.37MPa, a 10.19% increase from the last stress level. In the third stress level (1.5 MPa) E_{ic} increases 12.97 MPa, which is 12.85% within the stress level. E_{ic} Increases 13.52% by the end of the fourth (2.0 MPa) stress level and 13.3% by the end of the fifth stress level of 2.5 MPa. The final stress levels of 3.0 MPa E_{ic} increase 11.37%, with a final E_{ic} value of 100.8 MPa.

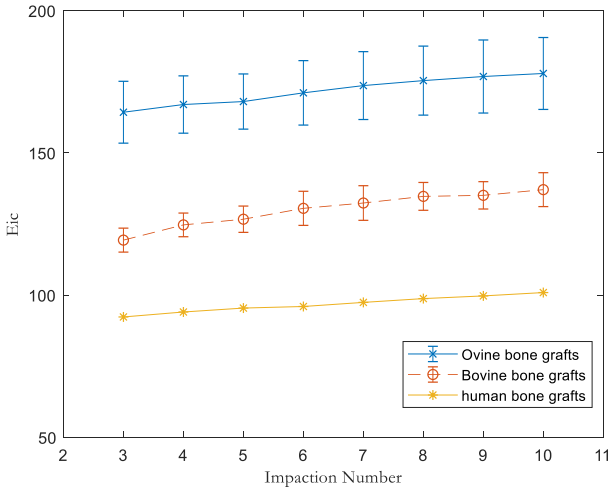

Figure 3.15 Increase in E_{ic} at the last stress level of 3.0 MPa at each loading cycle (3 – 10) for all tests between ovine, bovine and human bone grafts to show variation in, E_{ic} across the experiments.

Bovine bone grafts (Figure 3.15) measure a mean E_{ic} of 47 MPa to 137 MPa, whereas ovine bone grafts measure a mean between 48 MPa to 177 MPa. The standard deviation of E_{ic} across all 4 tests on bovine bone grafts was calculated to be 4.04 MPa at the first stress level (0.5MPa), 2.46 MPa at the second stress level (1.0 MPa), 3.5 MPa at third, 2.2 MPa at the fourth, 6.5 MPa and 6.7 MPa at final two stress levels (2.5 MPa) and (3.0 MPa) stress levels. Ovine bone grafts, on the other hand, have a deviation of E_{ic} across all 5 tests on bovine bone grafts was 9.2 MPa at first stress level (0.5 MPa), 10.5 MPa at the second stress level (1.0 MPa), 13.5 MPa at third, 12.8 MPa at the fourth, 11.1 MPa and 14.1 MPa at final two stress levels (2.5 MPa) and (3.0 MPa) stress levels. Human bone grafts, on the other hand, measure an E_{ic} value between 19 MPa to 100 MPa.

3.5. Discussion

Bone grafts from different species were harvested, morselized to be used in these tests. This experimental test aims to understand the variability of bovine and ovine bone grafts, assess if they capture the main features of the mechanical behaviour of bone grafts, and provide data to verify and validate future computational models. The results from the tests show that the overall mechanical behaviour of all three types of bone grafts are similar. All three species show an accumulation of strain, with the first stress level accounting for the highest magnitude of strain accumulation. The hysteresis starts to decrease as the stress level and the impaction cycles increase. At the same time, the instantaneous modulus increases as the applied stress increases. Ovine bone grafts recorded the highest elastic modulus, followed by bovine bone grafts and human bone grafts with the lowest modulus. However, the strain data is on the inverse scale, with human bone grafts accumulating the highest strain followed by ovine and bovine bone grafts accumulating similar strains but lower than that of human bone grafts.

The stress and strain results reported in these tests are consistent with the values obtained by Phillips et al. (2006a) whose results reported an elastic range of 11- 120 MPa for the bovine specimen. Comparatively, the experimental test reported an elastic modulus of 39 -137 MPa, which is higher than Phillips et al's study (14 – 110MPa). The strain values from the experiment with bovine specimen only accumulated a low 0.31 when compared to 0.53 reported in Phillips et al.'s (2006a) study. This higher elastic modulus and lower accumulated strain could be caused by the differences in the experiment. Such as, the use of 5mm bone graft cubes as opposed to bone grafts created using bone mills and the removal of blood and fat from the bone grafts before being subjected to the impaction process, which was not performed in Phillips et al.'s (2006) study. Both studies show a decrease in the rate of development of irrecoverable plastic strain as the number of impactions increases at each stress. The results in both studies indicate that the elastic behaviour

of the bone grafts and its instantaneous elastic modulus is dependent on the maximum stress and the number of load cycles experiences at a given stress level.

Comparing the results from other specimens, namely ovine and human bones, show that human bone grafts are less stiff than ovine or bovine, accumulating a higher strain than others. The results from the human bone grafts at the first loading cycle did not yield any strain value. Given that the bones were previously fractured could have affected the integrity of the bone grafts. As a result, the bones did not accumulate any strain at the first stress level. Once the applied stress increased to the second stress level of 1.0 MPa the bone grafts broke down and accumulated strain. Ovine bone grafts were the stiffest amongst the three species. The results from all three species indicate that ten compaction episodes are required to achieve 90% of its maximum stiffness at lower stress levels but, looking at higher stress levels 2.5 MPa and 3.0 MPa. However, there is an increase in accumulated modulus at every compaction episode although the accumulation rate decreases after the first three impactions. Various studies have reported different impaction numbers in examining the effect. The reported number of impactions so far are 10 (Voor et al., 2000a; Putzer et al., 2017), 20 (Albert et al., 2008b), 36 (Giesen et al., 1999), 60 (Phillips et al., 2006; McNamara et al., 2006), 150 (Cornu et al., 2003b) and (Ayers et al., 2014) used up to 150 impactions. Observing the current history of impaction bone grafting, the stress levels of the impactions have been increased sequentially and does not provide information on how much the prior loading history influence the impaction at higher stress levels. In other words, the study's limitations were that it is not clear what happens if the bone grafts are not sequentially impacted. Does impacting the bone grafts at higher stress levels reduce the number of impactions required to achieve the predicted 90% of its maximum stiffness? Also, what happens when the bone grafts are impacted at stresses beyond 3.0 MPa. Amongst current literature, only McNamara et al. (2014) explored impact stresses of magnitudes higher than 3.0 MPa (Ayers et al., 2014; Phillips et al., 2006). Regardless of the type of impaction techniques used, all studies have followed an increasing level of stress. What would be the outcome when they are impacted at higher magnitude forces at the start of the impaction

process? Additionally, the bone grafts used in this experiment were cube to reduce the variability. Changing the shape of the grafts can affect the results, as in a clinical scenario, cubes of bone grafts are generally not used.

The reported range of instantaneous elastic modulus varies amongst impaction grafting studies. The variability between research can be attributed to factors such as size, impaction kinetics, and techniques used in testing. For instance, McNamara et al. (2014) increased the confined compressive modulus of their impaction specimens by using a combination of human femoral heads plus hydroxyapatite and increasing the impaction stress to 6.8 MPa instead of 3.0 MPa (Phillips et al., 2006) and was able to record E_{ic} values in the range of 300 – 450 MPa. Verdonschot et al (Verdonschot et al., 2001) reported a modulus of 85 MPa using human femoral heads, which were compacted manually and then dynamically compressed 98 times at stresses up to 2.65 MPa. (Fosse et al., 2006) experimented with both human and bovine femoral heads but only subjected the bones to 1.4 MPa of stress and ten impactions and reported the E_{ic} of human bone grafts in the range of 24.2 – 50.9 MPa and bovine bone grafts in the range of 37 – 212 MPa. The E_{ic} values derived from this experiment were 25 – 140 MPa for bovine bone grafts, 60 to 200 MPa for ovine bone grafts. The values are consistent with the range of values reported in previous studies for apparent modulus of bone grafts from the bovine and ovine specimen (Voor et al., 2000a; Giesen et al., 1999; Fosse et al., 2006; Phillips et al., 2006). Looking at the elastic modulus in Figure 3.14 shows that there is little to no increase in the instantaneous elastic modulus at the first stress level. The elastic modulus recorded from the human bone grafts ranges between 19 – 100 MPa consistent with current research data (Verdonschot et al., 2001; Heiner et al., 2005; Cornu et al., 2009; McNamara et al., 2006; Putzer et al., 2017).

In conclusion, the results from ovine bovine and human bone grafts showed accumulation of permanent strain and an increase in instantaneous elastic modulus as impaction pressure increases which is consistent with the behaviour seen in other experimental studies. The experiment with human bone grafts required 13 femoral heads to prepare the necessary bone grafts. Replicating the experiment using human bone grafts was technically difficult due to the challenges of sourcing femoral heads and the ethics behind obtaining them. However, to do this using experimental testing methodology needs extensive planning and preparation time. The primary objective of this study was to acquire structural/apparent material properties of bone grafts to be used to create a numerical model replicating the experiment and try to match the experimental data. The data obtained from the experiment was sufficient and will be used as a validation experiment for a numerical model created using finite element analysis. The numerical model will serve as a standard to capture the changes from these variables and techniques.

Chapter 4 :

Exploration of computational modelling techniques

4.1. Introduction

The incorporation of the bone graft and long term fixation of a revision implant is based on the initial stability provided by the graft at the time of surgery (Welten et al., 2000; Glyn-Jones et al., 2004). To routinely achieve adequate stability, the mechanical behaviour of the bone graft has to be understood. Though numerous experimental and computational studies have focused on the mechanical characteristics of morselized bone grafts (Brewster et al., 1999; Giesen et al., 1999; Voor et al., 2000b, 2004; Fosse et al., 2006; Phillips et al., 2006; Barink et al., 2007; Albert et al., 2008b; Bavadekar et al., 2001; Cornu et al., 2003b; Schreurs et al., 2001; Brodt et al., 1998), the majority of these studies have been based on bone grafting in hip replacements in proximal femurs. Current numerical modelling studies use either a material constitutive modelling approach (Phillips et al., 2006b; Albert et al., 2009) or use a representative elastic modulus approach (Hanspeter et al., 2006; Phillips et al., 2007; Tsumura et al., 2005; Totoribe et al., 2018; Lunde et al., 2008) and model the grafts as a continuum. These continuum models rely completely on the experimental data to feed the material behaviour into the model. Changing any characteristics of the graft like size and shape distribution of particles requires new experimental data to feed the material model. Explicitly modelling the structure of the graft has the potential to forego this process. Hence the objective of the study was to find a suitable approach to model bone grafts by replicating the experimental study. To model bone grafts as a non-continuum model, computational modelling techniques, such as discrete element analysis and finite element analysis, were studied to find a method suitable to model bone graft particles. Once the bone grafts were modelled to look similar

to the experimental bone graft in size and shape, their mechanical behaviour was analysed for resultant stiffness by conducting a confined compression test experiment and comparing them with the experimental results from Chapter 3.

4.2. Computational Apparatus Setup

The numerical approach used to model bone grafts is based on the experimental setup from Chapter 3 which is an adaptation of Phillips et al. (2006) experimental setup. The custom apparatus from the experimental model consists of a test chamber 100mm high, 50mm in diameter and a wall thickness of 10mm, a load applicator with a diameter of 49mm and a base plate to fix the test chamber to a rigid base machined from blocks of stainless steel. A diagram of the device can be seen from Figure *4.1*. Bone grafts used in the experimental model consisted of 5mm cubes created from ovine bone and their material properties with a Youngs modulus of 1.46GPa, and poisons ratio of 0.2 were used to simulate the ovine material in the numerical model. The experimental test to be replicated was a uniaxial cycling compressive loading test of 60 load cycles with 10 load cycles per stress level ranging from 0.5 MPa to 3.0 MPa with a stress relaxation period between each stress level. The mechanical response to be replicated from these tests includes strain in the range of 0.2% – 0.27% and stiffness/instantaneous modulus in the range of 45 – 170 MPa.

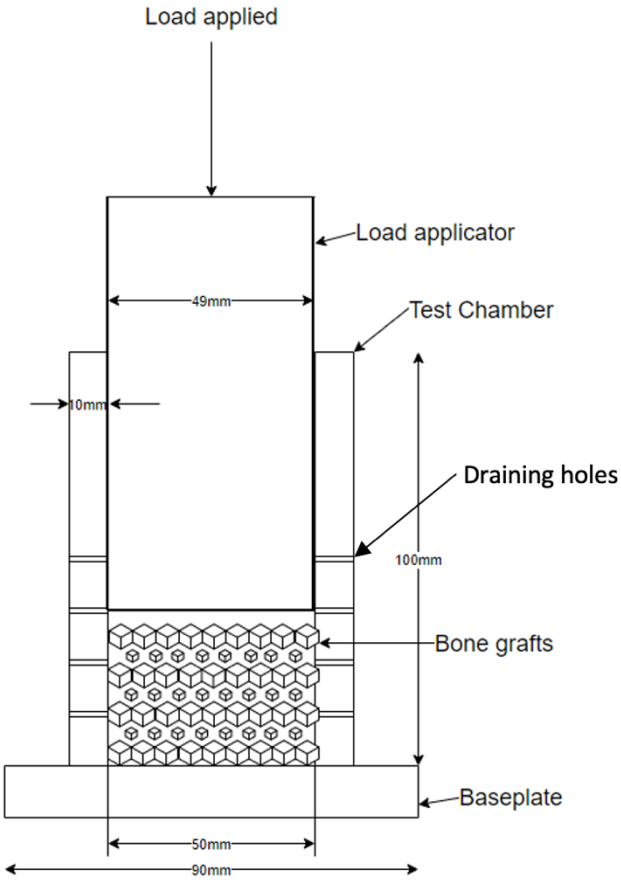

Figure 4.1: Confined Compression experiment adapted from Phillips et al. (Phillips et al., 2006)

4.2.1. Numerical model creation process

The numerical model apparatus consists of a cylindrical test chamber. The young's modulus of the chamber was set to 210 GPa and a Poisson's ratio of 0.3. The cylinder was given a rigid body constraint and was encastered, so it does not move in any direction. The particles created were allowed to fill the chamber under the gravity load applied to the particles. The surface interaction between the contacts was defined as per each method used in the model. An impactor was introduced into the model positioned behind the bone grafts. The impactor was given a rigid body

constraint and displacement was restricted to move only in the direction parallel to the inner walls of the cylinder. The load was applied from the distal end of the impactor.

4.2.2. Modelling of bone graft for impaction bone grafting

In this study, various modelling methods were explored, namely DEM and Abaqus explicit.

4.2.2.1. Discrete element method (DEM)

The discrete element method is l used to model and understand macroscopic particulate material behaviour (García-Rojo et al., 2005). Discrete element modelling has been extensively used in civil engineering applications to model soils concerning the foundation of structures and buildings. For this reason, the discrete element model was explored to model and simulate bone grafts. Modelling of bone grafts using DEM was tested on two different software's, namely Abaqus and Rocky.

Abaqus DEM:

The DEM model was created using Abaqus 2017, where the Discrete Element method was embedded in the software. Abaqus DEM produced bone graft particles that were completely elastic. Abaqus only provides minimal options to try to induce/spoof plasticity into the DEM through contacts or changing other parameters like damping and friction. However, even with the parameters available to tune (contact definitions, friction, Youngs modulus & Poisson ratio), the results from the model did not yield a response comparable to the experimental test. As a result, the second approach on discrete element modelling was attempted using ROCKY DEM.

Rocky DEM:

Rocky DEM uses a mesh-free method and was chosen to overcome the downfalls in Abaqus of having minimal parameters to tune. Rocky DEM allowed for the use of an elasto-plastic model, which allowed for the simulation of plastic energy dissipation on contact without introducing the

overhead of long simulations. However, the results failed to achieve a response close to the experimental results as the viscoplastic behaviour induced through the rocky simulation was insufficient. DEM's in these simulations struggle to capture the mechanical behaviour due to the inability to account for large deformations of the particles.

Numerical analysis in the form of the finite element method was deemed the next practical approach where bulk elastic and non-linear material behaviour of a complex component can be successfully simulated. Using the finite element modelling method, bone grafts can be simulated using either implicit or explicit analysis. However, the problem to be solved using bone grafts involves the use of multibody contact and using an implicit analysis to model such a problem would result in excessive computational costs. Hence using the explicit finite element method was used to try to simulate the behaviour of bone grafts.

4.2.2.2. Abaqus Explicit Finite Element Analysis

The experimental setup was modelled identical to the experimental model as explained in the computational experiment setup. The bone grafts were modelled as a deformable solid cube with 5mm sides meshed as a linear tetrahedral element comprising 93 elements per cube. Young's modulus of ovine bone grafts was estimated to be around 1.4 GPa from literature (Oftadeh et al., 2015; Mittra & Qin, 2003) and the Poisson's ratio to be 0.3 (Brodt et al., 1998). The particles were aligned and stacked as a linear stack, as seen in Figure 4.2.

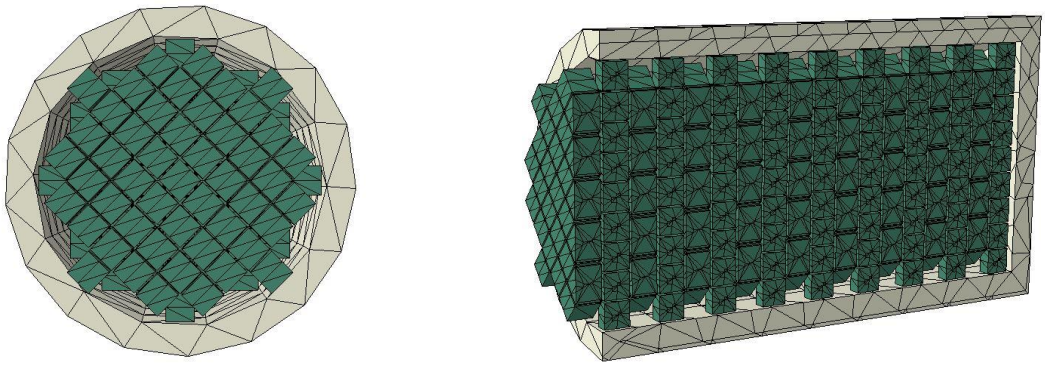

Figure 4.2: Linear pattern arrangement of bone-graft cubes (left) linear pattern arrangement of bone-graft cubes along the length of the cylinder (right)

A gravity load was applied to the bone graft cubes. The surface interaction between the chamber and the cubes were set to general contact hard. The coefficient of friction was set to 0.5 and the density to $1.5\ 7\ g/mm^3$. The stable increment for each element was estimated to be 7.33 e^{-08} seconds in explicit modelling whilst modelling quasi-static analysis like bone grafts where complex nonlinear effects involving intricate contact conditions are in place It was found that a discrete mass matrix improves computational efficiency and accuracy. Mass scaling improved the computational efficiency while retaining the necessary degree of accuracy required for the problem. It was found that forcing a large time step of 7.33 e^{-05} seconds increased the solution time to approximately 96 hours and resulted in huge surges of kinetic energy in the system, crushing the supporting bone and resulting in distortion errors. Introducing mass scaling reduced the solution time from approximately 96 hours to 8 hours per simulation. To determine stable mass scaling time increments, various mass scaling increments were tested (7.33 $e^{-05}\ to$, 9.0 e^{-07} and the lowest stable value was found to be 1.0 e^{-06} seconds.

4.3. Results

Figure 4.3 shows the stress vs strain plot for 30 loading and unloading cycles. It can be observed from the graph that upon loading for the first time, the bone graft particles get compressed, and strain gets accumulated. There is a significant increase in strain at the start of each stress level, with the first stress level of 0.5 MPa inducing a strain of 0.04% on the first loading cycle, upon subsequent loading and unloading cycles and the strain accumulated by the end of the first loading cycle is around 0.05%. This increases to 0.09% at the second stress level (1.0 MPa), 1.125% by the end third stress level (1.5 MPa), 1.15 by the end of the fourth (2.0 MPa), 1.175% and 1.21% respectively by the end of the fifth (2.5 MPa) and sixth (3.0 MPa) stress level.

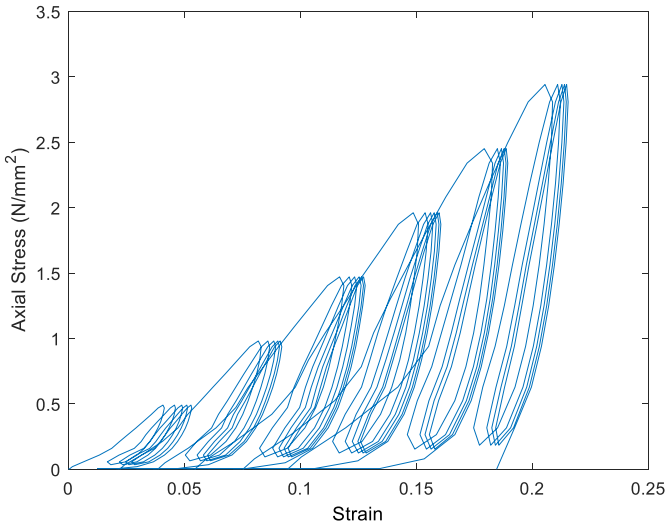

Figure 4.3 Results from Abaqus FEM using bone graft cubes 30 loading cycles and 6 stress levels.

4.4. Further exploration of explicit finite element analysis of bone grafts

The bone graft particles in this model were switched from a stacked arrangement to a random gravity poured and filled pattern, as seen from Figure 4.4. The bone graft particles were spaced

evenly between each other in random patterns and allowed to drop into the chamber when subjected to a gravity load to fill the chamber in a pseudo-random orientation. The rest of the processes were created identical to the experimental tests.

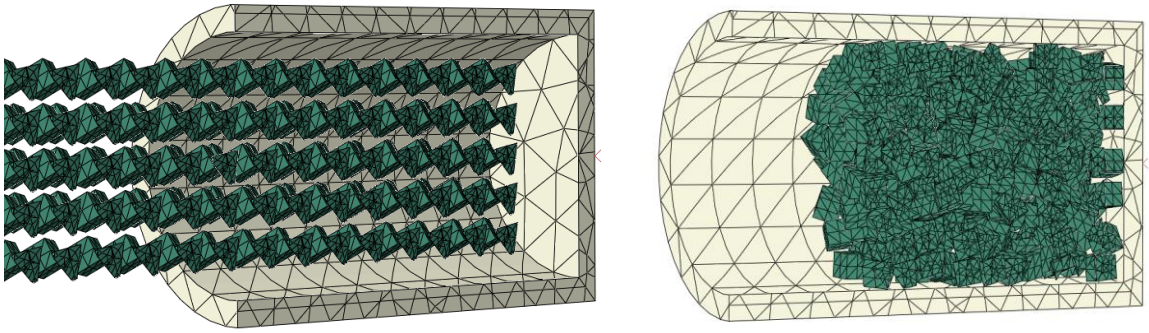

Figure 4.4 Bone graft cubes (a) modelled by increasing the distance between each other and angled so that they form a random pattern when dropped into the chamber. (b) Bone graft cubes after they have been dropped into the chamber forming a random pattern or accumulation

The results from the simulations were processed to evaluate the instantaneous elastic modulus and then compared with the experimental tests from chapter two to validate the computational model. In this model, the full range of impaction was carried out identical to the experimental tests consisting of 60 impaction cycles with 10 cycles per stress level in the range of 0.5 MPa to 3.0 MPa. The particles were assumed to be completely plastic, where the stiffness is assumed to be zero after yield, and the particles were given yield stress of 11 MPa. This was calculated to be 0.8% of Young's modulus (Oftadeh et al., 2015; Mittra & Qin, 2003).

The instantaneous elastic modulus was evaluated for all 60 loading and unloading cycles using the equation (4.1)

$$Eic = \frac{(\sigma_a^L - \sigma_a^{UL})}{(\varepsilon_a^L - \varepsilon_a^{UL})} \qquad 4.1$$

Where the axial stress is in the positive end, the loading phase is σ_a^L and the axial stress at the end of the unloading phase σ_a^{UL}. The axial strain at the same positive end of the loading phase is ε_a^L and the axial strain at the end of the unloading phase ε_a^{UL}.

4.4.1. Results

Comparing the computational model with the experimental results from Figure 4.5 (a) & (b), the computational results look very similar. Upon loading for the first time, the bone graft particles get compressed, and strain gets accumulated. There is a significant increase in strain at the start of each stress level, with the first stress level of 0.5 MPa inducing a strain of 0.04% on the first loading cycle, upon subsequent loading and unloading cycles and the strain accumulated by the end of the first loading cycle is around 0.051%. This increases to 0.1% at the second stress level (1.0 MPa), 0.125% by the end third stress level (1.5 MPa), 0.52 by the end of the fourth (2.0 MPa), 0.18% and 0.23% respectively by the end of the fifth (2.5 MPa) and sixth (3.0 MPa) stress level. The accumulated strain between the two models was on a comparable scale. The first stress level of 0.5 MPa accumulated a strain of 0.061% on the computational model and 0.049% on the experimental test. At stress level of 1.0 MPa the computational model accumulated a strain of 0.1% and the experimental test 0.091%, 0.13% and 0.12% at stress level of 1.5 MPa, 0.17% and 0.15% at 2.0 MPa, 0.19% and 0.18% of strain accumulation at 2.5 MPa and finally 0.22% for the computational model and 0.20% for the experimental model at an axial stress level of 3.0 MPa.

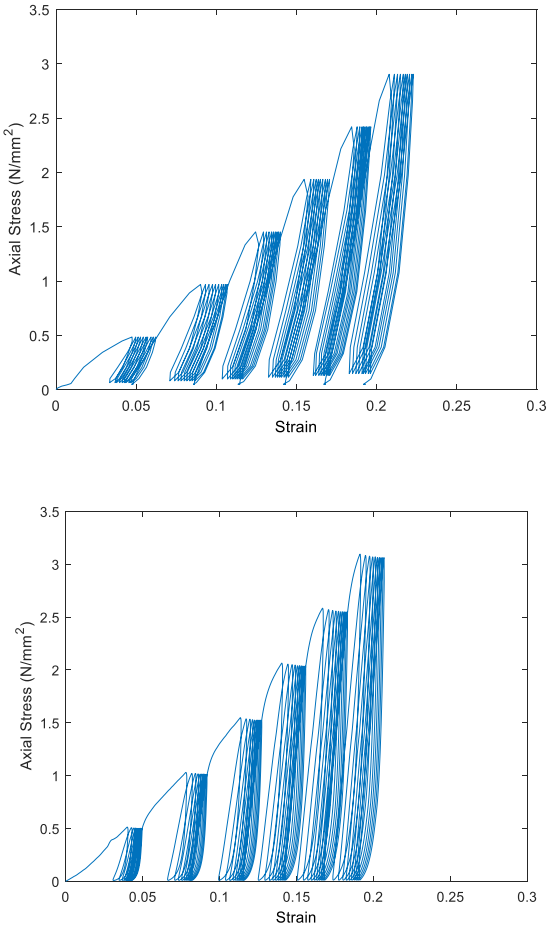

Figure 4.5: Stress vs strain graph with 5mm cube bone graft particles (a) Computational results from randomly stacked bone graft particles with 0.8% yield strain and assumed to be completely plastic. (b) Representative experimental results with 5mm ovine bone graft cubes

The instantaneous confined elastic modulus (E_{ic}) for the computationally modelled ovine bone grafts start at 33 MPa after the first loading cycle increasing to 0.4 MPa, which is a 0.26% increase by the end of the 10th loading cycle. In the second (1.0 MPa) and third stress level (1.5 MPa), the average increase in E_{ic} is 4 & 4.8%. E_{ic} Increases 0.3% in the fourth and 7.5% in the fifth stress level of 2.0 MPa and 2.5 MPa, further increasing by 5.3% at the final stress levels of 3.0 MPa to a final value of 151 MPa. E_{ic} Increases from 33.97 MPa at the end of the first stress level to 57.62 MPa at the end of the first load cycle at the second stress level of 1.0 MPa which is an increase of 17%. This increase in E_{ic} between stress level decreases to 10% between the stress level 1.0 MPa

– 1.5 MPa and between 1.5 MPa -2.0 MPa. Between stress levels 2.0-2.5 & 2.5 to 3.0 MPa the average increase in E_{ic} was 12%.

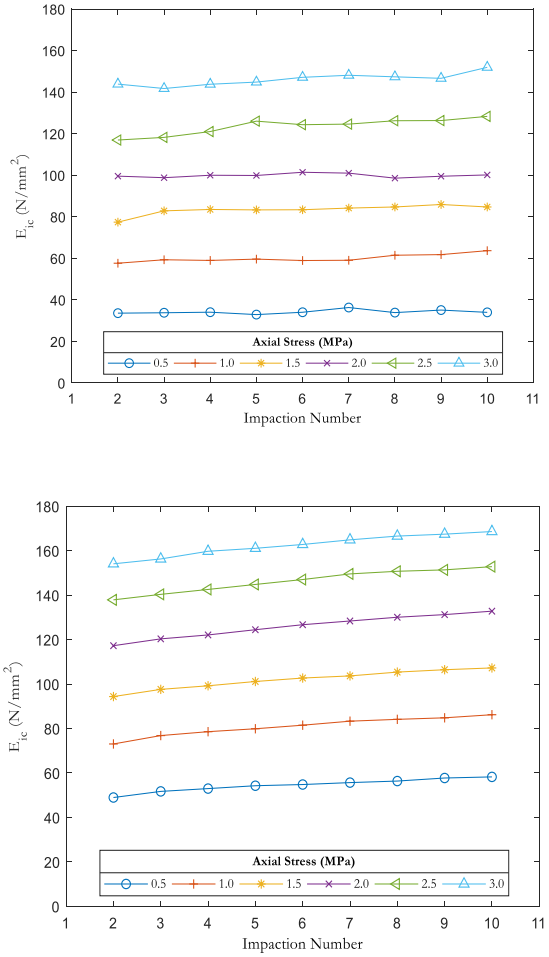

Figure 4.6 Instantaneous elastic modulus achieved at each stress level from a (left) computational model, (right) mean experimental results with 5mm ovine bone graft cubes.

Comparatively, the instantaneous elastic modulus achieved from the experimental mean's as seen from Figure 4.6 (b) start at 48 MPa after the first loading cycle increasing to 64 MPa, which is around an average of 9% increase by the end of the 10th loading cycle at first (0.5 MPa) stress level. At the end of the second (1.0 MPa) and third stress level (1.5 MPa), the average increase in E_{ic} is 19MPa an increase of 10%. E_{ic} Increases 12% by the end of the fourth (2.0 MPa) stress level

and 9% by the end of the fifth stress level of 2.5 MPa. At the final stress levels of 3.0 MPa E_{ic} increases 9.4% with a mean final E_{ic} value of 177 MPa.

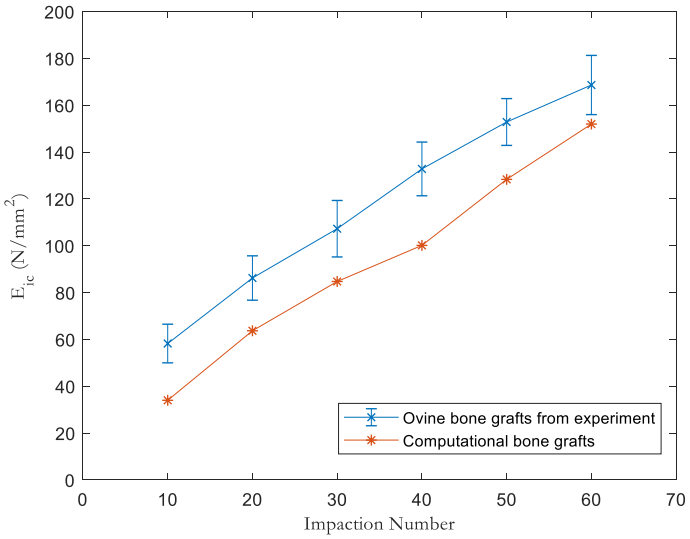

Figure 4.7 Increase in E_{ic} at the end of 10th loading cycle at each stress level for all tests between experimental ovine (all tests) and computational ovine bone grafts to show variations in E_{ic} between the two

The graph shows that the increase in E_{ic} for ovine bone grafts from the experimental test compared with the computational model at the end of the 10th loading cycle at each stress level for 5 tests using ovine bone grafts. Ovine bone grafts from the experiment measure a mean E_{ic} of 48 MPa to 177 MPa, whereas ovine bone grafts from the computational model measure between 38 MPa to 155 MPa. It can be deduced from the graft that the Standard deviation of E_{ic} across all 5 tests on ovine bone grafts was 8.2 MPa at the first stress level (0.5MPa), 9.4 MPa at the second stress level (1.0 MPa), 12 MPa at third, 11.46 MPa at the fourth, 10 MPa and 12.6 MPa at the final two stress levels (2.5 MPa) and (3.0 MPa) stress levels. Comparing the elastic modulus achieved between the computational and experimental means, the computational model achieved an elastic modulus E_{ic} values lower at a rate of 41.6% at 0.5 MPa stress level, 26.1% at 1.0 MPa, 26.6% at 1.5 MPa, 24.6% at 2.0 MPa, 16% at 2.5 MPa and 9.9% at 3.0 MPa.

4.5. Sensitivity Analysis

The results presented from the computational study (3.4) indicate that the bulk behaviour of bone grafts can be modelled with an explicit finite element model and by implementing an elastic-plastic material. However, the stress and strain values achieved from the computational study were similar but not identical to experimental test results using ovine bone graft cubes with 5mm edge length. The result achieved from the computational model was approximately 20% lower with a maximum achieved instantaneous elastic modulus of 159 MPa as compared to the 168.7 MPa for 5mm ovine bone grafts cubes. To be able to use the computational model as a stand-alone technique to understand the material behaviour of the bone grafts, tuning of the computational model is necessary. The behaviour of the particles in the computational model can be controlled using three effective parameters, namely, Young's modulus, yield strain, and the coefficient of friction. Research suggests that the average value of young's modulus of ovine cancellous bone is 1.1± 0.4 GPa (Mittra et al., 2003) and the yield strain value to be 0.6% in tension and 1.01% in compression (Niebur et al., 2000), the friction coefficient was found to be between 0.3 – 1.3 (Zhang et a.,l 1999). This provides significant variability in the input parameters, which needs to be studied to better understand and match the computational model with the experimental results.

As a result, in this sensitivity study, the parameters influencing the final bulk elastic modulus will be studied understand the interaction between each input parameter and its effect on the resultant bulk modulus E_{ic}. The data achieved from this study will be used to tune the computational model to try to match the computational and experimental results. Once the values are matched, the results will be used to verify that the computational method can be applied to other similar materials by estimating the optimum parameters necessary to predict the response when the experimental material is changed from ovine bone grafts to bovine bone grafts of similar size and shape.

The current modelling technique takes approximately 8 hours to run, and therefore it is not possible to perform an exhaustive search for the optimal parameters. An effective process is needed to help identify the appropriate material parameters. However, multiple mathematical simulations can be used to identify the material parameters like principal component analysis (PCA), Monte-Carlo simulations, Orthogonal matching pursuit (OMP) and Design of experiments (DoE). In this thesis, a Design of experiment (DoE) type of approach was employed. DoE is a widely used method for determining the interaction between different parameters. A DoE is an organised approach that rationally connects experiments to study the influence of and the interactions between all factors in a precise manner with limited experiments. Using this approach, a response surface methodology was employed to try and identify the best parameters to describe the experimental mechanical behaviour in the computational model.

A response surface is an analytical equation that allows for the estimation of interaction between different inputs and therefore describes the response to the various inputs. To develop a response surface a series of experiments are needed to be run where the input parameters are varied. There are several ways these experiments can be run out of which design of experiments is the most common approach used. The choice of experimental design depends on the number of resources available and choosing a design that requires fewer runs so that the objectives of the experiments and the independent factors can be investigated within the budget. In this case, the total number of factors to be investigated is three. These three factors are independent of each other. As a result, the proportion of these different factors must sum to 100% to achieve the best combination of parameters required for the computational model. Thus, three designs were identified when designing these experiments, namely, Full Factorial Array (FFA), Central Composite Face Cantered design (CCF), and Box-Behnken design (Trutna, 2012). A Full factorial array is the most common experimental design where all input factors are run with all possible combinations. Even if the number of factors 'k' are small, a three-level full factorial required for this study needs 3^k

runs accounting to 27 runs. On the other hand, CC requires 5 levels for each factor investigated accounting to 20 runs for all three factors. Box-Behnken requires only 3 Levels for each factor. The following table shows the number of experiments needed for each of these designs.

Type of Design	Number of runs
Full Factorial Array – 3 Levels	27
Central composite face centred (CCF) – 5 Levels	20
Box-Behnken – 3 Levels	15

Table 4.1 Number of runs required by Central Composite and Box-Behnken designs

To reduce computational time by up to 4 weeks, a Box-Behnken approach was decided as a reasonable method given the time in hand and the data needed to understand the interaction. In addition to this, the Box Behnken provides fitted values, which are as close as possible to observed values. This minimises the residual error of the prediction and provides a good graphical analysis through simple data patterns. All of which can be obtained with fewer runs as compared to FFA & CCF (Trutna, 2012). The Box Behnken can be summarised as a statistical method to design and explore the interaction and relationship between an objective function (resultant bulk modulus) and a set of independent variables, namely, Young's modulus, friction and yield strain, which were classified as attribute data (i.e., low or high). This design aims to optimise the resultant bulk modulus (objective function) which is influenced by the various independent variables.

4.5.1. Methods

A Box Behnken design was used to create response surfaces using fewer runs than full factorial techniques. Response surface is an expression of the function of independent variables. This response can be expressed from the equation (4.2)

$$Y = f(x_1, x_2, \ldots . x_n) \quad 4.2$$

The goal of using this design is to optimize the response variable *Y* (resultant bulk elastic modulus) and x_1, x_2 & x_3 the independent variables called factors (k).

The design consisted of factorial design points; k(k+1) runs used to analyse factors in three-level factor runs. A second-order polynomial equation can explain the response surface methodology expressed from the equation (4.3)

$$Y = b_0 + b_1x_1 + b_2x_2 + b_3x_3 + b_{11}x_1^2 + b_{22}x_2^2 + b_{33}x_3^2 + b_{12}x_1x_2 + b_{13}x_1x_3 + b_{23}x_2x_3 \quad 4.3$$

Where Y is the resultant bulk elastic modulus b_0 the value of the fitted response at the centre point of design, $b_{1\ldots3}$ linear, $b_{11\ldots33}$ quadratic and $b_{12,13,23}$ the interaction respectively.

$x_{1\ldots3}$ the coded independent variables, quadratic terms are $b_{11}x_1^2$ and cross product terms like $b_{13}x_1x_3$.

4.5.2. Experimental design

According to Table 4.2, the input variable parameters of Young's modulus, friction and yield strain interaction between each other were investigated. A series of 15 runs were conducted by changing the input variables and keeping all other parameters for the simulation constant.

Run	Youngs modulus (x_1)	Friction (x_2)	Yield Strain (x_3)
1	-1	1	0
2	0	0	0
3	1	1	0
4	0	1	-1
5	0	-1	-1
6	0	-1	1
7	1	0	1
8	-1	-1	0
9	-1	0	-1
10	0	1	1
11	0	0	0

12	0	0	0
13	1	0	-1
14	1	-1	0
15	-1	0	1

Table 4.2 Factor setting for Box-Behnken design

This image has been removed due to copyright restriction, Available online from (Trutna, 2012)

Figure 4.8 Box Behnken design block diagram for a three-factor experiment (Trutna, 2012)

4.5.3. Computational experiment setup

The computational experiment setup was modelled identical to the computational model as explained in **Error! Reference source not found.**. The bone grafts were modelled as a deformable s olid cube with 5mm sides meshed as a four-node linear tetrahedral element consisting of 93 elements per cube. The custom apparatus from the experimental model consists of a test chamber 100 mm high, 50 mm in diameter and a wall thickness of 10 mm. After filling the chamber with bone graft particles, an impactor of 100 mm high and 49 mm diameter was introduced into the test chamber. The material definition for the apparatus was given as 210 GPa, and general hard contacts were specified for their interactive properties. The material definition of the bone grafts was changed based on the experiment.

MINITAB 19.25 statistical analysis software was used to generate the experimental design. Analysis of the variance was evaluated using the statistical analysis software. Based on the selected independent variables, Youngs Modulus (X_1), Friction (X_2), and yield strain (X_3) are shown in Table 4.2. The range of values of the independent variables were coded as the variables, x in the range of +1 and -1 levels.

Youngs Modulus		Friction		Yield Strain	
Real Value	Coded Value	Real Value	Coded Value	Real Value	Coded Value

X_1	x_1	X_2	x_2	X_3	x_3
0.97 GPa	-1	0.5	-1	0.4%	-1
1.27 GPa	0	0.8	0	0.6%	0
1.57 GPa	1	1.1	1	0.8%	1

Table 4.3 Computational range and independent variable levels with coded values

The response obtained from the simulations were analysed by performing a regression of the predicted versus the Box Behnken results for the training data. Further to the regression analysis Pareto figures were plotted to characterise the standardised effect of each of the coded values and their interactions, main effects plots to describe the effects of each of the coded values and response surface plots to describe the change in final bulk modulus and visualise the change graphically.

Each of the variables were transformed into coordinates inside a dimensionless scale. The variable level X_i were coded as x_i with regards to the following equation in a way that X_0 corresponds to the central value.

$$x_i = \left(\frac{X_i - X_0}{\Delta X_i}\right) \; i = 1,2,3, \dots k \tag{4.4}$$

Here, x_i corresponds to the dimensionless value of independent variable, X_i the actual real value of the independent variable, X_0 the actual real value of the independent variable at the centre point, and finally ΔX_i is the step change.

Following the above equation (4.4), the relationship between the coded value and the real independent variable is given by equation (4.5)

$$x_1 = \left(\frac{X_1 - 1.27}{0.30}\right), x_2 = \left(\frac{X_2 - 0.8}{0.3}\right), x_3 = \left(\frac{X_3 - 0.6}{0.2}\right) \tag{4.5}$$

4.5.4. Results

The estimated correlation coefficient for the response surface is not sufficient as a correlation coefficient only provides the information if the variable is either positive significant (+1) or not significant (0) or negative significant (-1). As a result, ANOVA analysis was also to analyse the differences and significance further to characterise the results and get the best response.

Youngs Modulus (x_1)	Friction (x_2)	Yield strain (x_3)	Resultant Instantaneous Bulk Modulus in MPa					
			10^{th} load cycle		30^{th} load cycle		60^{th} load cycle	
			Computational	Predicted	Computational	Predicted	Computational	Predicted
-1	1	0	37.13	36.96	106.17	106.25	210.62	215.41
0	0	0	37.44	37.29	106.56	106.56	206.52	200.48
1	1	0	48.25	49.33	126.36	127.87	206.12	311.40
0	1	-1	55.1	53.25	134.91	130.90	285.33	267.92
0	-1	-1	38.27	38.13	86.27	86.185	210.01	161.31
0	-1	1	39.89	39.41	82.41	79.960	127.35	169.91
1	0	1	37.44	37.29	106.56	106.56	158.67	206.62
-1	-1	0	59.31	60.83	121.73	125.87	164.11	195.77
-1	0	-1	34.49	35.57	77.21	78.867	277.58	169.85
0	1	1	42.27	40.44	98.93	94.785	158.29	153.09
0	0	0	37.44	37.29	106.56	106.56	206.52	184.05
0	0	0	37.44	37.29	106.56	106.56	206.52	206.62
1	0	-1	59.31	60.83	121.73	125.87	287.81	206.62
1	-1	0	56.17	54.78	131.68	130.02	146.19	266.63
-1	0	1	31.07	32.61	82.09	86.09	154.90	175.03

Table 4.4 Parameter levels of Box Behnken (coded values) and the results of computational simulations and the predicted response values for resultant bulk modulus at the end of stress level 0.5MPa, 1.5MPa & 3.0MPa

The regression analysis of the results shows that the relationship between the computational bulk modulus and the predicted bulk modulus has a strong correlation with a slope of the lines represented from the regression equations below in Table 4.5 and Figure *4.9* show the scatter plot with the relationship between the computational results and the predicted results.

Stress Range	Regression equation
0.5 MPa	$Y = 0.9898 * x + 19.95$
1.5 MPa	$Y = 0.9889 * x + 139.39$
3.0 MPa	$Y = 0.9036 * x + 19.95$

Table 4.5 Results from the regression analysis and the best-fit equation between computational modulus and the predicted modulus with the slope of the lines at different stress levels

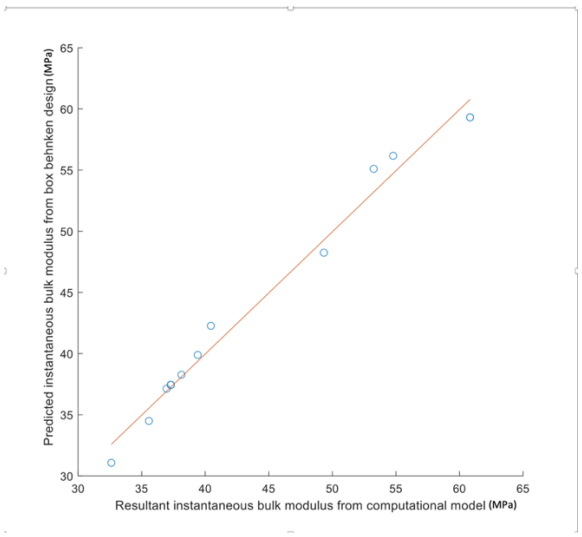

(a)

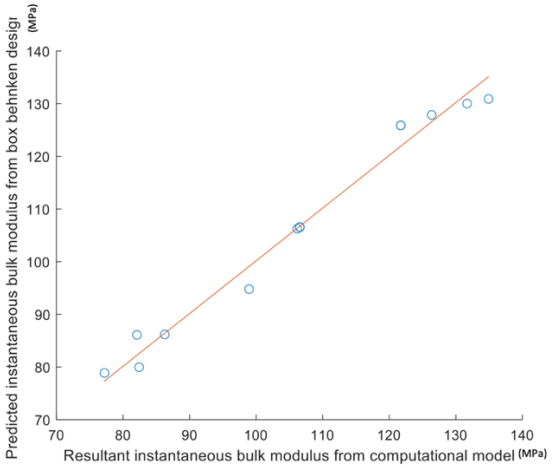

(b)

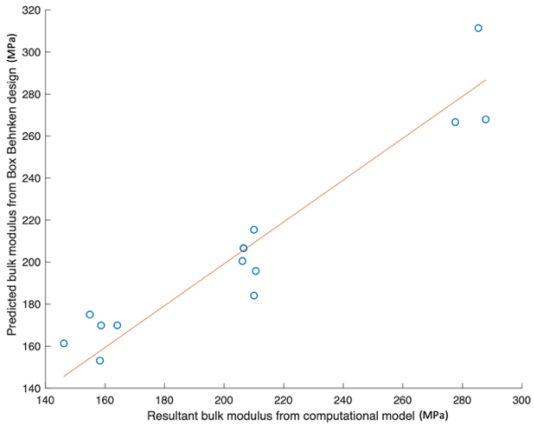

(c)

Figure 4.9 *Scatter plot showing the relationship between the computational results and the predicted results at stress levels (a) 0.5 MPa, (b) 1.5 MPa, (c) 3.0 MPa.*

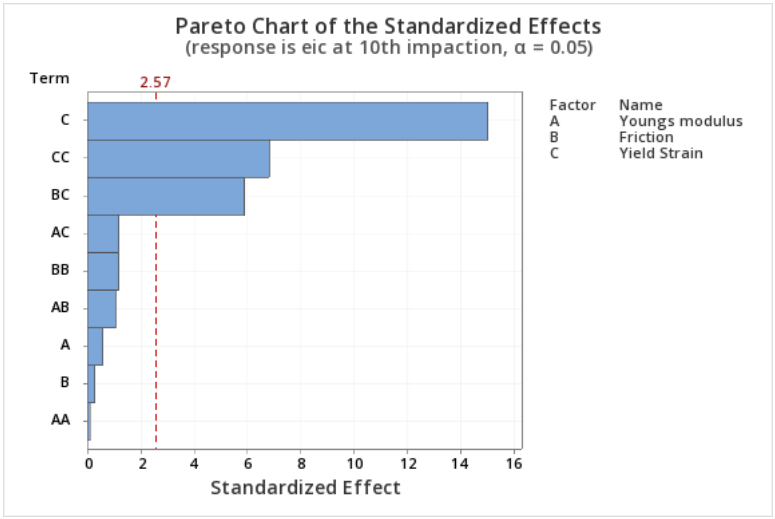

(a)

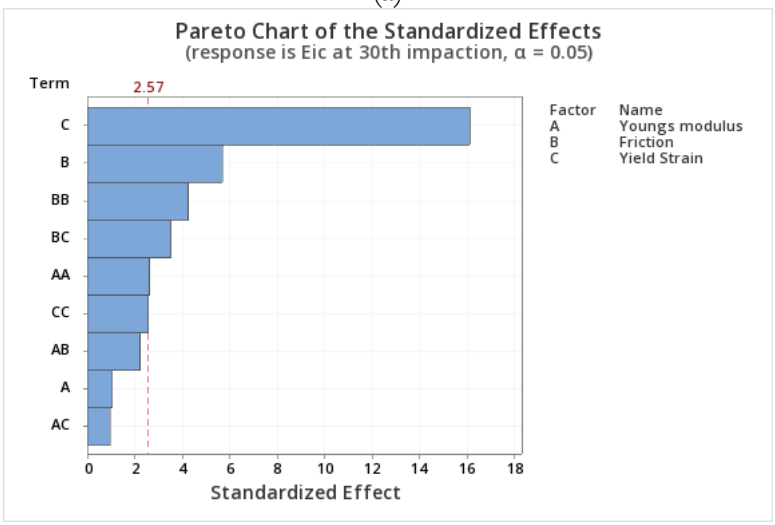

(b)

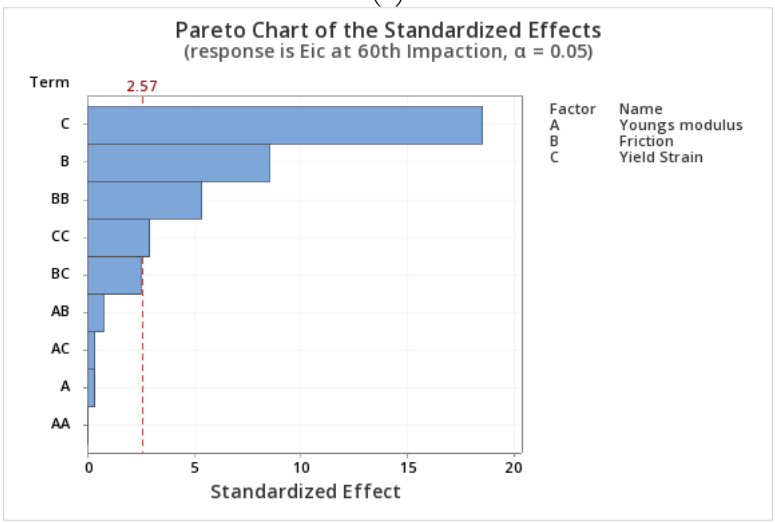

(c)

Figure 4.10 Pareto chart indicating the interaction effect between each variable independently (A, B, C), between each other (AA, BB, BC) and their interaction effect with other variables (AB, BC, CA) at stress levels (a) 0.5 MPa, (b) 1.5 MPa, (c) 3.0 MPa.

Figure 4.10 shows that at all stress levels, yield strain shows the highest effect. Friction plays an important role in the interaction as the stress level increases. The standard effect of friction at 0.5 MPa is less than significant. However, at 1.5 MPa, the effect of friction rises to the second-highest and further increases at 3.0 MPa stress level. It can be observed from the chart that Young's modulus has the least effect on the results. The yield strain and friction interaction shows significant interaction at the lowest stress level and decreases as the stress level increases. The interaction between Young's modulus and Yield strain is lower, providing the least amount of difference. The interactions between Young's modulus and friction are higher than Young's modulus's effect but are lower than the standardised effect required to be considered an influence. The interactions between each of the independent variables with themselves do provide significant interaction in terms of friction beyond 1.5 MPa. The self-interaction between yield strain is highly significant at the lowest stress level but decreases at 1.5 MPa, similar to Young's modulus's self-interaction. However, at 3.0 MPa stress level, friction's self-interaction increases slightly whilst Young's modulus's self-interaction drops to zero.

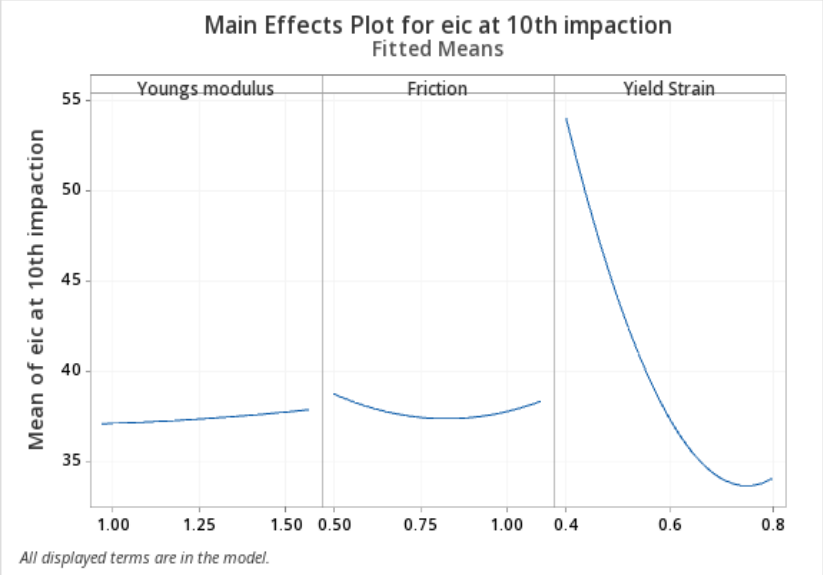

(a)

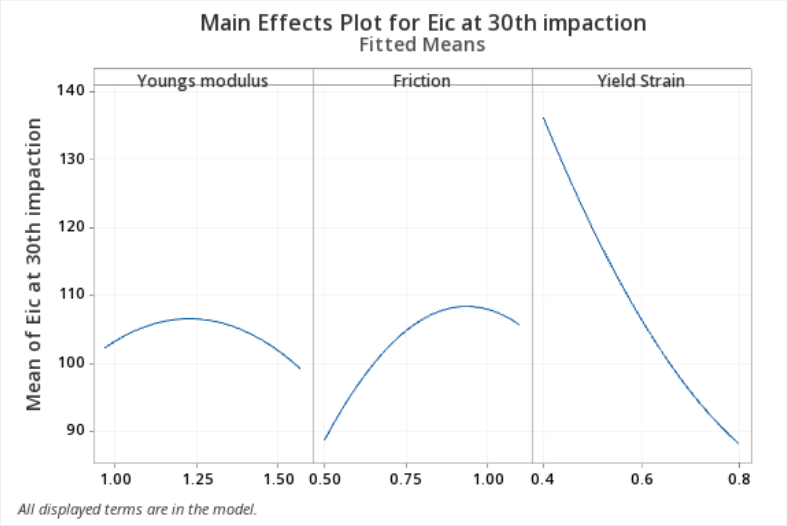

(b)

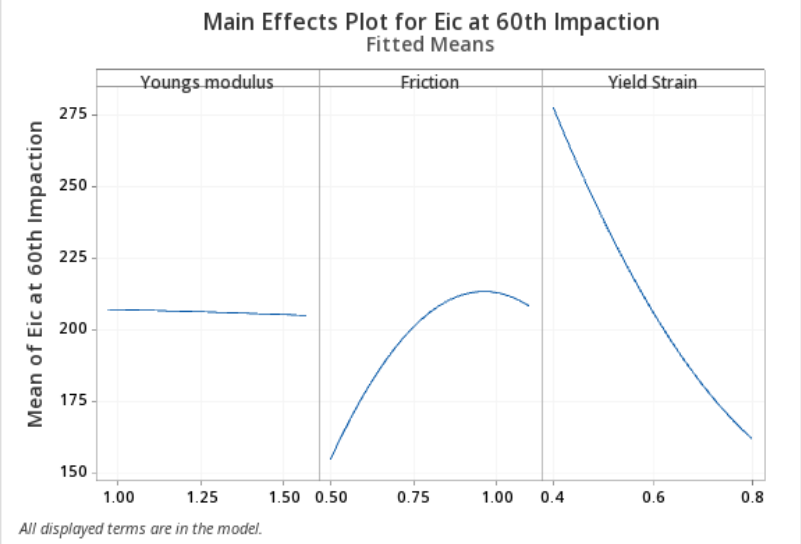

(c)

Figure 4.11 Main effects plot of final resultant bulk modulus to the independent input variables at (a) 0.5MPa, (b) 1.5MPa, (c) 3.0MPa Stress levels

The above Figure 4.11 show the main effects plot for all three independent input variables, Young's modulus, friction and yield strain at stress levels 0.5 MPa, 1.5 MPa and 3.0 MPa. At 1.5 MPa & 3.0 MPa. Yield strain follows a downward slope on all stress levels; however, the downward slope stops when the yield strain reaches 0.78% and starts to increase beyond 0.78%. At higher stress levels of 1.5 MPa and 3.0 MPa, the pattern is identical with the instantaneous bulk modulus decreasing by 35.7% till the strain increases to 0.65%. Beyond this, the rate at which the instantaneous bulk modulus decreases goes down to 10.7%. Friction follows a concave pattern at 0.5 MPa stress level. However, as the stress level increases, the pattern is steeper than Young's modulus, increasing 15 to 15.3% in resultant bulk modulus until the friction value reaches 0.89. The resultant bulk modulus starts decreasing for both 1.5 MPa and 3.0 MPa stress levels. The change in resultant E_{ic} with an increase of Young's modulus is minimal with the E_{ic} increasing effect of 4% at 0.5 MPa stress level and a decreasing effect of 4% at 3.0 MPa. At 1.5 MPa stress level, however, changes in Young's modulus follows a convex pattern increasing resultant E_{ic} until 1.25 MPa stress level and decreasing beyond 1.25 MPa.

4.5.5. Response surface / Contour plots

Response surface was generated to describe how E_{ic} changes in a given direction by adjusting the designed variables. This change can be visualised graphically with E_{ic} plotted versus the levels of Young's modulus, friction and yield strain. Contour plots can be used to explain the same effects in a less complicated way to view the response surface in a two-dimensional graph. These contour graphs (Figure 4.11 a, b & c) show the contour lines of the independent variables that have the same response value Y on E_{ic}. One of the three variables is selected as a control variable and held constant. Youngs modulus was selected as the hold variable and 1.27GPa was selected as it is the middle value of the range. It is easier and more convenient to understand the interaction between two independent variables and match the experimental observations.

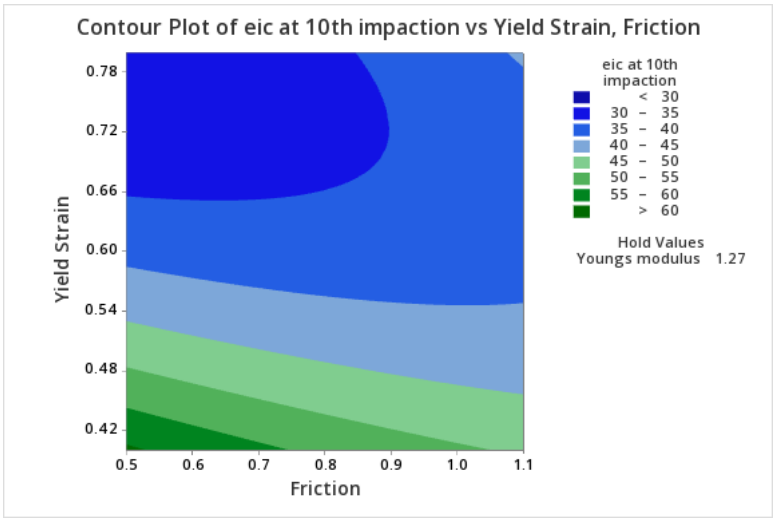

(a)

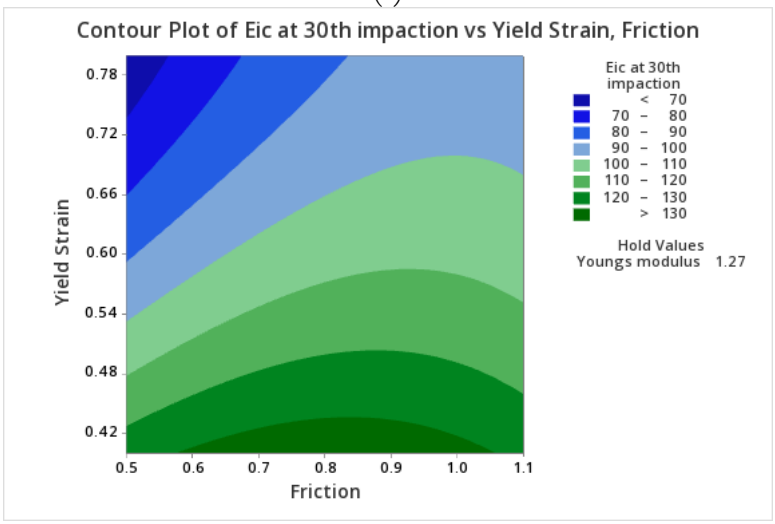

(b)

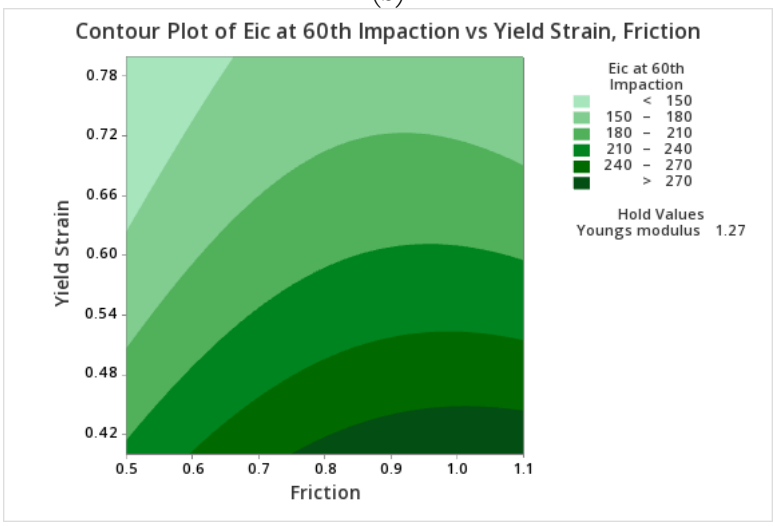

(c)

Figure 4.12 Effect of Yield strain and Friction on E_{ic} on a 2D Contour Plot at (a) 0.5MPa, (b) 1.5MPa & (c) 3.0MPa

Looking at the contour plot (Figure 4.12 a, b & c) created from the effect of yield strain and friction, it can be observed that the contour plot follows an elliptical pattern with significant interactions between yield strain and friction. Friction and yield strain show parallel lines towards each other at the lowest level of friction and low level of yield strain at 0.5 MPa, accumulating the highest modulus for the stress level. However, the highest level of friction and the lowest level of yield strain at 1.5 MPa accumulate the lowest E_{ic} values. The highest stress level of 3.0 MPa friction and yield strain follow an elliptical only pattern with the highest friction level and lowest yield strain values accumulating the highest modulus E_{ic} values.

The T-values and P-Values specify the importance of each coefficient, a T-value and P-value less than 0.05 indicates the significance of the corresponding coefficient. SE coefficient values close to the SE coefficient constant (1.08) represent no effect whist values further from the constant exhibit significant effect.

Term	Coefficient	SE Coefficient	T – Value	P - Value
Constant	37.44	1.08	34.58	0
Youngs modulus (x_1)	0.39	0.663	0.59	0.582
Friction (x_2)	-0.192	0.663	-0.29	0.783
Yield strain (x_3)	**-9.97**	**0.663**	**-15.04**	**0**
Youngs modulus * Youngs modulus (x_1^2)	0.101	0.976	0.1	0.921
Friction * Friction (x_2^2)	1.161	0.976	1.19	0.287
Yield strain * Yield strain (x_3^2)	**6.666**	**0.976**	**6.83**	**0.001**
Youngs modulus * Friction (x_1x_2)	1.002	0.938	1.07	0.334
Youngs modulus * Yield strain (x_1x_3)	1.122	0.938	1.2	0.285
Friction * Yield strain (x_2x_3)	**5.523**	**0.938**	**5.89**	**0.002**

(a)

Term	Coefficient	SE Coefficient	T – Value	P - Value
Constant	106.56	2.43	43.88	0
Youngs modulus (x_1)	-1.59	1.49	-1.07	0.334
Friction (x_2)	**8.47**	**1.49**	**5.7**	**0.002**
Yield strain (x_3)	-23.99	1.49	-16.13	0
Youngs modulus * Youngs modulus (x_1^2)	**-5.72**	**2.19**	**-2.61**	**0.047**
Friction * Friction (x_2^2)	**-9.31**	**2.19**	**-4.25**	**0.008**
Yield strain * Yield strain (x_3^2)	5.64	2.19	2.57	0.05
Youngs modulus * Friction (x_1x_2)	-4.7	2.1	-2.23	0.076
Youngs modulus * Yield strain (x_1x_3)	-2.03	2.1	-0.96	0.379
Friction * Yield strain (x_2x_3)	**7.45**	**2.1**	**3.54**	**0.017**

(b)

Term	Coefficient	SE Coefficient	T – Value	P - Value
Constant	206.52	5.08	40.63	0
Youngs modulus (x_1)	-1.05	3.11	-0.34	0.748
Friction (x_2)	**26.59**	**3.11**	**8.54**	**0**
Yield strain (x_3)	**-57.69**	**3.11**	**-18.53**	**0**
Youngs modulus * Youngs modulus (x_1^2)	-0.13	4.58	-0.03	0.978
Friction * Friction (x_2^2)	**-24.63**	**4.58**	**-5.37**	**0.003**
Yield strain * Yield strain (x_3^2)	13.35	4.58	2.91	0.033
Youngs modulus * Friction (x_1x_2)	3.35	4.4	0.76	0.48
Youngs modulus * Yield strain (x_1x_3)	-1.62	4.4	-0.37	0.729
Friction * Yield strain (x_2x_3)	-11.09	4.4	-2.52	0.053

Table 4.6 Results of the regression analysis of Box Behnken Design at (a) 0.5 MPa, (b) 1.5MPa, (c) 3.0MPa stress level (statistically significant values are highlighted in bold)

The ANOVA results of the regression analysis as seen from Table 4.6 across the different stress levels with the significant variable being the yield strain followed by friction and the self-interaction between yield strain and friction to have the most significant effect. Multiple regression analysis of the computational data gave the following second-order polynomial equations given in Table 4.7

Stress level	Polynomial equation Y (E_{ic})
0.5 MPa	$Y = 206.0 - 21.7x_1 - 90.7x_2 - 347.2x_3 + 1.1x_1^2 + 12.9x_2^2 + 166.7x_3^2 + 11.1x_1x_2 + 18.7x_1x_3 + 92.0x_2x_3$
1.5 MPa	$Y = 25.4 + 218.3x_1 + 185.6x_2 - 354.4x_3 - 63.6x_1^2 - 103.5x_2^2 + 140.9x_3^2 - 52.2x_1x_2 - 33.8x_1x_3 + 124.1x_2x_3$
3.0 MPa	$Y = 184 - 13x_1 + 590x_2 - 507x_3 - 1.5x_1^2 - 273.6x_2^2 + 334x_3^2 + 37.3x_1x_2 - 26.9x_1x_3 - 184.9x_2x_3$

Table 4.7 Regression equation from multiple regression analysis of the computational results in uncoded units units for Youngs modulus(x_1), friction(x_2) and yield strain(x_3) at different stress levels.

The linear effect of yield strain & friction, the quadratic effect of yield strain, the interaction between yield strain and friction has the most influence (Table 4.7). Other factors such as the linear and quadratic effect of Young's modulus and friction, the interaction terms between Young's modulus friction and yield strain have very less significance and can be neglected and eliminated from the model. As a result, the final second-order polynomial equation with a 95% confidence can be interpreted, as seen from Table 4.8

Stress level	Polynomial equation Y (E_{ic})
0.5 MPa	$Y = 206.0 - 347.2x_3 + 166.7x_3^2 + 92.0x_2x_3$
1.5 MPa	$Y = 25.4 + 185.6x_2 - 354.4x_3 - 103.5x_2^2 + 124.1x_2x_3$
3.0 MPa	$Y = 184 + 590x_2 - 507x_3 - 273.6x_2^2 + 334x_3^2 - 184.9x_2x_3$

Table 4.8 Reduced Regression equation of the computational results in uncoded units for Youngs modulus(x_1), friction(x_2) and yield strain(x_3) after removal of insignificant factors in each stress levels

4.5.6. Estimation of input variable values to match the experimental results

The sensitivity study using the Box Behnken design described the interactions and the effect each of the variables has on the resultant E_{ic} bulk modulus. To estimate the optimum input variable values necessary to achieve a resultant bulk modulus in the same range of the experimental results, a response optimiser was used. The results at the final stress level of 3.0 MPa, the final accumulated

instantaneous modulus was the target to be tuned. The response optimiser uses the optimization plot to determine the value set for the predictors within the given parameters.

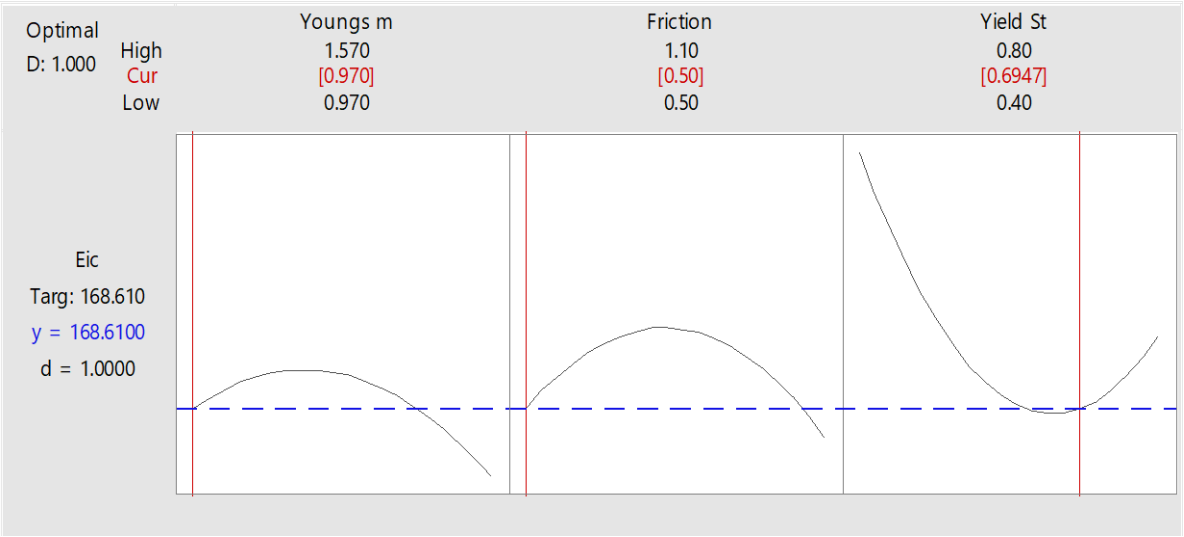

Figure 4.13 Response optimization results for a target E_{ic} value of 168.7MPa (Mean value achieved from experimental results)

It can be observed from Figure 4.13 that the target for the tuning process was set to 168.7 MPa, which is the mean aggregate value obtained from the experimental results at the end of the compression test. The response optimiser returned results with a high value, a low value and an optimised value. The response optimiser value was chosen to be the best fit value in from this test as they were closer to the Youngs modulus, friction and yield strain values observed in literature (Mittra et al., 2003; Bayraktar et al., 2004; Zhang et al., 1999; Niebur et al., 2001).The estimated optimum value from the figure was implemented into further simulations and the best fit input variables were determined to be 0.97 GPa for Youngs modulus, 0.5 for friction coefficient and a yield strain of 0.69%.

It can be seen from the results in Figure 4.14 that the optimisation response after the sensitivity analysis has improved the results of the computational model. The graph shows the resultant bulk

modulus E_{ic} in the final 10 impactions at 3.0 MPa. the second graph shows E_{ic} the final 10 impactions at 3.0 MPa after the optimised input parameters are used, the range of error of the computational model has dropped considerably, with the modulus lying within the SD error of the experimental tests.

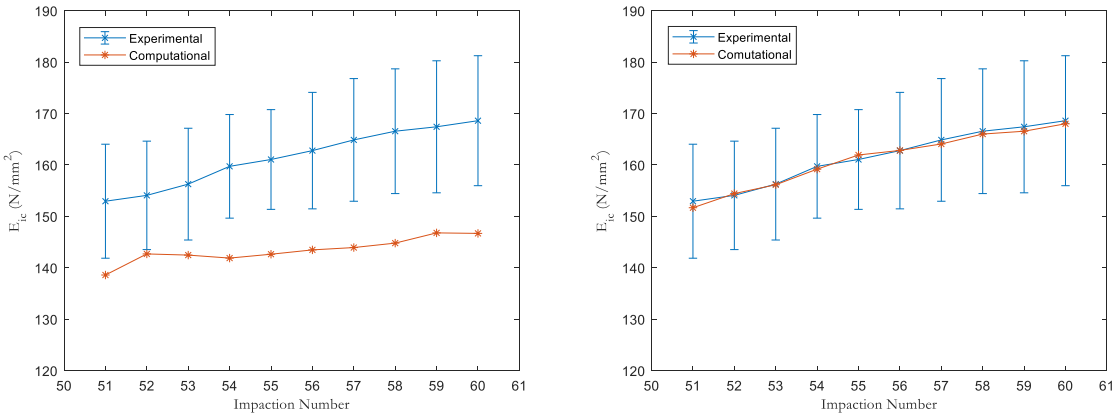

Figure 4.14 (a) Before tuning of input parameters, (b) After tuning of input parameters at the final stress level of 3.0MPa compared with the standard deviation error of the experimental results from ovine bone grafts.

The computational model was then checked at all loading levels with the experimental model. This can be seen from Figure 4.15, where the graph on the left shows the differences of the computational model before the tuning of the material parameters, the computational model lagging with its bulk modulus observed to be 50% lower than the experimental meal at the first load cycle.

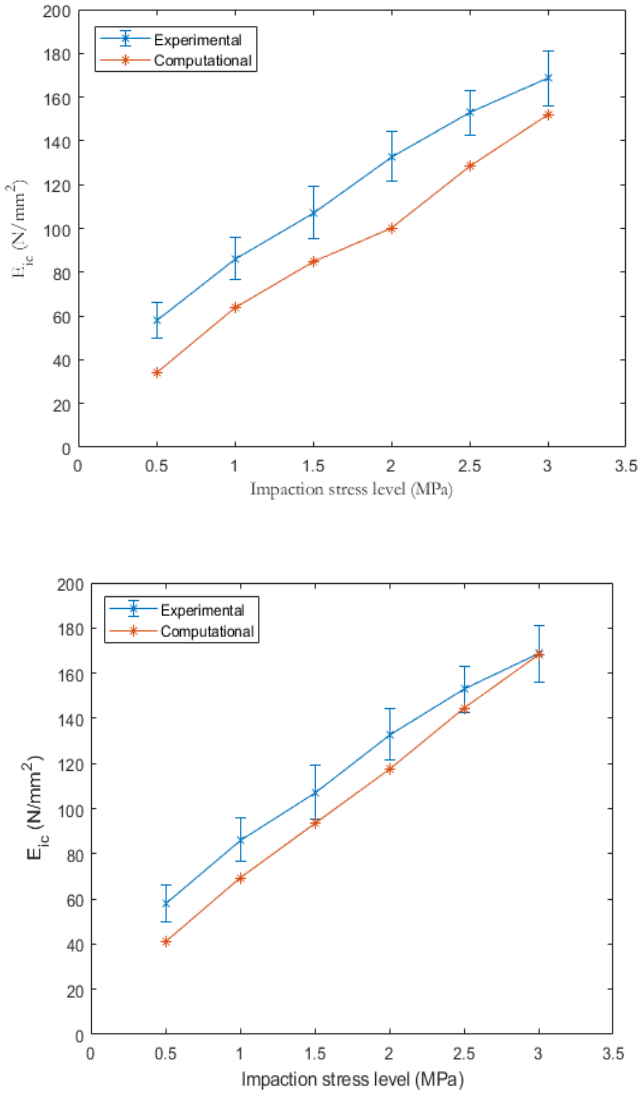

Figure 4.15 (a) E_{ic} at the end of each stress level before tuning, (b) E_{ic} at the end of each stress level after tuning compared with the standard deviation error of the experimental results with ovine bone graft.

This deficit in E_{ic} continued through the first four loading cycles, where the computational model produced 151.22 MPa as the final E_{ic} value as opposed to the mean of the experimental model, which recorded 168.78 MPa. Looking at the graph above on the right, it can be observed that the difference between the computational and experimental model has improved with the last two loading level cycles lying within the SD error range of the experimental results. The E_{ic} value obtained from the computational model at the end of the first loading cycle was 15.52% less than the experimental mean. This difference in value decreases as the loading cycle increases. The

second loading cycle had a deficit of 8.14%, the third 3.74% fourth loading cycle 4.55 %, the fifth loading cycle 5.26% and 0.3% at the final loading cycle. Though the predictions from the model are lower, they do lie within the experimental range.

4.6. Tuning of the computational model for bovine bone grafts

The results from the experimental tests using 5mm ovine bone grafts and a computational model with 5mm bone graft cubes fall within the SD value of the experimental tests. To validate this study, the same process of estimating the best input variable considerations was done for 5mm bone graft cubes from bovine samples from Chapter 3.

The mean final bulk modulus from the experimental tests with 5mm bovine bone graft cubes was used as a target value against the regression equation from the sensitivity study to calculate the value of input parameters necessary to achieve a response on the computational scale. The results from the regression value were determined to be 0.97 GPa Young's modulus, 0.5 friction and a yield strain value of 0.77%.

A computational model was run with the input parameters derived from the sensitivity study and compared with the existing experimental results. The results of which can be seen (Figure 4.16). It can be seen that at the final stress level of 3.0 MPa, the computational model accumulates a E_{ic} value higher than the experimental mean through the loading cycles and finally match the experimental value at the end of the loading and unloading cycles.

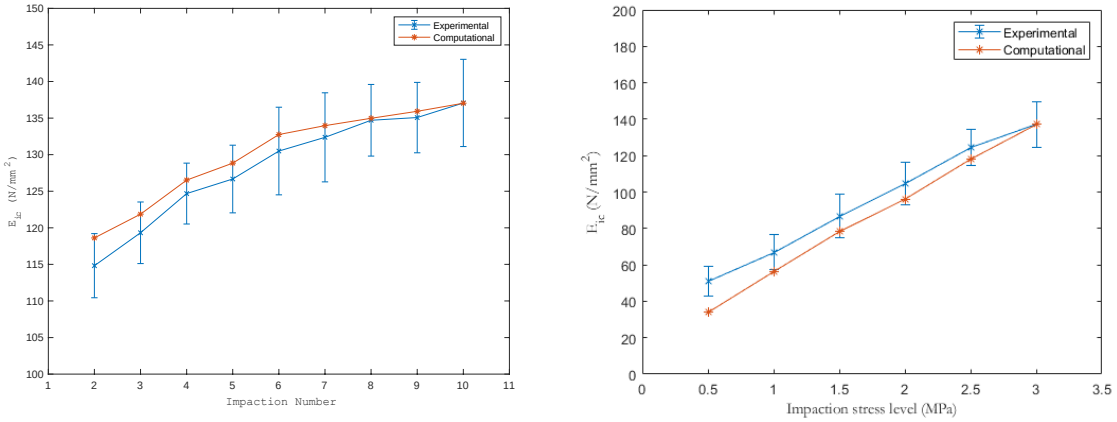

Figure 4.16 Results from the computational model compared with the results from experimental tests run with bovine bone graft cubes of 5mm sides. (left) computational results at the final stress level of 3.0MPa, (right) computational results compared at the last loading cycle of each stress level

The graph on the right shows computational model results at the end of the 10th loading and unloading cycle for all six stress levels. It can be seen that the computational model converges to the experimental mean as the stress level increases. There is not much convergence at the first load cycle where the computational model records 39.86 MPa and the experimental mean value recorded was 51.10 MPa which is 12.24 MPa higher. The variance across the 4 experimental tests was recorded to be 5.94 MPa. The computational model falls within the experimental variance value from the second stress level. At the end of the second stress level, the computational model records an accumulated E_{ic} of 62.22 MPa. The experimental mean recorded 66.89 MPa resulting in a deficit of 4.67 MPa, which is well within the 5.94 MPa SD value of the experimental tests. This can be seen at the other stress levels as well, where the results from the computational model fall within the SD range of the experimental mean.

4.7. Discussion

It can be observed that from the initial results using explicit finite element modelling and by modelling each particle separately, the simulation was able to capture a cyclic hysteresis loop like

the experimental study in Figure 4.3. There is an increase in strain almost immediately on the application of load. During the unloading phase, the strain reduces gradually and much slower than the results with DEM's. Stiffening can be observed on subsequent loading and unloading cycles at each stress level. There is some noise observed in all but the last stress level. This could be due to the bone graft particles being cubes that are stacked. Hence, when they are compacted, they do not have adequate stress to compact the particles to undergo irrecoverable deformation at the lower stress levels and hence move around in the unloading phase. This is not seen in the final stress level of 3.0MPA as they seem to get impacted to a point where they undergo irrecoverable deformation, and as a result, they don't move around when the stresses are removed. Although the computational model does capture a similar trend compared to the experimental model, there is still room for improvement in the computational model. As a result, a further study was conducted on the computational model by creating an identical bone graft in the form of cubes, randomly stacking the bone graft cubed and introducing plasticity into the particles to make the particle behave in a much more realistic manner.

The results presented from this study indicate that including plasticity in the computational model, the behaviour of the bone grafts changes significantly. Upon loading, there is an increase in strain almost immediately. During the unloading phase, the accumulated strain is stored in the graft for longer periods suggesting that they have undergone irrecoverable permanent deformation. Bone grafts experimentally are not completely elastic; they exhibit elastic and plastic properties, which clearly can be seen from **Error! Reference source not found.** Figure 4.5(a). Comparing the graph w ith results from the representative sample of the experimental test, the strain accumulated from the simulation is on a similar scale with a mean total accumulated strain of 0.18%, as seen in Figure 4.5. Accumulated strain on both these graphs was in the same range as the computational model accumulating an average of 0.01% higher than the representative experimental result.

Looking at the instantaneous elastic modulus values between the two (Figure 4.5), however, shows there are differences in the behaviour of the experimental and simulated results. The results from the computational model are on averaged 20% lower than the experimental results, as seen in Figure 4.6. At the end of the first load cycle, the computational model yielded a E_{ic} value of 33MPa, whilst the experimental model yielded 48 MPa. Within the same stress value of 0.5 MPa, the increase in E_{ic} over the loading cycles was not evident in the computational model where the E_{ic} from the computational model increased only 0.2% when compared to 9% on the experimental model. The average increase of E_{ic} at each stress level was only 3.3% for the computational model, while the experimental model recorded an average increase of 10% throughout the test. Looking at the elastic modulus values recorded at the end of the 10th cycle at all stress levels and comparing the computational results with all the experimental tests using 5mm Ovine bone grafts, the computational model predicts a lower elastic modulus as compared to the experimental data. It should be noted that the experimental results include the variations achieved from all 5 tests using ovine bone grafts, and the computational model's results do not fall within the values of the experimental variations. The error/deficit in E_{ic} from the computational model decreases as the stress level increases with the final stress level recording a E_{ic} value 9.9% less than the experimental mean. However, the computational model records a value up to 40% lower than the experiments at the lower stress level. This could be because the assumed elastic modulus of the bone grafts at 1.47 GPa are higher than the elastic modulus of the bone grafts from the experiment. As a result, they accumulate a lower instantaneous modulus than the experimental results at lower stress values between 0.5MPa to 2.0MPa.

Furthermore, in the experimental tests, the bone grafts were filled by hand and thereby the testing chamber was filled with the particles filled up in a completely random scattering pattern every time the experiment is repeated. By randomly scattering the particles in the computational model, it

achieved an increase in the distance between the particles and dropping them from a distance at an angle into the chamber. However, the randomised pattern achieved from the simulations will be the same when the simulation is repeated.

The computational model had to be tuned to develop a computational model that closely matches the experimental tests. As a result, a sensitivity was performed on the model to tune the model closer to the experimental results. The input parameters were studied to help tune the model and match the experimental results. Using the same methodology, it was possible to tune the model to match the experimental results at the first (0.5 MPa), Mid (1.5 MPa) and high end (3.0 MPa) of the applied stress levels. The analysis found that the yield strain was the most important factor affecting the resultant bulk modulus E_{ic} across the whole stress range, which means some of the particles have been impacted to the limit that they have started to yield and exhibit plastic deformation. However, the total accumulated modulus is 168.7 MPa which is 82% lower than the apparent elastic modulus of the particles at 0.97 GPa, suggesting there are gaps between the particles and only some particles have been impacted beyond their yield strength.

Friction within the model was the second most significant contributing factor to the prediction of the instantaneous elastic modulus at 1.5 MPa and 3.0 MPa. However, friction doesn't play an important role at the lower end of the stress range as the particles could be still in relative motion. As the stress level increases, the relative motion exhibited by some of the particles is reduced to static friction, preventing the particles from filling up the chamber's gaps.

The interaction between Yield strain and friction plays the next important factor in the first (0.5 MPa) and mid (1.5 MPa) stress range, beyond which the interaction effects is minimal. At the lower

end of the stress level, there are no interaction effects played by friction. Still, as the stress level increases, the effect of friction becomes more prevalent with friction becoming the second-highest important factor at the high end of the stress level. This could also be because static friction between the particles results in some particles being loaded beyond their yield values. The resultant E_{ic} recorded could be because of some of the particles yielding and exhibiting plastic deformation.

Young's modulus had no real influence on the behaviour of the bone grafts, with Young's modulus and friction account for less than 10% change in bulk modulus at all stress levels, whereas yield strain accounted for 35% change. Looking back at the three input parameters used to tune the model. The analysis revealed that two of the three parameters (yield strain & friction) play a significant influence. Using these two parameters alone, it was possible to tune the computational model to match the experimental results in the higher stress level of 3.0 MPa. To achieve the instantaneous elastic modulus closer to the apparent elastic modulus, the particles need to be impacted at stresses much higher than 3.0 MPa.

Regression analysis was used to estimate the ideal input values, and the computational model with the optimised parameters produced a final E_{ic} value very close to the experimental results with an observed error of 0.03%. In the lower stress levels, the accumulated modulus in the computational model falls close to the SD range of the experimental mean but was still at the lower end of the spectrum with an average observed error of 2% to the experimental model. The reason for this being an estimation of the input values, was that they were only carried out for the final bulk modulus and not for the accumulated modulus at each stress level. The final instantaneous elastic modulus achieved from the model is more important than the elastic modulus accumulated at the lower stress levels. As seen from the results, the bone grafts are not well impacted at the lower stress levels. Impacting the bone grafts a 0.5 MPa does not produce an instantaneous modulus in

the range of the impacted instantaneous modulus from experiments in the literature (Verdonschot et al., 2001; Giesen et al., 1999; Phillips et al .,2006; Ayers et al., 2014) and the final bulk modulus achieved through impaction is used as a measure of the stability of the impacted bone. As such, less importance was given to the computational model to match the experimental model at all stress levels and matching the end output with a minimal margin of error was achieved. The results from the regression value determined that Young's modulus of 0.97 GPa, 0.5 friction and yield strain of 0.69% was the best-suited input parameters required to achieve the equivalent 168.6 MPa instantaneous modulus achieved by the experimental results in Chapter 3.4 using ovine bone grafts. Existing research has reported the elastic modulus of 6 – 8-month-old ovine bone grafts in the range of 0.97 ± 0.21 GPa (Nafei et al., 2000), which falls under the input parameters measured from the sensitivity tests.

The final part of this study explored whether the same response surface could be used to estimate the parameters for the bovine material. The results from the regression value were determined to be 0.97GPa Young's modulus, 0.5 friction and a yield strain value of 0.77%. Existing research has reported the instantaneous elastic modulus of bovine bone grafts were between 8 – 212 MPa (Voor et al., 2000b; Oftadeh et al., 2015; Mittra & Qin, 2003; Fosse et al., 2006) and the reported elastic modulus of bovine bone grafts in the range of 0.98 ± 0.17 GPa (Zhang et al., 1999). The experimental tests using bovine bone grafts accumulated a mean final resultant modulus of 137.72 MPa. The results from this simulation show that the computational model did match the experimental results in terms of hysteresis behaviour and accumulated apparent modulus with a variance of less than 1 MPa (0.03%) at the last loading cycle. This methodology to tune the computational model for both bovine and ovine bone graft is efficient, requiring only fifteen runs to achieve the results. However, the study's limitations were that only three values per parameter were used; increasing the number of values can help understand the effects of each parameter

more intricately. Secondly, the behaviour of human bone grafts was not explored as data from one experimental test was not enough to capture the variations in the bone grafts to have the range of parameters needed to study their behaviour.

Chapter 5 :

Exploration of variables based on impaction technique

5.1. Introduction

The results presented from the sensitivity study was able to identify the parameters required to simulate responses on par with experimental tests with both bovine and ovine bone graft particles. The best input parameters for the computational model using ovine bone grafts were determined to be 0.97 GPa – Young's modulus, 0.5- friction coefficient, and a yield strain of 0.69%. Similarly, bovine bone grafts recorded a higher yield strain of 0.77% for a similar Young's modulus and friction coefficient as ovine.

A fundamental difficulty in impaction bone grafting is determining how vigorous the impact force must be applied and when the graft is adequately impacted (Flannery et al., 2010). Based on previously published data, the majority of the impaction stresses used are in the range of 0.5 MPa – 3.0 MPa (Bavadekar et al., 2001; Brodt et al., 1998; Giesen et al., 1999; Heiner et al., 2005; Fosse et al., 2006; Phillips et al., 2006). In some cases, there has been research where the bone grafts were subjected to stresses of more than 3.0 MPa (McNamara et al., 2014; Flannery et al., 2010). A study by Noble et al (Noble et al., 2018) suggested that the average value of peak impaction force was 3765 ± 1094 N (3.8 MPa ± 1.11MPa) for head neck taper junction. On the contrary, a study by Wiebe et al. (2012) suggested that the impact stress of a hammer by surgeons in clinical situations can go to as high as 15.4kN (15.71 MPa). However, the test was conducted in an experimental environment and not in a surgical environment. Studies on controlled experimental testing also show impact forces of 15,781 ± 4,555 N (16.1 MPa ± 4.64 MPa) in a study by Scholl et al. (2016) and looking at the experiment setup, the impaction forces were measured at the striking pad of

the hammer, and it was found that the impact forces decrease as the load transducer is brought further from the striking pad of the surgical hammer. The study used an ortho impactor with an overall length of 22.86cm. The distal end of the ortho impactor was in direct contact with the bone grafts, but the impaction forces were not measured at the distal end of the ortho impactor. As such, there is the question as to how much impaction force is realistically achievable. To capture both the surgical and experimental spectrum in this chapter, the stresses range between 0.9kN – 17.6kN (0.5 – 9.0 MPa) applied directly to the bone grafts.

In the research literature (Brodt et al., 1998; Phillips et al., 2006; Albert et al., 2008b; Grimm et al., 2002), the delivery of the impaction energy has been tested sequentially over the load spectrum, rising from a low to high impaction stress rather than at a single, specified impaction level. In this chapter, the delivery of impaction energy will be tested individually rather than sequentially to determine if vigorous impaction of bone grafts at higher loads can produce adequately impacted bone grafts quicker than increasing loads sequentially.

Clinically the grafts are impacted in layers; however, there is little information on the influence of impacting bone grafts sequentially on the overall mechanical behaviour of the graft. Some papers report that preparing cylindrical confined compression; the specimen is layered (Bavadekar et al., 2001; Cornu et al., 2009; Voor et al., 2000b; Kuiper, 1997; Phillips et al., 2006). However, seldom have they been impacted in layers and most of these studies use impacted bone grafts as a single mass/object. Though they have their advantages, such that they are relevant to the study, it does not translate to a clinical scenario where bone grafts are often impacted sequentially in layers. To explore the reason, in this chapter, the bone grafts are split equally into dual layers and impacted one after the other to analyse the behaviour of the bone grafts and their differences in stiffness, permanent plastic strain and fill ratio compared to a single layer impaction.

Changing the impaction force and the number of impactions, it is possible to understand what happens in the bone graft after each impaction and predict the change in volume of the bone graft particles and change the fill ratio of the impacted bone. In addition to analysing the behaviour during impaction, these bone graft post impaction were also analysed by further subjecting them to threshold forces equal to a physiological loading condition as observed on the tibia (Bergmann et al., 2014). The standardised contact forces acting on a knee implant after a revised knee surgery were calculated to be around 200 to 300% of the person's body weight (Bergmann et al., 2014).

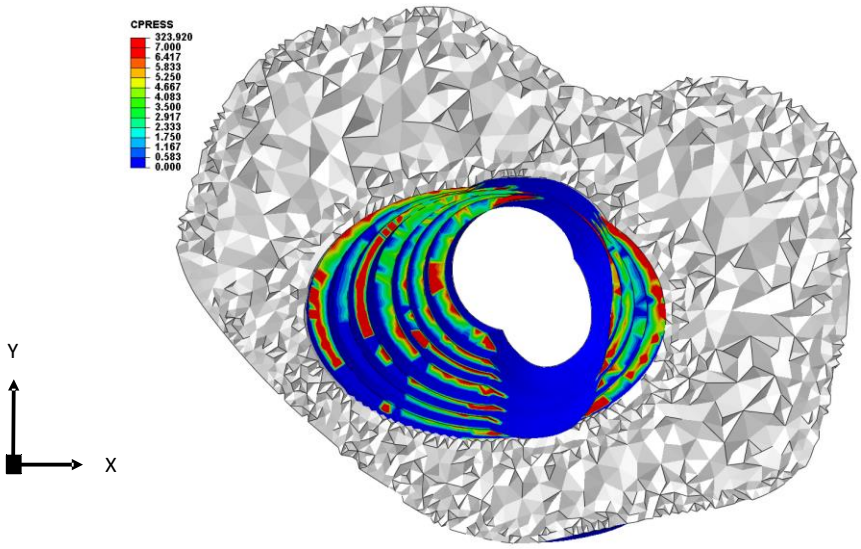

Figure 5.1 Metaphyseal bone sleeve contact stress reported in MPa (Awadalla et al., 2019)

A study conducted by Awadalla and associates (Awadalla et al., 2019) analysed the sleeve size in combination with stems on the primary stability and load transfer of a revision total knee impact with AORI type IIB defect treated with metaphyseal sleeves. They reported the peak strain on metaphyseal sleeves during physiological load. Through personnel communication, the strain values were converted into stresses, and the stress ranges were in the order of 2 – 5 MPa, as seen from Figure 5.1. As a result, 2.0 MPa was chosen as the comparable scenario for physiological loading conditions.

Currently, in literature, there is no good definition of a stable impacted bone graft. However, the parameters that define grafts' stability are instantaneous bulk modulus, strain accumulation, and hysteresis during the loading and unloading cycles. Previously, in chapter 4.3, it was observed that the modulus of the bone grafts converges to a steady value after cumulative series of impactions (Figure 4.6), there is reduced or no further accumulation of permanent strain, and there is minimal hysteresis during the impaction cycles (Figure 4.5**Error! Reference source not found.**). This can b e hypothesised as one of the defining characteristics of a stable graft. In this chapter, the accumulation of strain and the instantaneous bulk modulus is analysed to achieve a well-compacted graft.

The change in surface area and the fill ratio of the particles are analysed against the impact force and the number of impactions. The change in surface area of the particles captures the deformation caused by the impact force within the particles. The fill ratio of the bone graft is the ratio of the particles to the volume of the chamber at the same height as the particles. The change infill ratio will explain the rate of compaction, the maximum achievable stiffness and the resultant forces/energy needed to obtain the bulk stiffness.

5.2. Methods

The computational model followed the same protocols as the other computational simulations in chapter **Error! Reference source not found.**. Based on the results from the last chapter (4.5.4), t he input parameters with the best correlation were ovine bone grafts. Ovine bone grafts are often used as an exemplar of what would be ideally used in place of human tissue. As a result, they were used for the input parameters for this experiment. The Young's modulus of the bone graft particles was set to 0.97 GPa, the friction coefficient to 0.5 and the yield strain to be 0.8%, with the particles

assumed to be completely plastic. A total number of 480 bone graft cubes were used per experiment.

5.3. Test procedure

Two analyses were performed with the bone grafts:

1. All the bone graft particles were filled into the testing chamber and subjected to 60 load cycles at constant stress with a stress relaxation period between every ten impaction cycles. The range of stresses was between 0.5 MPa to 9.0 MPa to capture the range of forces reported surgeries and experimental tests (Bavadekar et al., 2001; Brodt et al., 1998; Giesen et al., 1999; Heiner et al., 2005; Fosse et al., 2006; Phillips et al.,2006; McNamara et al., 2014; Flannery et al., 2010; Noble et al., 2018; Zhao et al., 2012; Scholl et al., 2016). The increments of stresses were at 0.5 MPa intervals between each of the tests.
2. The next set of experiments were carried out by separating the particles into two groups, Group A and Group B each consisting of 240 particles. In the first group, A particles were filled into the test chamber, which was subjected to 30 load cycles and then particles from group B were introduced into the chamber on top of the impacted group A particles, and then the particles are impacted for a further 30 load cycles. The particles were impacted for a total of 60 load cycles with a stress relaxation period after every 10 load cycles. The stress range for these impactions was from 0.5 to 5.0 MPa increasing 0.5 MPa per test.

The resultant file from both the set of tests was subjected to a further 30 loading cycles at regular loading threshold levels of 2.0 MPa with a stress relaxation period between every ten loading cycles.

The results from the procedure were used to estimate variables like the volume change, the deformation of the particles and fill ratio to explore the behaviour of the graft.

5.3.1. Estimation of fill ratio

The volume of the particles before impaction was calculated using the formula.

$$V_p = a_p^3 \quad 5.1$$

Where, a_p the length of each side of each bone graft cube. The volume of the particles after impaction was calculated from the EVOL function on Abaqus, which records element volume; summing up all the elements in each particle gives the volume of the particles.

The final height of the particles was calculated from the displacement data. The volume of the cylinder beneath the impactor was calculated using the formula

$$V_c = \pi r^2 h_i \quad 5.2$$

Where, r is the radius of the inner chamber, h_i height of the surface of the impactor in contact with the particles.

The maximum number of particles that the space below the impactor can take in the chamber was calculated using the formula

$$N_{max} = {V_c}/{V_p} \quad 5.3$$

Where, V_c is the volume of the cylinder beneath the impactor, V_p is the volume of each particle.

Finally, the fill ratio of the chamber below the impactor is calculated using the formula

$$Fi_b = \left({N_{used}}/{N_{max}}\right) * 100 \quad 5.4$$

Where, Fi_b the fill ratio of the particles before impaction, N_{used} is the total number of particles used in the experiment and, N_{max} the maximum number of particles the chamber can take at that particular height.

This process was repeated to calculate the volume of the particles after impaction and used to calculate the final resultant fill ratio. The results were compared to try achieving the highest fill ratio possible.

5.4. Results

Looking at Figure 5.2**Error! Reference source not found.**, at stress level 1.0 MPa, the particles are still intact and undergo a very low to no deformation. Some deformation can be seen at a 2.0 MPa stress level right next to the impactor. However, there does not seem to be much deformation occurring beyond the first few bone particles, which are not near or in contact with the impactor. At stress levels, 3.0 MPa deformation starts accumulating near the impactor and at the end of the cylinder. At the stress levels, 4.0 MPa & 5.0 MPa, the deformation in the particles increases substantially, with some particles near the rigid edges being crushed more than the particles in the centre of the chamber. Beyond 5.0 MPa, the deformation of the particles increases where there is a boundary with the rigid body, namely, the walls of the cylinder and the impactor. This can be seen on the simulations beyond 6.0 MPa at both walls of the cylinder where the particles are being crushed into flat surfaces. The highest displacement of the impactor is recorded till the stress levels reach 5.0 MPa after which, the displacement of the impactor is reduced between stress levels.

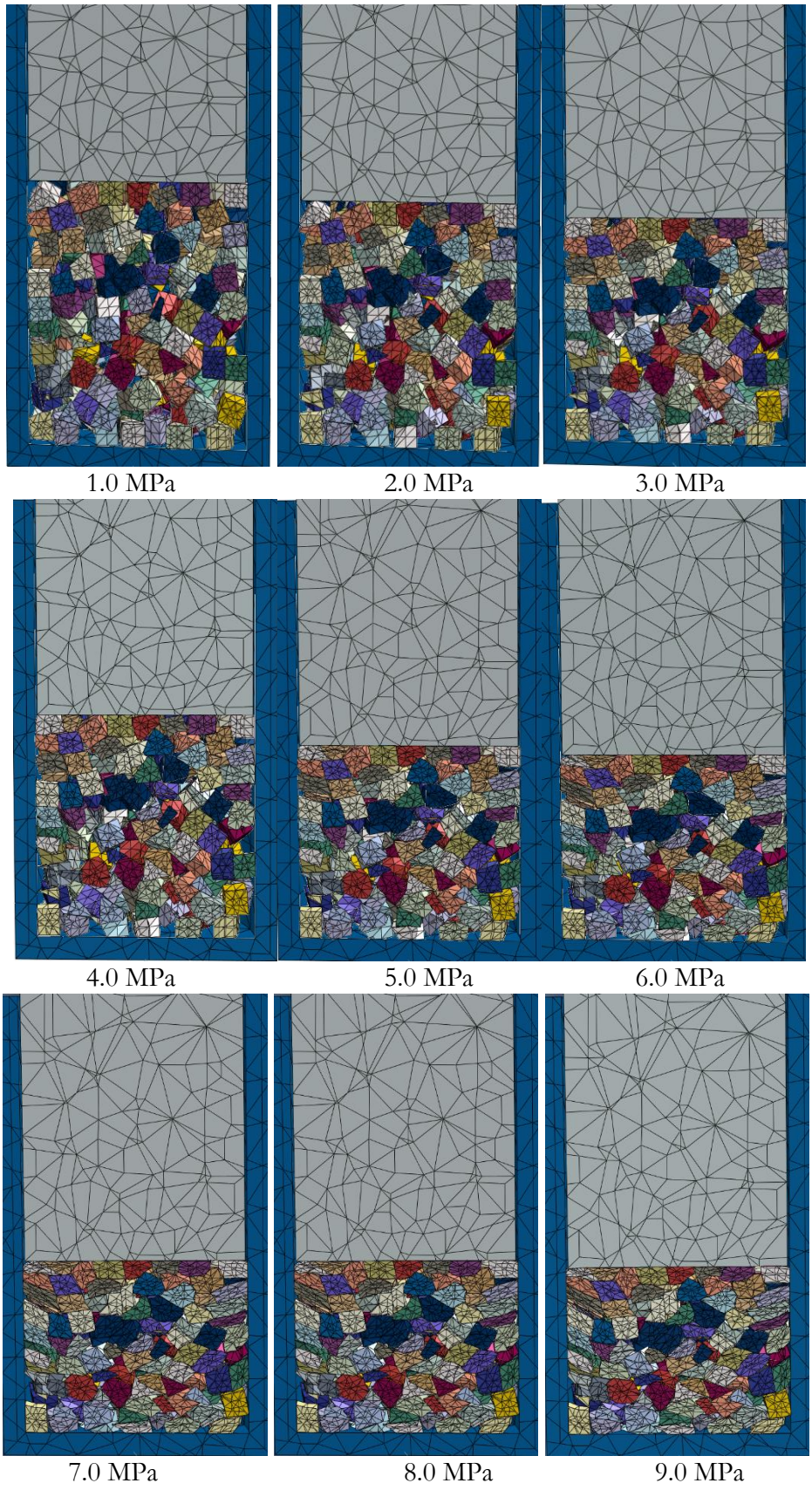

Figure 5.2: Finite element model results depicting the deformed particles at each stress level from 1.0MPa to 9.0 MPa after single layer impaction at the end of the 60th impaction cycle

The final bulk modulus, surface area post impaction and fill ratio were calculated and summarised in Table 5.1 for all simulations with 60 cycles constant stress level. The total surface area of the particles before impaction was calculated to be 60375.00 mm^3, which accounts for a pre impaction fill ratio of 48.80 %.

Stress in MPa	Instantaneous Modulus in MPa	Total Surface area of bone grafts in mm^3	Fill Ratio after impaction in %
0	0	60375.00	48.80
0.5	38.25	59972.91	52.57
1	57.59	60010.02	54.82
1.5	78.38	60081.20	56.36
2	115.54	60072.62	58.96
2.5	144.78	60109.03	61.68
3	179.54	60096.19	64.03
3.5	214.70	60197.73	66.06
4	251.71	60217.55	68.26
4.5	282.33	60273.36	70.44
5	318.30	60369.66	71.38
5.5	370.44	60492.05	69.98
6	413.33	60708.08	69.34
6.5	444.50	60801.47	69.52
7	457.51	60859.42	68.52
7.5	483.40	61028.32	68.67
8	476.67	61501.98	68.35
8.5	507.84	61487.27	65.75
9	501.78	61372.09	66.09

Table 5.1 Results of the first phase of computational simulation with 60 constant stress impactions.

It can be observed from Table 5.1 that at the lowest stress level of 0.5 MPa, there is not much of an increase in fill ratio, which only increases from 48.8 to 52.57% with an estimated instantaneous bulk modulus of 38.24 MPa. As the stress is increased, the increase in bulk modulus and the fill ratio is linear till the stress level reaches 2.5 MPa. As the stress is increased from 2.5 to 3.0, there is an increase in the fill ratio from 61.6% to 64%, which is the highest increase between two stress levels. Beyond this stress level, the fill ratio increases to a maximum value of 71.38 at 5.0 MPa stress level, after which there is no increase of the fill ratio beyond the stress level. There is a

decrease in the fill ratio after 5.0 MPa stress, although an increase in the instantaneous bulk modulus was observed. Additionally, sustained stress deforms the bone grafts, thereby increasing the surface area of the bone grafts, which was used to calculate the deformation of the bone grafts in the simulation. The highest increase in modulus can be found at a stress level of 9.0MPa which accounts for a 1.05% increase in surface area.

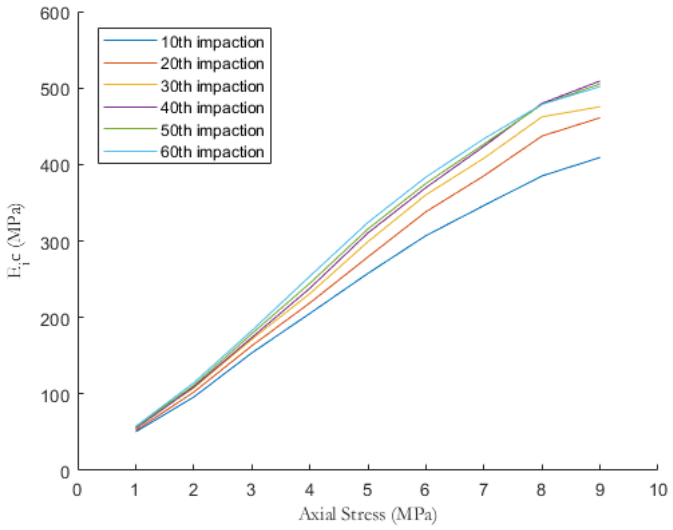

Figure 5.3 Graph depicting the increase in bulk modulus at the end of 10th, 20th, 30th, 40th, 50th & 60th impaction

Figure 5.3 shows that at lower stress levels, consecutive impaction cycles shows a linear increase in accumulation of modulus. As the stress level is increased, the differences between consecutive impactions become evident. The graph shows that the most instantaneous modulus of the particles occurs in the first 30 impaction cycles. Impacting the particles beyond the first 30 impactions, the increase is negligible. Similarly, comparing the fill ratio with the axial stress against all computational simulations from Figure 5.4 (a), it can be observed that the fill ratio increases from 52% at 0.5 MPa to 71.2% at 5.0 MPa axial stress. After which, the curve turns to flatten till 6.0 MPa. Then the fill ratio decreases up to 4% when the axial stress is increased to 9.0 MPa. This

could result from the bone grafts being subjected to excessive deformation at the distal end in contact with the cylinder and the proximal end in contact with the impactor.

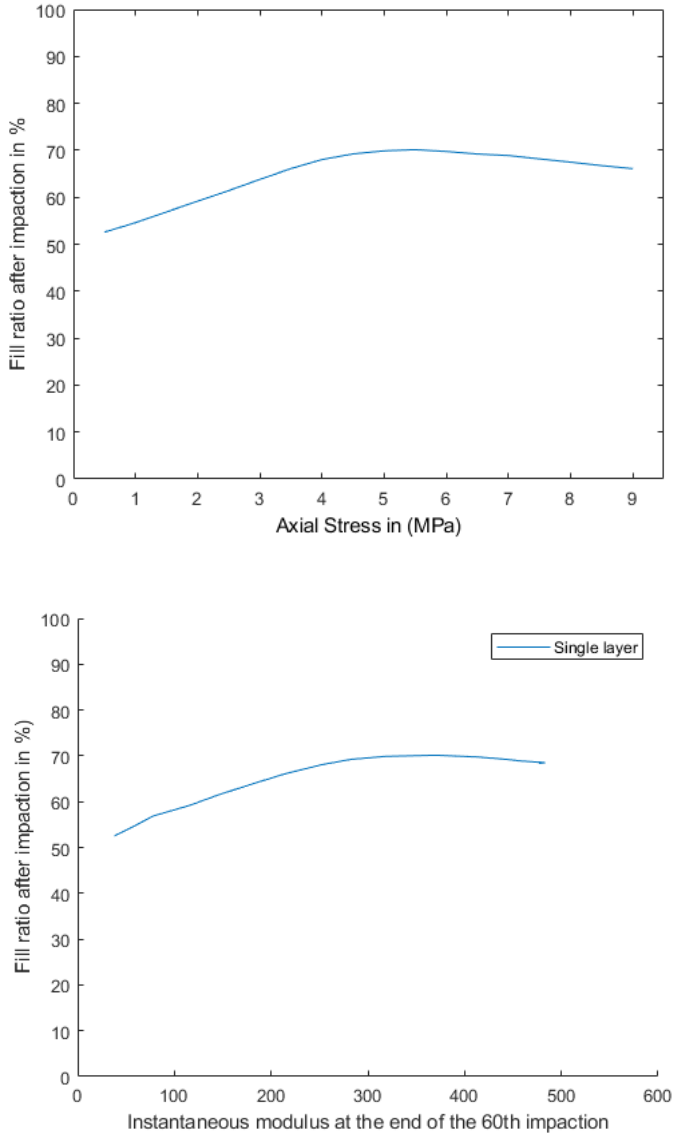

Figure 5.4 Graph depicting (a) increase in fill ratio after impaction against the axial stress and (b) fill ratio vs bulk modulus at the end of 60 impaction cycles.

A similar curve can be found in Figure 5.4 (b), which compares the rise of fill ratio compared against the instantaneous bulk modulus. It can be seen from the graph that the fill ratio increases as the bulk modulus accumulate to around 300 MPa. After which, an increase in axial stress does not have an increasing effect on the fill ratio; even though the bulk modulus increases, there is no

increase in the fill ratio. The fill ratio stays almost constant between 300 and 400 MPa, after which the fill ratio starts decreasing.

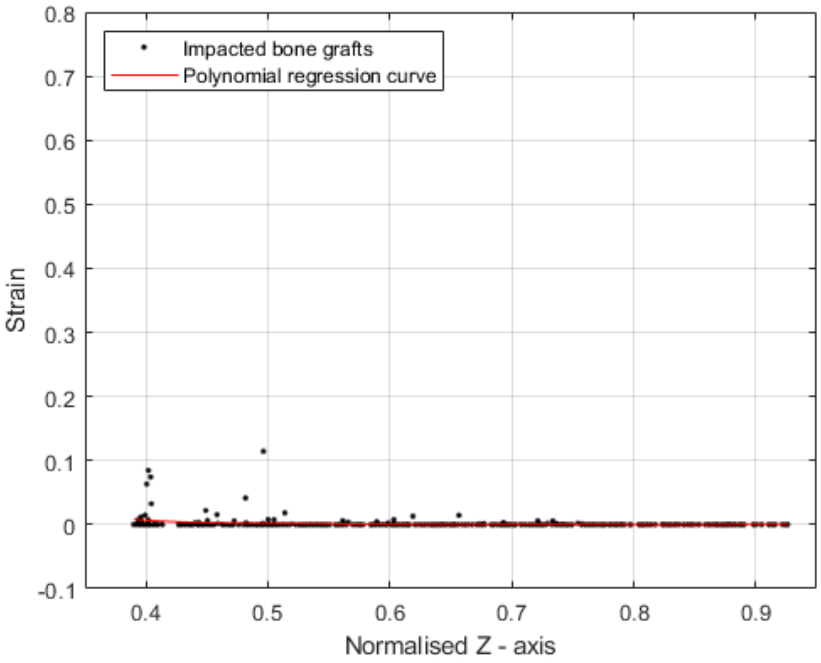

(a) 1.0 MPa

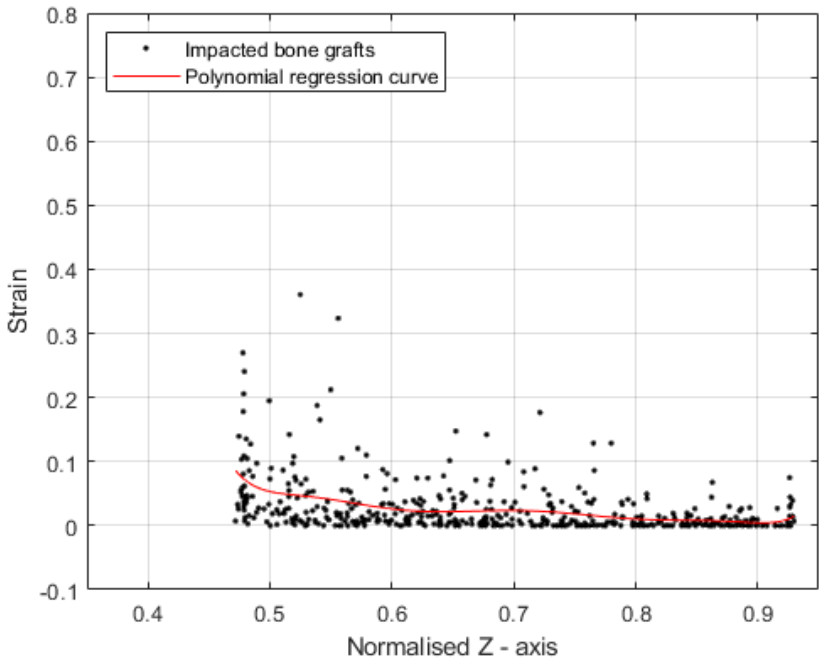

(b) 2.0 MPa

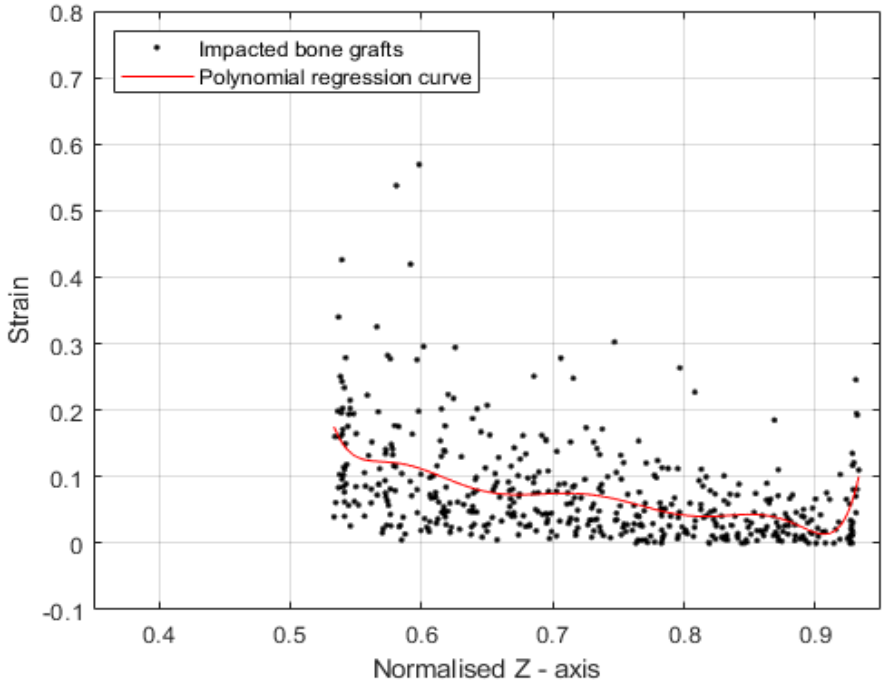

(c) 5.0 MPa

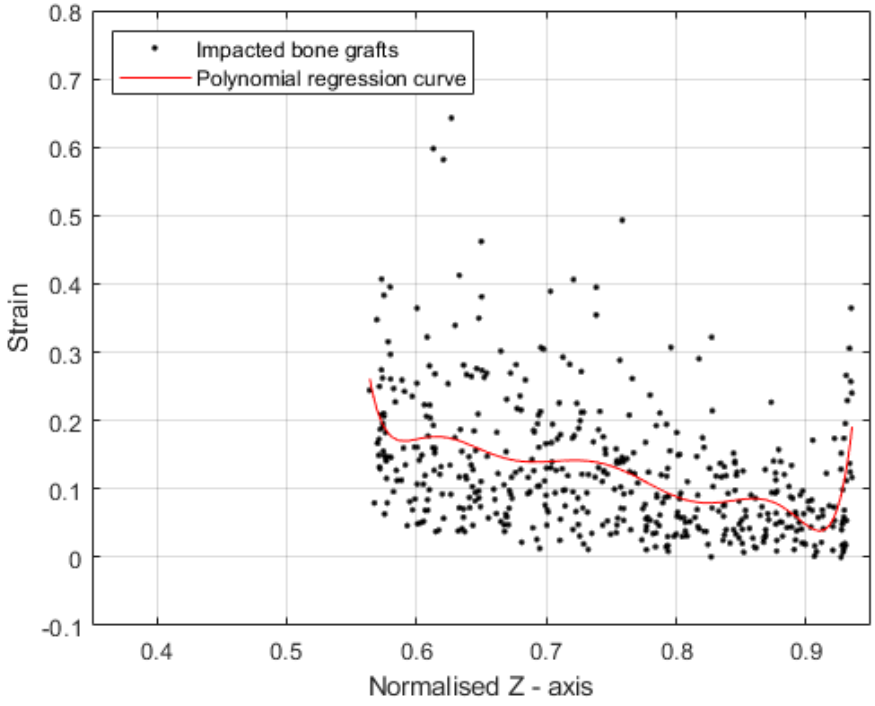

(d) 7.0 MPa

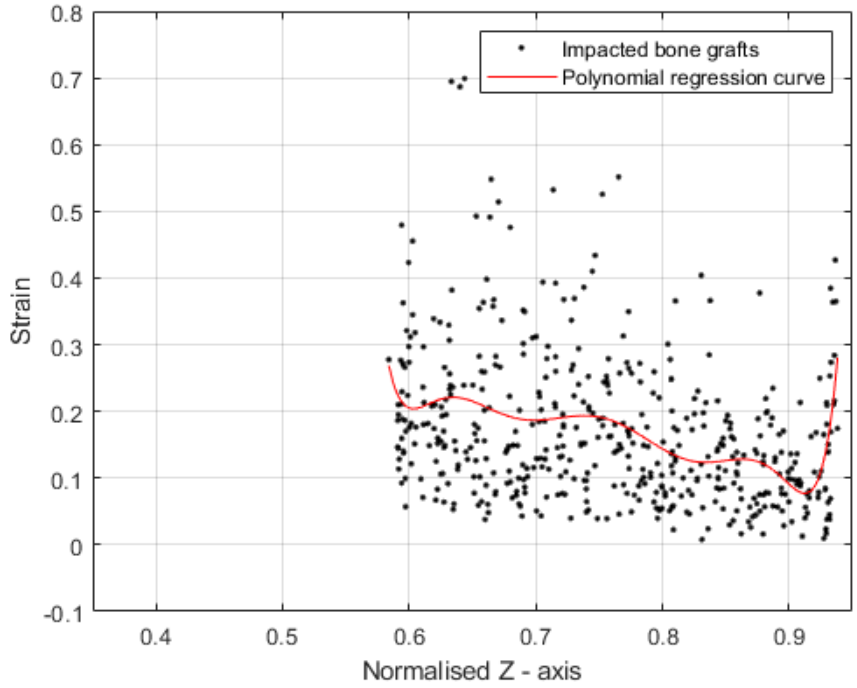

(e) 9.0 MPa

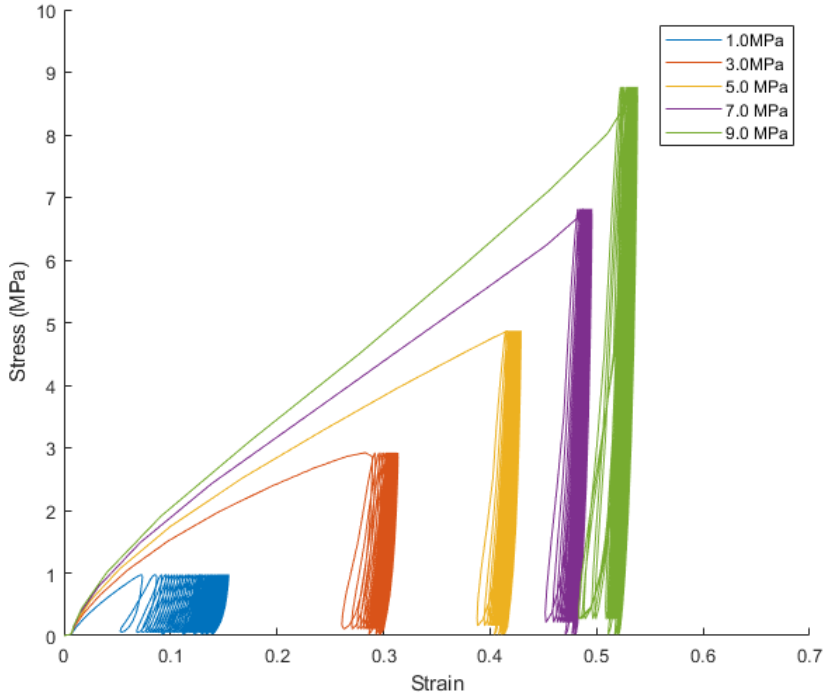

(f)

Figure 5.5 Accumulated permanent plastic strain in each bone graft particle after 60 impaction cycles from the proximal end (impactor – 0.4) to the distal end (base of the cylinder – 0.95) at stress levels of 1.0MPa (a), 3.0MPa (b), 5.0MPa (c), 7.0MPa (d) & 9.0MPa with a 9th degree polynomial regression curve and the average accumulated strain across the bone graft at similar stress levels (f)

Figure 5.5 (a) – (e) shows the accumulated permanent plastic strain distribution for all grafts on a scatter plot with a regression curve fitting line. At lower stress levels, the permanent plastic strain accumulation is distributed only through low, with an increase in strain observed only at the distal end of the cylinder. The accumulated permanent plastic strain increases as the stress levels are increased to 3.0 MPa. The distribution of strain increases further down the bone grafts; however, the distribution is not uniform and tends to concentrate more on the proximal end than the distal end of the bone grafts. At 5.0 MPa stress level, the increase in strain can be observed at both ends of the cylinder, with the bone grafts in the middle accumulating a lower strain than the two rigid ends. At stress levels beyond 5.0 MPa, the strain continues to increase at the two ends of the cylinder and continues to stay lower at the centre of the cylinder. Looking at the stress vs strain graph from Figure 5.5(f), at 1.0 MPa stress level, there is a total accumulated strain of 0.15. The hysteresis loop from this stress level starts at 0.05 strain and keeps increasing till the last loading cycle at the same stress level. At 3.0 MPa, the bone grafts accumulate a total strain of 0.3. At 5.0 MPa, the strain accumulated is 0.4, and at the final two stress levels of 7.0 MPa and 9.0 MPa, the accumulated strain is in the range of 0.45 – 0.55 As the stresses are increased, the hysteresis of the bone grafts reduces, with the first impaction cycle accumulating the largest jump in strain accumulation. Subsequent impaction cycles increase the strain, but their rate of increase decreases considerably as the stresses are increased. The difference in the accumulation of strain between stress levels decreases as the stresses increase beyond 5.0 MPa. The cyclic hysteresis loops followed by the simulations show that impacting the bone grafts at lower stress levels shows more hysteresis than impacting the bone grafts at higher stress levels.

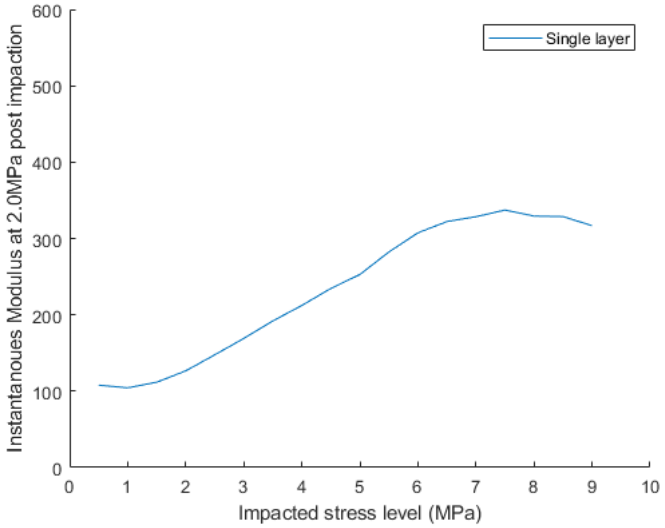

(a)

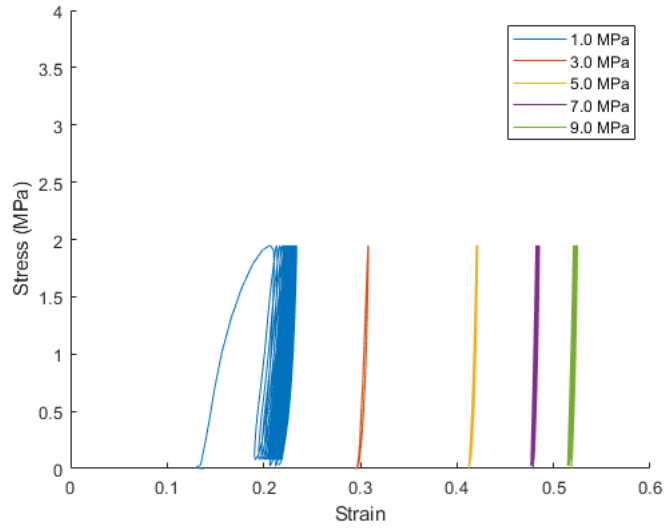

(b)

Figure 5.6 Graph depicting the resultant instantaneous bulk modulus (a) and accumulated permanent strain at 1.0, 3.0, 5.0m 7.0 and 9.0 MPa (b) post impaction when subjected to loading at 2.0MPa

A set of 18 simulations was run, with the results from the initial 60 cycles and a further 30 cycles at 2.0MPa, and the responses obtained from them can be seen in Figure 5.6 It can be observed from the graph that for the tests performed at less than 2 MPa stress levels when subjected to 2.0 MPa physiological stress, the grafts undergo further impaction. At stress levels beyond 2.0 MPa when subjected to loading conditions on these bone grafts after impaction, their resultant bulk modulus of the particles keep increasing from a little over 100 MPa to 346 MPa on particles

impacted with stresses up to 7.0 MPa. After which, the graph starts to stabilise, fluctuating between a maximum of 340 MPa to a minimum of 312 MPa on bone graft particles impacted beyond 7.0 MPa stress level. The accumulated strain values from Figure 5.6(b) show that the bone grafts undergo further impaction when subjected to physiological stresses if they are impacted at stresses less than 2.0 MPa beyond which there is little to no further accumulation of strain when subjected to physiological stress; however, their average strain level depends on the prior loading to when the bone grafts were impacted.

5.4.1. Layered impaction bone grafting results

A series of nine simulations were run where the bone grafts were split into two groups and impacted in two layers with impaction stresses ranging from 0.5 MPa to 9.0 MPa. The results from the simulations under 5.0 MPa showed that they followed a similar trend to the experimental results. However, the simulations recorded very high deformations at stress levels beyond 5.0 MPa, as seen in Figure 5.6. Although the impaction stresses in literature go up to 17kN, there are reports which suggest that the average impact stress exerted by a surgeon is in the range of 3.5kN. To ensure the validity of the results are in the range of the experiments, henceforth, only simulations with stress levels up to 5.0 MPa are only reported. As seen in Figure 5.7, the results show that at stress level 1.0 MPa, the particles are still intact and undergo very low to no deformation. Some deformation can be seen at a 2.0 MPa stress level right next to the impactor. However, there does not seem to be much deformation occurring beyond the first few bone grafts, which are near or in contact with the impactor. At 3.0 MPa stress level the deformation starts accumulating near the impactor, the end of the first layer and at the end of the cylinder. As the stress levels 4.0 MPa & 5.0 MPa, the deformation in the particles increases substantially with the first layer of impaction accumulating deformations in the centre of the cylinder and the second layer of impaction accumulates deformation in the particles near the rigid edges.

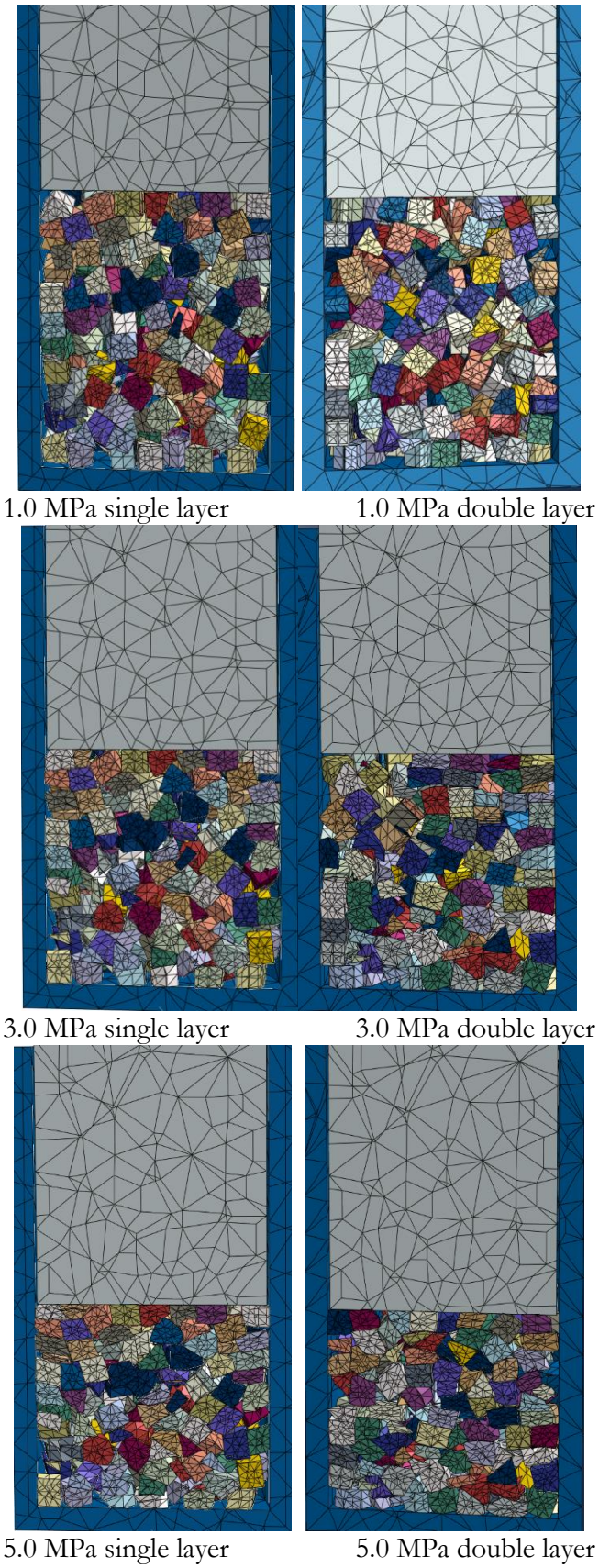

Figure 5.7 Finite element model results depicting the deformed particles at 1.0MPa, 3.0 MPa 5.0 MPa stress levels compared between single and dual-layer impaction at the end of the 60th impaction cycle

Comparing a single layer impaction and dual-layer impaction from Figure 5.8, the overall bulk modulus achieved from impacting the bone graft in the layer is lower than a single layer impaction.

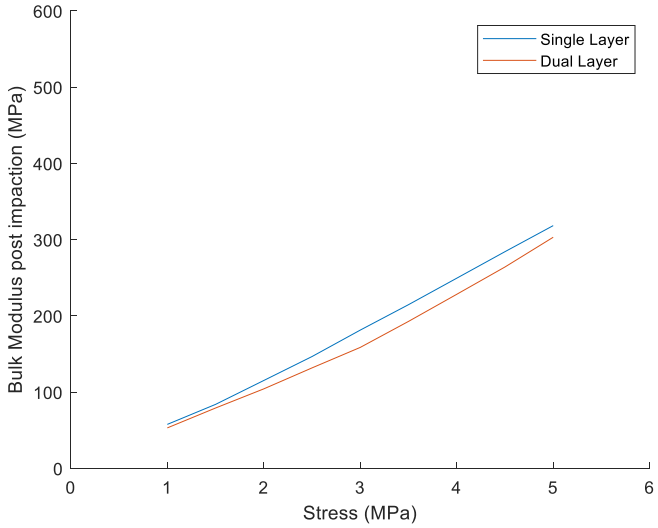

Figure 5.8 Graph comparing the increase of bulk modulus over increased Axial stress at the end of 60 impaction cycles between single layer impactions and dual-layer impaction

The results from the layered impaction were also compared with the single-layer impaction in terms of the change in the fill ratio at their stress levels and the effect of fill ratio vs instantaneous modulus. These results can be observed in Figure 5.9. It can be seen from the two graphs that the results from both single layer impaction and dual-layer impaction have a similar rate of increase in fill ratio up to 5.0 MPa. Looking at the bulk modulus, it can be observed that a single layer impaction reaches a higher bulk modulus than the dual-layer impaction. However, dual-layer impacted bone grafts show an increase in the fill ratio whilst accumulating a lower modulus.

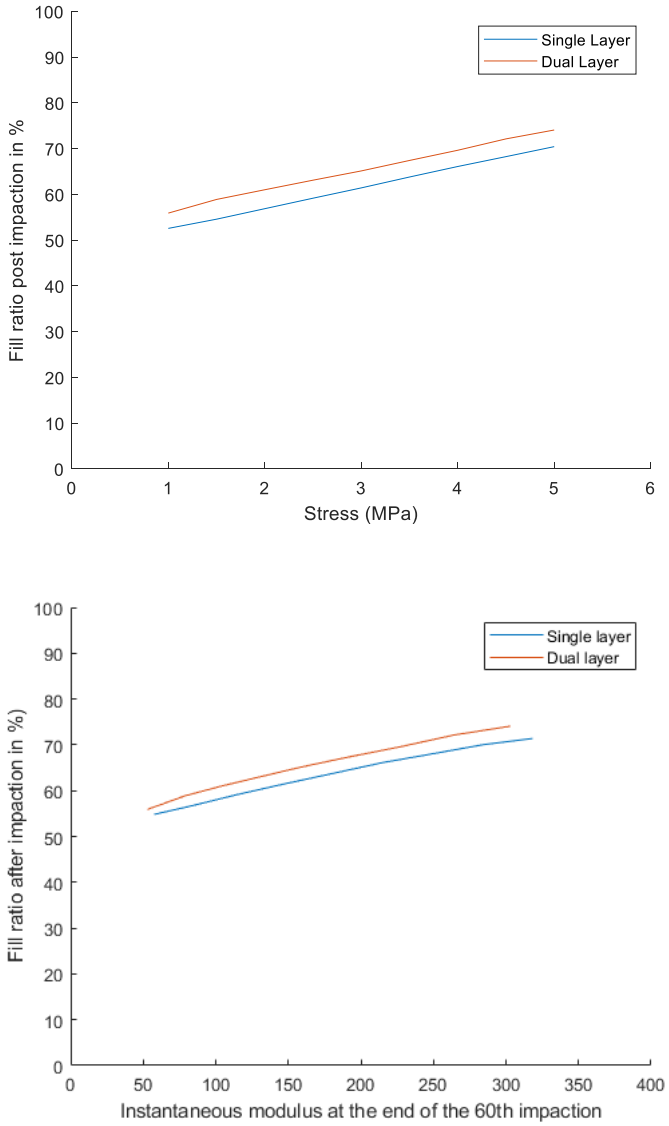

Figure 5.9 Graph comparing (a) increase in fill ratio after impaction against the axial stress and (b) fill ratio vs bulk modulus between single layer impaction and dual-layer impaction.

The models impacted in two layers of bone grafts were impacted further another 30 cycles at a physiological loading level of 2.0 MPa and compared with the single-layer impaction results from Figure 5.5. It can be observed from figure 5.10 that the results from the dual-layer impaction provide a lower increase in modulus as compared with single-layer impaction at the physiological load. The difference in the achieved modulus increases as the stress level increases. The dual-layer impacted bone grafts reach their peak at 250 MPa when compared with the single-layer impacted bone grafts, which peak at around 350 MPa. It can be noted from the graph that both single layer and dual-layer impacted bone grafts achieve the maximum modulus at physiological load when

impacted at 5.0 MPa. Comparing the accumulated strain between single and double layers, it was observed that the accumulated strain values in the double-layer impaction are higher than the single-layer impaction. There was little to no strain accumulation observed when the bone grafts are subjected to physiological loading stresses of 2.0 MPa after impacting at stresses beyond 2.0 MPa.

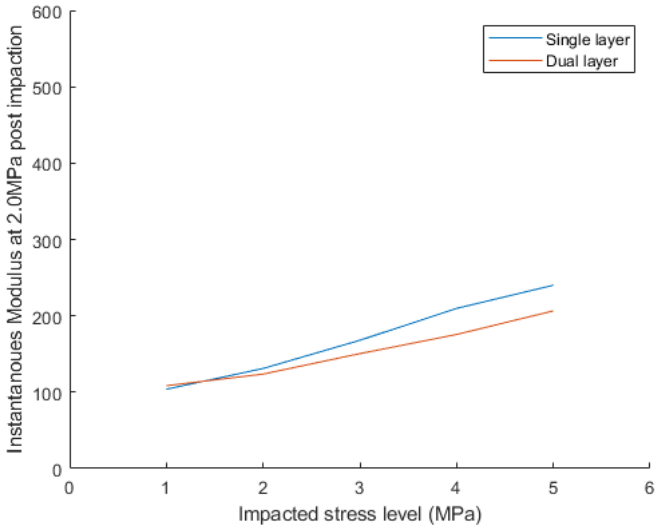

(a)

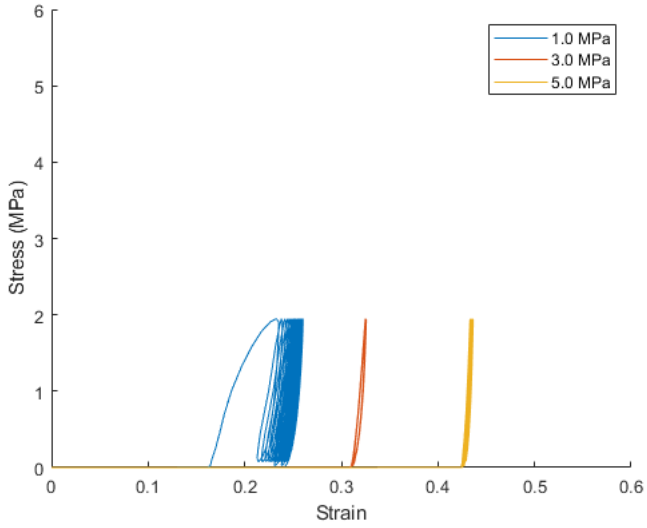

(b)

Figure 5.10 Graph comparing the resultant instantaneous bulk modulus (a) and accumulated permanent strain at 1.0, 3.0 & 5.0 MPa stress levels (b) post impaction with when subjected to loading at 2.0MPa between single layer impaction and dual-layer impaction.

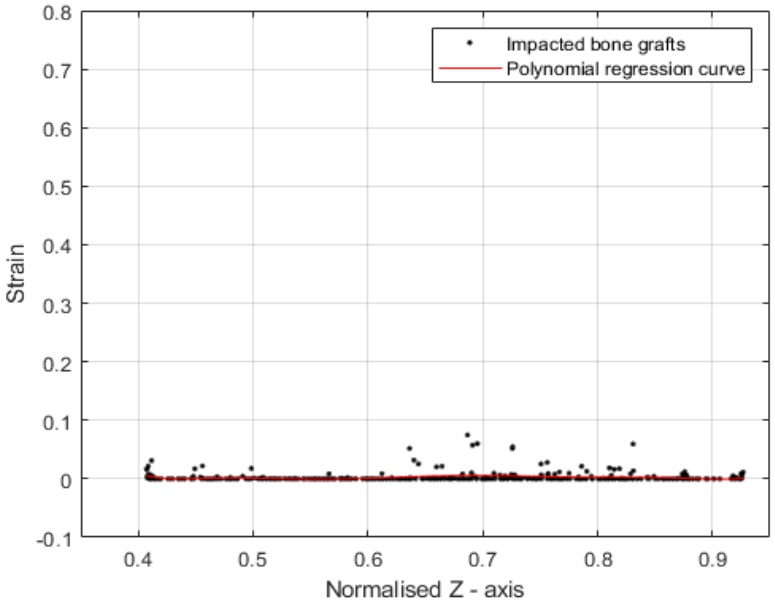

a) 1.0 MPa

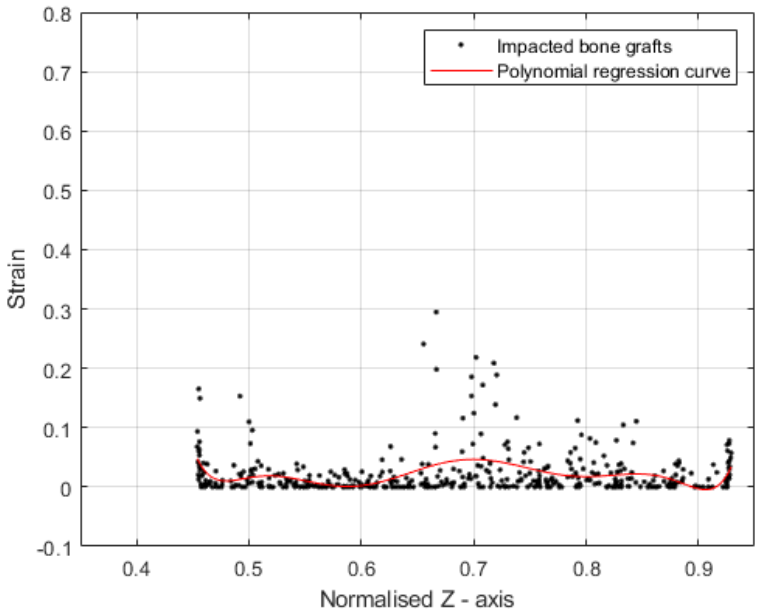

b) 2.0 MPa

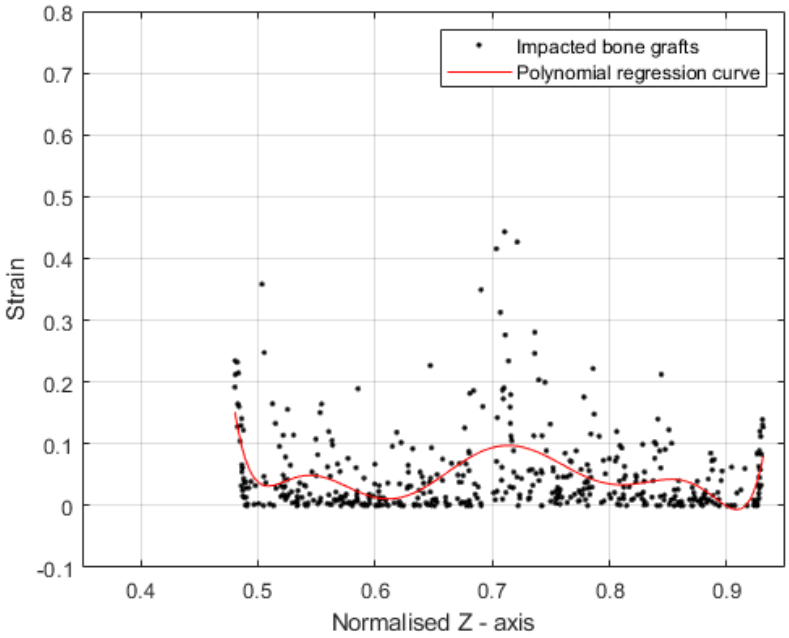

c) 3.0 MPa

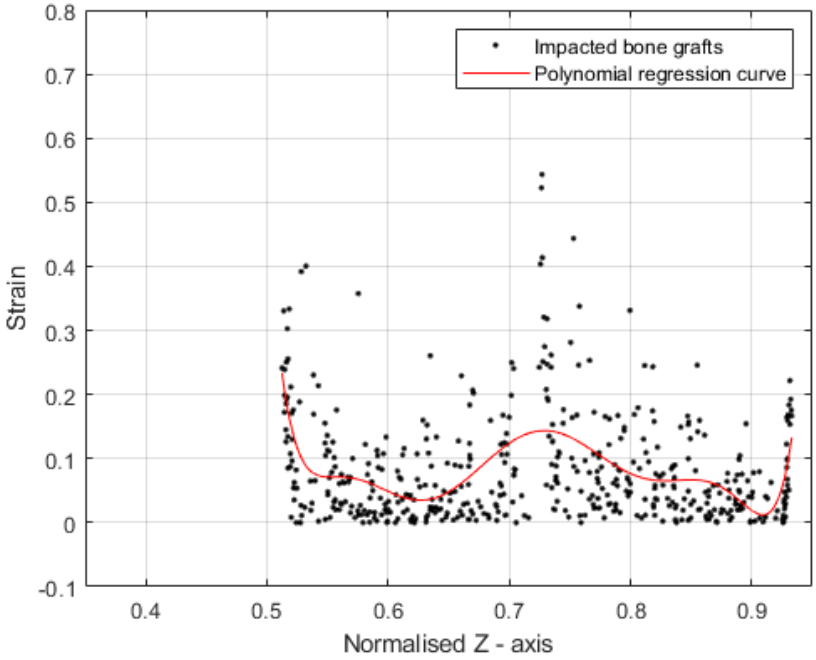

d) 4.0 MPa

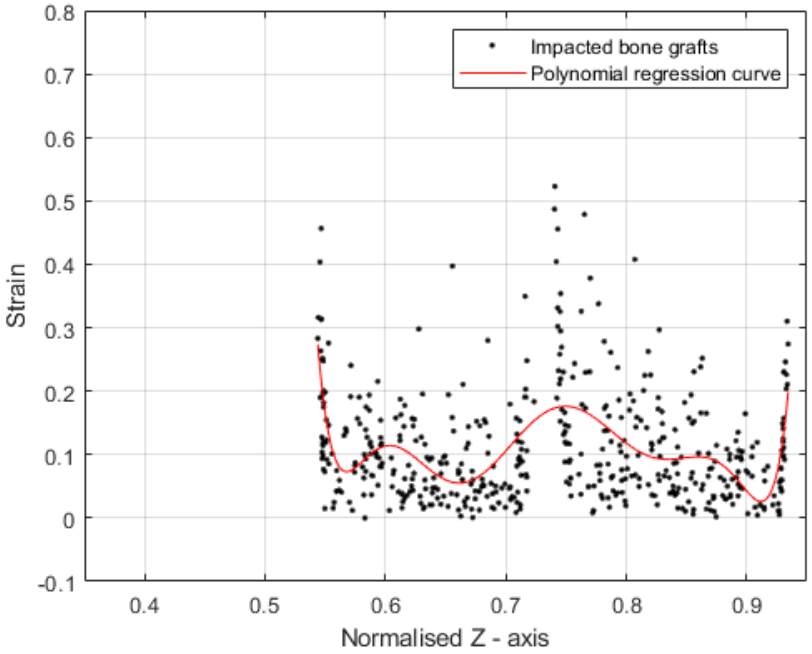

e) 5.0 MPa

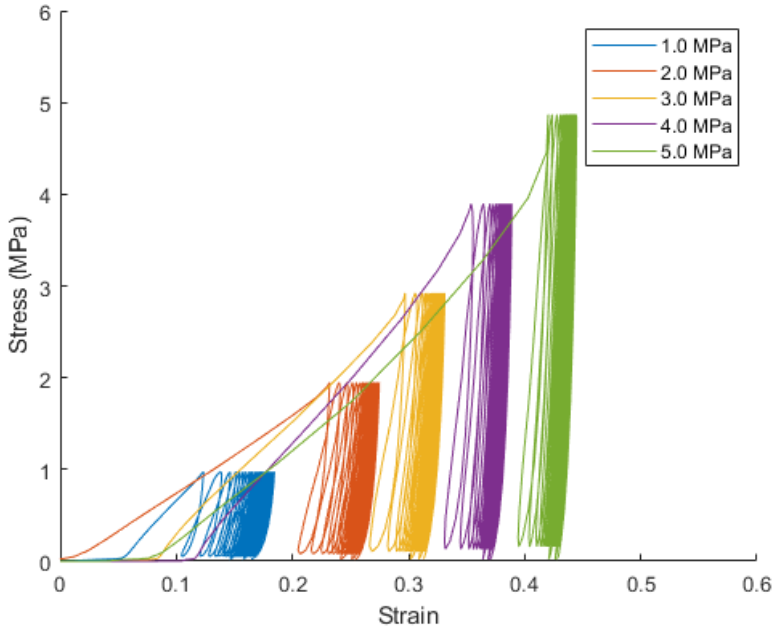

f) 1.0 MPa – 5.0 MPa

Figure 5.11 Accumulated permanent plastic strain in each bone graft particle after impaction in two layers with 30 cycles per layer from the proximal end (impactor – 0.4) to the distal end (base of the cylinder – 0.95) between stress levels of 1.0MPa - 5.0MPa (a – e), with a 9th degree polynomial regression curve and average accumulated strain across the bone grafts at similar stress level (f)

Figure 5.11 (a – e) shows the distribution of permanent plastic strain for all grafts on a scatter plot with a regression curve fitting line. The permanent plastic strain accumulation is distributed better

at the first layer than the second layer at lower stress levels. However, the accumulated strain is low, with an increase in strain propagated better in the first layer than in the second layer. The accumulated permanent plastic strain increases as the stress levels are increased to 3.0 MPa the distribution of strain can be observed at the distal end of the cylinder, the proximal end of the first layer and the proximal end of the second layer. The regions between these three locations accumulated less strain than their counterparts. At 5.0 MPa stress level, the increase in strain can be observed at both ends of the cylinder with the bone grafts in the proximal end of the first layer accumulating a lower strain than the two rigid ends but higher than the distal end of the second layer and the middle region of the first layer. Looking at the stress vs strain graph from Figure 5.11 (f), it can be seen that at the 1.0 MPa stress level, there is a total accumulated strain of 0.18 which is higher than the single-layer impaction, the hysteresis loop from this stress level starts at a higher 0.1 and keeps increasing till the last loading cycle at the same stress level. At 3.0 MPa, the bone grafts accumulate a total strain of 0.32, and at 5.0 MPa, the strain accumulated is 0.43. The accumulation of strain in the dual-layer impaction is like that of the single-layer but at a slightly higher rate than single layer impaction. The cyclic hysteresis loops followed by the simulations are like single layer impaction showing that impacting the bone grafts at lower stress levels shows more hysteresis than impacting the bone grafts at higher stress levels.

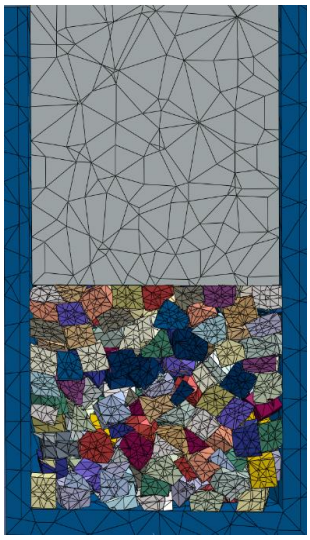

10th impaction single layer

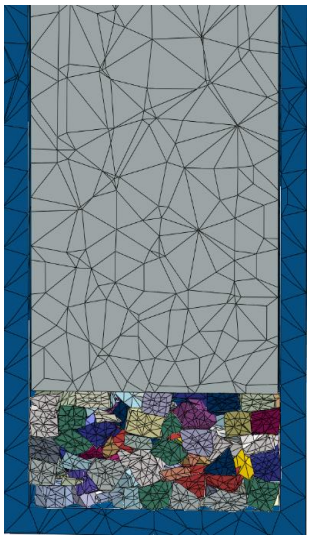

10th impaction – first layer, dual-layer

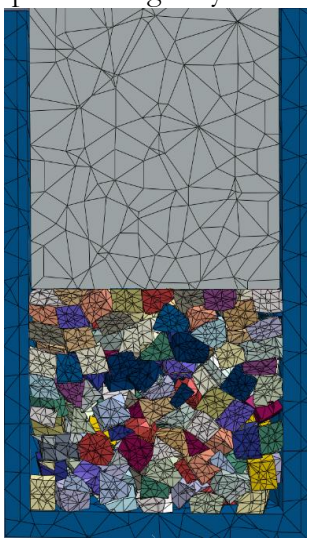

20th impaction single layer

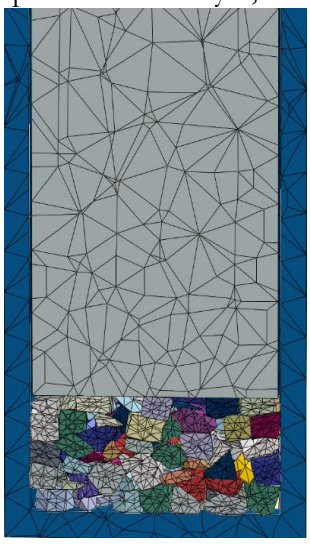

20th impaction – first layer, dual-layer

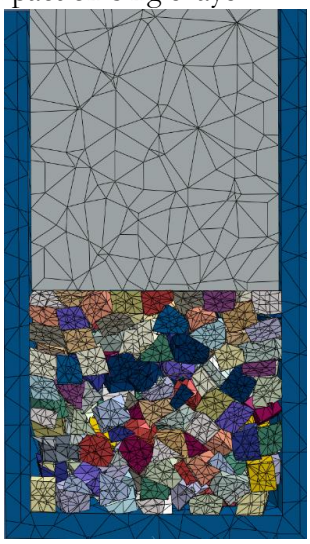

30th impaction single layer

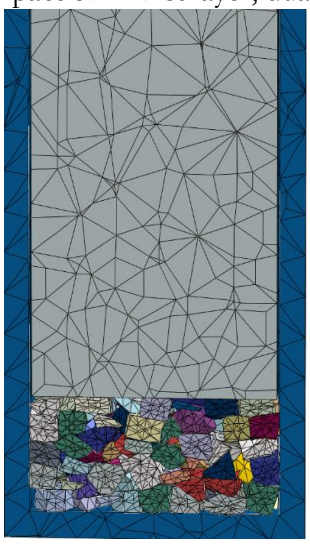

30th impaction – first layer, dual-layer

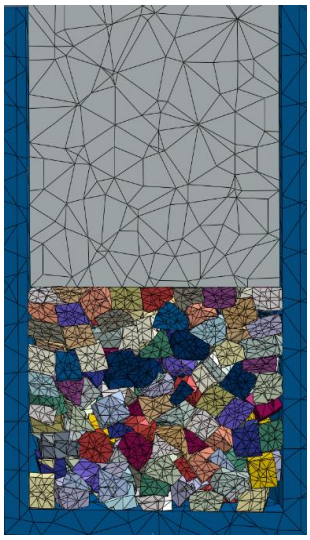

40th impaction single layer

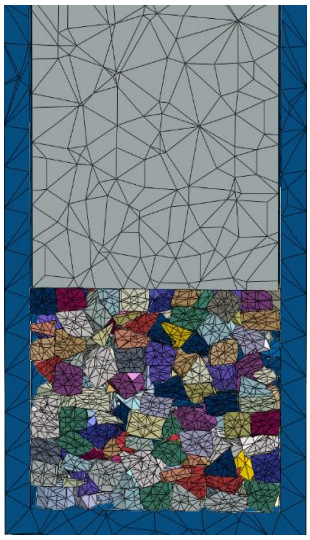

10th impaction – second layer, dual-layer

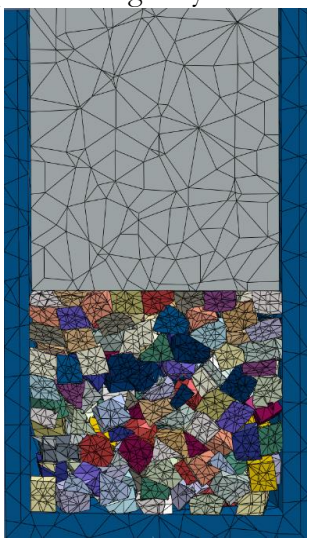

50th impaction single layer

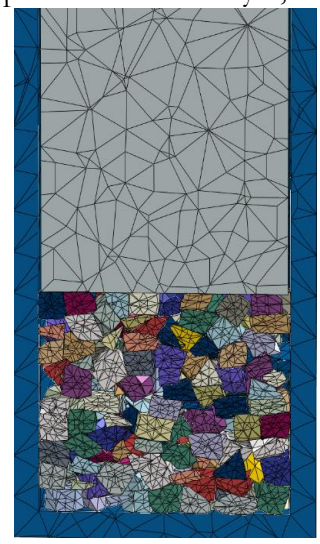

20th impaction – second layer, dual-layer

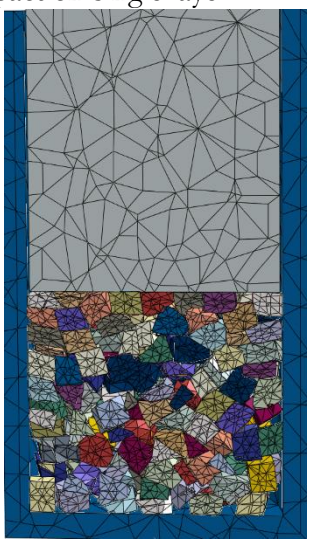

60th impaction single layer

30th impaction – second layer, dual-layer

Figure 5.12 Finite element model results depicting the deformed particles at 5.0 MPa stress levels compared between single and dual-layer impaction at the end of 10th, 20th, 30th, 40th, 50th & 60th impaction cycle

The progression of deformation through the impaction cycles at 5.0 MPa for the single-layer impaction and dual-layer impaction can be seen in Figure 5.12. In the single-layer impaction, the particles are being impacted as the number of impactions increases, and the particles deformation increases. However, the deformation is accumulated only at the ends near the impactor and at the end of the cylinder from the impaction number 30 and above. In the double-layer impaction, on the other hand, the first 30 impaction cycles are concentrated on the first layer of the bone grafts, which get impacted thoroughly, and the deformation in the particles are evenly distributed in the first layer of the impaction. As the second layer is introduced, the top layer of particles gets compacted, but there is not much difference observed in the bottom layer of the bone grafts. Only the top layer of the bone grafts close to the impactor undergoes deformation throughout the impaction cycles on the second layer.

5.5. Discussion

In this study, the data from the computational model was analysed to investigate the influence of impact stress, the number of impactions and the influence of layered impaction technique on the fill ratio, the bulk modulus and the accumulated permanent strain. The study looked at the behaviour of these bone grafts during impaction, post impaction, and at physiological stress levels were also analysed in terms of accumulated permanent plastic strain, bulk modulus and deformation to further understand the mechanical behaviour of the bone graft.

Analysing the permanent plastic strain and the deformation of the particles (Figure 5.5), the results from the study revealed that stresses less than 3.0 MPa does not compact the bone grafts. It only compresses them and rearranges them between the gaps in the chamber and in-between particles. This can be seen from the strain data from Figure 5.5 (a), where there is little to no permanent strain accumulated from the particles at 1.0 MPa, Figure 5.5 (e) suggests that the hysteresis loops from the graft keep continue to increase when impaction suggesting that they are not being

compacted at 1.0 MPa adequately. It is necessary to impact the bone grafts to the expected physiological stress level. If this does not occur at initial loading, further compaction will happen in the bone grafts resulting in the implant migrating through the graft. Though there is an accumulation of permanent strain in the particles at 2.0 MPa stress levels, there is very minimal deformation in the particle, as seen in Figure 5.5. When the impaction stresses were increased beyond 5.0 MPa, the particles were not uniformly deformed; only some of the particles yield and permanent deformation takes place. As seen from Figure 5.5(a - e), this results in some particles accumulating a permanent strain value twice as much as the average strain. The number of outliers increases, moving further away from the average permanent strain values as the stresses are increased beyond 5.0 MPa.

The majority of the consolidation in the particles occurs in the first 10 to 20 loading cycles which record the highest increase in bulk modulus (Figure 5.2**Error! Reference source not found.**) and p ermanent strain accumulation (Figure 5.5), continuing beyond 30 impaction cycles has no benefit. The higher the stress, the higher the increase in bulk modulus and permanent plastic strain achieved. Impacting the bone grafts beyond the 10 cycles does provide an increase in bulk modulus and permanent plastic strain when the stresses at which the bone grafts are impacted is increased beyond 4.5 MPa below that, the plastic strain does not make a significant difference in modulus (Figure 5.2). Impacting the bone grafts for 10 cycles is sufficient to achieve 90% of the bulk modulus for the stress level.

Under physiological loading conditions Figure 5.6 shows the variations of bulk modulus observed as a function of initial impaction stress. The bulk modulus below 2 MPa impaction stresses is less than the bulk modulus at 2 MPa. As a result, the particles undergo further impaction when subjected to normal physiological loading conditions, and this would result in subsidence of the implant. Again, this can be again seen in the strain graph from Figure 5.6 (b), where there is hysteresis at 1.0 MPa. By looking at the strain values of those bone grafts impacted at stresses

beyond 2.0 MPa, there is little to no strain accumulations showing that the bone grafts have been compacted enough to constitute a stable graft. Hence, for tibial impaction, the ideal impaction stress for impaction bone grafting should be higher than 2.0 MPa so that the bone grafts are impacted adequately to sustain/support the expected physiological stresses. From a general perspective, the mechanical environment of the graft must be assessed to identify the likely stress levels and then impaction needs to be done at similar or higher stress levels. The stresses the bone grafts need to sustain in physiological conditions for an acetabular cup in revision hip replacements or the stresses that the bone grafts must sustain to support a femoral stem may well be different. Hence it is necessary to assess the typical loading level of the implant specific to the region and impact the bone graft at higher stress levels to adequately impact the bone grafts.

Impacting the bone grafts at stresses higher than 5.0 MPa results in some particles being impacted more than others and can be outside the range achievable by a surgeon in a clinical scenario, which is explained later in the discussion. This can be seen from the results of the fill ratio (Figure 5.3 (a)) and instantaneous bulk modulus (Figure 5.3 (b)), where the fill ratio and bulk modulus plateau's when the stress is increased beyond 5.0 MPa. This may be a consequence of the modelling assumptions used in the study. The simulations of the bone grafts were created using first-order elements. For first-order elements, though they are good at describing the strain or stress fields in the elastic range and with finite plastic deformation, they are less reliable when the meshes are subjected to large deformation, as seen in simulations where the stresses are increased beyond 5.0 MPa. Increasing the stress beyond 5.0 MPa results in extreme deformation occurring within the bone grafts. As a result, beyond 5.0 MPa, as seen from Figure 5.3 (a) & (b), the bulk modulus versus fill ratio response does not follow the same linear pattern. Looking at the stress vs the strain graph from Figure 5.5 (f), impacting the bone grafts at stresses beyond 5.0 MPa only results in an overall strain increase. Although, in theory, it constitutes a stable graft bed, it also crushes the bone grafts creating large un-even deformations within the graft, as seen from Figure 5.7. To account for the large deformations in the grafts, further analysis is required by refining the meshes using

higher-order elements to better capture the stress/strain field. In addition, to higher-order elements implementing an automated remeshing to limit the consequences of excessive deformations. Further experimental tests at higher stresses are required to see if the trends align with each other can help explain the behaviour of the simulations at stresses beyond 5.0 MPa. However, until further exploration is performed, the results from the simulations at stress levels beyond 5.0 MPa should be treated with caution.

Analysing the permanent plastic strain and the deformation of the particles in the dual-layer impaction technique (Figure 5.7), the results from the study revealed that at stresses less than 3.0 MPa, there is no significant difference between the single and dual-layer impaction in terms of deformation. There is localised crushing of the bone, which can be seen in both the layers at stresses below 3.0 MPa. The strain plots from Figure 5.11 show that there is permanent stain accumulation around the bone grafts in contact with the impactor at lower stresses. At stress levels beyond 3.0 MPa, the strain accumulation is observed near the rigid ends of the cylinder in both layers of impaction. Some particles in this region undergo extreme deformation accumulating up to 60% strain at 5.0 MPa showing that they have been crushed severely. At the same time, the strain accumulation is spread out through the graft better in the dual-layer impactions as seen from Figure 5.11. This shows that the bone graft particles have been deformed more uniformly than the single-layer impaction, where the deformation was only observed in the localised regions. As seen from Figure 5.7 – Figure 5.11, the double-layered technique shows that layering impaction produces a higher average permanent strain whilst accumulating a lower final instantaneous bulk modulus. This is because of the localised crushing of the particles that occur twice in the dual-layer, one near the impactor and base of the cylinder in the first layer and the second near the impactor in the second layer. Sequential impaction of the lower layer ensures that the graft in the distal end of the cylinder is compacted before impacting the top layer resulting in a higher fill ratio than the single-layer impaction technique.

There have been many studies published on the magnitude of intraoperative impaction forces. The intraoperative forces from these studies are highly dependent on the set up which in turn is dependent on the rigidity of the setup. Heiney et al., (2009) studied the impact forces at the femoral head into a Morse taper and reported a mean impaction force exerted by an orthopaedic surgeon to be 4.4 kN, Nassutt et al. (2006) measured the assembly forces below the femoral head and found them to be in the range of 0.27 – 7.85kN. Based on these studies, it can be hypothesized that the average threshold forces that can be exerted by a surgeon using an impaction hammer between the head impactor and the bone grafts to be 8kN. Though there are studies that report impact forces as high as 17kN (Scholl et al., 2016; Wiebe et al., 2012), they were performed in a controlled experimental environment where the impaction location are rigidly fixed and did not account for the movement of the patient during impaction in the case of Wiebe et al. (2012). Or, the impaction forces are not measured at the head of the impactor and the bone grafts instead at the striking pad of the hammer in the case of Scholl et al. (2016). Hence, based on the literature and knowledge of experimental setups compared to the clinical environment, it is unlikely that the impaction forces at the impactor would exceed 10 kN. In this study, forces of the impactor were simulated up to 10 kN and the simulations from the model were able to capture the response of the bone grafts with good confidence. The diameter of the impactor used was 49mm and applying forces of 9.4 kN to the impactor resulted in 5.0 MPa stress which is higher than the stresses used in literature (0.5 - 3.0MPa) (Bavadekar et al., 2001; Brodt et al., 1998; Giesen et al., 1999; Heiner et al., 2005; Fosse et al .,2006; Phillips et al., 2006) and within the range of stresses easily achievable by surgeons. Hence, it can be hypothesised that impacting the bone grafts at 5.0 MPa achieves a higher impacted instantaneous modulus and permanent plastic strain than impacting bone grafts at lower stress levels.

However, there is another factor that needs to be considered. The surface area of the impactor in surgery varies, and so does the surface area of the graft bed. Hence the higher the surface area of the graft bed and impactor, the higher the forces required to generate the sufficient stress to impact at 5.0 MPa. The graft bed of a typical proximal tibia is conically shaped. As a result, when layered impaction is used, the forces required to reach peak stress of 5.0 MPa would be lower at the bottom layer than at the top layer. Comparing the surface area of the impactor used in this study to the proximal tibia, the surface area of the tibia is likely to be higher. As a result, the impaction stresses equivalent to 9.4 kN would be much lower. If the impaction forces a surgeon can generate is only 8 kN, then the this may be enough to impact the lower layers of the graft bed, but it will not be sufficient to impact the top layer of the proximal tibia. However, these assumptions are based on data for ovine bone grafts. The results from the single experiment with human cancellous bone show that a lot more compaction occurred in the human cancellous bone at lower stress levels. So, if human bone grafts use the surgeons are more likely to achieve the forces required to compact the graft.

In conclusion, this study studied the effect of impaction force and the number of impactions to understand what happens in the bone graft after each impaction. The accumulation of strain and the change in the fill ratio of the impacted bone were investigated. The study found that a minimum of 10 repetitions is needed to achieve 90% of its maximum stiffness for a given compaction force. The results from the study also showed that the model behaves as expected till the stresses are 5.0 MPa. The stress vs strain graphs at physiological loading conditions from Figure 5.6 (b) & Figure 5.10 (b) shows that the bone grafts behave like a linear elastic material. There was little to no increase in hysteresis when impacted at stresses 3.0 MPa and above. There is an argument that impacting the bone graft at 3.0 MPa is adequate and meets the criterion of a stable graft. However, impacting the bone grafts at stress levels higher than 3.0 MPa yields higher instantaneous modulus (Figure 5.1) and strain values (Figure 5.5(f) & Figure 5.11(f)). Impacting the bone graft at 4.0 MPa or 5.0 MPa stress levels can reduce the number of impactions needed

to achieve the maximum impacted modulus, which is achievable when impacted at 3.0 MPa stresses, thereby reducing the repetitions and reducing the time. Suppose the bone grafts are impacted at stresses under 2.0 MPa. In that case, there is a good chance the bone grafts are not adequately impacted and when subjected to physiological loading, especially when the stresses exerted on the bone grafts and implants can be more than 2 MPa. This could lead to implant migration, hence impacting the bone grafts in multiple layers help distribute the accumulation of strain between the bone grafts more evenly across the graft-bed and faster than the experimental in-vitro study in literature, which caps at 3.0 MPa.

Chapter 6 :

Overall Discussion

6.1. Discussion

Failure of hip and knee replacements is often accompanied by a problematic bone loss in the bone due to the removal of the failed implant. Impaction bone grafting has the potential to restore bone stock and reduce the size of the defect in the bones. However, the procedure is complex and achieving a stable impaction bone graft is hard due to the lack of understanding of how these bone grafts behave. Several studies have been done to understand the properties of bone grafts which were centred around hip replacements, though the process used in impaction bone grafting in knee replacements are similar. Current studies are focused on mechanical testing of bone grafts or numerical, which are created using a continuum modelling technique where any change in the composition of the model requires repeating the experimental test to validate and derive a new constitutive model. As a result, there is no standard technique that one could use to test, retest and explore the characteristics or the mechanical properties of bone grafts either in isolation or as a part of revision construct. This thesis examined the mechanical properties of bone grafts using experimental testing, replicated the response using a finite element model, it tuned and validated the model to match the experimental results. Finally, it used the computational model to explore the influence of the impaction procedure on the mechanical behaviour of the bone graft. The results from this study provide valuable information that will help explain and help the surgeons understand the properties of bone grafts and develop strategies to minimise the risk of failure in impaction bone grafting.

Clinically, the properties of bone grafts are highly variable based on the type, shape, composition, the additive contents in the used bones, and parameters related to impaction of the bone graft. For example, the shape of the construct, the position, and the area. To reduce variability in the tests, bones grafts were cut from femoral and tibial heads into identical shapes and sizes. This thesis examined and compared the response of bone grafts created from bovine and ovine bone grafts against existing literature by Phillips et al. (2006a). A comparison study was conducted with human bone grafts to compare the range of instantaneous modulus and accumulated strain between the different bone The study showed that human bone grafts accumulated a higher strain of 70% than bovine and ovine bone grafts, which accumulated a much lower strain of 2% (ovine) and 23% (bovine) whilst deforming and compressing less than the human bone grafts. The instantaneous modulus values achieved from all three types of bone grafts were 20 -140 MPa (bovine), 60 – 200 MPa (ovine), 19-100 MPa (human), which is consistent with data published in the literature (Voor et al., 2000a; Giesen et al., 1999; Fosse et al., 2006; Phillips et al., 2006; Verdonschot et al., 2001; Heiner et al., 2005; Cornu et al., 2003a; McNamara et al., 2006; Putzer et al., 2017). The overall mechanical behaviour from both ovine and bovine species behaved similarly to human bone grafts. Though the gold standard of grafting material remains to be autogenous bone grafts followed by allogenous bone grafts, xenogeneic bone grafts have become more popular to be used as a suitable replacement for human bone grafts. Xenogeneic bones are typically chemically cleaned and sterilised, resulting in a void of any living cells to promote bone regrowth. Chemical cleaning and sterilization may affect the mechanical behaviour of xenogeneic bone grafts, the bone grafts used in the study were not chemically cleaned or sterilised. However, xenogeneic bone grafts can be used as a substitute to fill the gap alongside autografts (Bow et al., 2019; Campana et al., 2014; Wang & Yeung, 2017).

Experimental testing has always been the gold standard in explaining the response and behaviour of materials in science. This provides insights into the materials with real data to confidently demonstrate findings in research. However, the major limitations of mechanical testing in impaction bone are that it's difficult to visualise what's happening inside the bone grafts during the test. Advanced computer modelling techniques can provide a realistic picture of bone grafts' underlying mechanical and physical properties. Though computational modelling techniques cannot replace the experimental testing concepts completely, they can be used to complement and expand the knowledge gathered from experimental tests. This thesis is one such example where the results from the final chapter give a better insight into what computational models are capable of. The results from the thesis show that when impacting a large defect, there were only localised crushing of the bone grafts at the top layer at stresses less than 3.0 MPa. At stresses above 3.0 MPa, the deformation of the bone grafts is move evident at the rigid ends of the cylinder, namely the point in contact with the impactor and the lower end of the cylinder. The reason for localised crushing is likely due to the rigidity of the impactor and the distal end of the cylinder. At these locations, there is a steep change in stiffness resulting in highly localised stresses. In other regions of the graft, the graft particles are elastically supported by other particles.

One of the limitations of this approach is that the use of bone grafts as cubes. In a clinical scenario, bone grafts do not come in a set standard shape but can be of various irregular shapes and sizes. However, in theory, using this computational model, it is easy to model any geometry of shapes and assign them with the material properties of bone grafts and fill it to study the influence of shape in impaction.

The second limitation of this study is that this research was performed predominantly using ovine and bovine bone grafts due to the availability. Ethically sourcing human bone grafts in quantities required for repeatable tests to capture their material properties and then simulate them into a computational model though difficult, would provide more clinical relevance. Alternatively, the

experimental apparatus can be modified and adapted to test using fewer resources to overcome resource shortages.

This thesis explored two different modelling techniques to model bone grafts for impaction bone grafting (DEM & FEA). A finite element method (FEA) by modelling each bone graft particle as a separate entity was deemed the best and most logically plausible approach. DEM or Discrete element modelling is a powerful technique and has been used to perform very sophisticated analyses of some very complex material behaviour. Although, in theory, it seemed like a much more attractive and less processor-intensive approach, it was dismissed largely because to obtain an accurate prediction using discrete element analysis, there is a need to tune many parameters. These are parameters in simulations that cannot be directly measured and hence aren't available in the literature for the bone. Although computational models like finite element analysis are adapted more frequently to extend the knowledge of bones and better understand the theory of bone behaviours. One scenario would be where there is a need to tune many parameters even while using the finite element method, which has limited computational models. The flexibility in using finite element models in this thesis was the ability to use three parameters, namely young's modulus, friction, and yield strain to replicate the overall material behaviour of the bone grafts.

Predicting the accurate material properties for the bone grafts can improve our understanding of the bone's biomechanical behaviour. Using existing literature, the finite element model used in this thesis drew on three parameters; for Young's modulus, Poisson ratio, friction and plasticity, with the later fourth parameter plasticity component of the model is assumed as completely plastic. This idealised value was tuned to fit the experimental response. However, the limitation of the model is that the research performed relied on using ovine bone grafts due to the availability and ethical considerations for the use of human bone grafts. The results from the simulations of ovine bone grafts at high-stress levels beyond 5.0 MPa proved to be highly demanding for the first-order elements used in the model resulting in large deformations in the graft. The numerical model with

480 bone graft cubes meshed as 4 noded tetrahedral second-order elements drew a processing time of six hours whilst using eight CPU cores. The quality of the meshes could be improved by using higher-order elements, sequentially re-meshing the particles during the impaction process and perhaps, using a different plasticity model such as the ones used by (Kelly & McGarry, 2012). They assigned and provided two distinct loading paths in the von Mises-pressure stress plane and emulated a crushable foam model, which are much better at capturing localised crushing a material when compared to a metal-based yield criterion as used in the current model. Using their model could help simulate a much more accurate plastic deformation within each bone graft and help explain the stress-strain fields in the bone grafts more efficiently. Moreover, the experimental study shown in Figure 3.15 found that the human bone grafts have a lower bulk modulus and accumulated far more permanent plastic strain than ovine bone grafts at the same applied impaction stress. A mesh convergence study will better understand the FEA model and help verify the numerical model. Additionally, modelling the bone grafts using higher-order elements and sequential remeshing of the bone grafts will help explain the stresses and strain fields better when this model is used to capture the mechanical behaviour of human bone grafts. However, even though computational modelling has improved considerably in the past few years, modelling complex structures like bone are still computationally demanding. Building models with increased complexity would exponentially increase in time, resources, and computing power to complete each task.

In this thesis, the major variables based on mechanical properties that determine the response of the bone grafts were determined to be young's modulus, friction, and Yield strain. Though these factors do play an important role in the mechanical properties of the bone grafts, they are not the only factors contributing to a stable bed that is necessary to prevent failures in the replacement due to subsidence or resorption of bones. The other factors that could affect the stability of the bone grafts were preparation and impaction techniques. Variables based on the impaction technique was explored to analyse the impaction force and the number of impactions needed to

achieve a stable graft bed. The study showed that impacting the bone grafts in layers results in better consolidation of the bone grafts in the graft bed and an even distribution of the impact forces evenly to all the bone grafts in the graft bed. Impacting the bone grafts in two layers at a stress threshold of 5.0MPa for 20 impactions achieves a fill higher permanent strain than single layer impaction. The mechanical stability of the bone graft depends on the stiffness, strength, and cohesive properties of the graft. As a result, impacting the bone graft in layers improves the grafts mechanics in terms of strength. Hence, from a clinical point of view, impacting the bone grafts at higher stress levels (3.5MPa – 5.0 MPa) in two layers or more and sequentially compacting them in each layer provides a better-impacted graft bed. This thesis did not explore other influencing factors such as the shape and size of the bone grafts. This thesis developed a framework that can help to better understand the mechanics of impaction bone graft material. Currently, the models are used to identify the parameters that achieve a desired mechanical behaviour. Further experimental tests to confirm that the simulations' results are further needed to close the loop. Exploring a different range of sizes and shapes with this technique can help confirm the results from the simulations whilst significantly reducing the number of experiments needed. Finally, from a clinical perspective, this technique's limitation is that it comprises a rigid system and does not account for energy lost in realistic clinical scenarios. The study doesn't account for energy lost in the movement of the patient during impaction, or the strength and force exerted by the surgeon onto the impactor. The results achieved in this study and that achieved in the operating table are not on the same scale.

6.2. Conclusion

This thesis aimed to create a robust method to create and explore the mechanical behaviour of impaction bone grafting. The numerical model was validated for the use of ovine, and bovine bone graft particles, and the responses from the numerical model were able to predict a reasonable response using only three parameters. Yield strain and young's modulus was found to be the most

important factors that influence the mechanical behaviour of the bone grafts. Compression stiffness, accumulated strain and instantaneous modulus were proportional to the impaction forces used. The key challenge found with impaction bone grafting is that they are highly variable. Current literature studies have relied on experimental testing to develop a constitutive model to answer one specific question or explore one variable parameter. The results presented in this thesis capture the response of bone grafts using a simple material model without constitutive modelling. Hence, the graft particle parameters like dimensions of the bones, type of bones, changes in impaction technique, time and process etc, can be changed without having to go through the usual pipeline used in current literature were each different parameter is experimentally tested to create an equivalent constitutive model, and then their influences are explored to explain the mechanical behaviour.

Impacting the bone grafts at stress levels higher than 3.0 MPa resulted in compaction of the bone grafts faster and with a fewer number of impaction cycles than in lower stress ranges. Current literature studies have examined impaction bone grafting with a sequential increase of impact forces, and seldom have they gone past 3.0 MPa in terms of impact forces. Besides a handful of studies (Heiner et al., 2005), impaction bone grafting has been tested using a single layer technique. While preconditioning of the bone grafts is the gold standard (Brodt et al., 1998; Phillips et al., 2006; Fosse et al., 2006; Voor et al., 2000b; Giesen et al., 1999; Xu et al., 2011), sequential impaction of the bone grafts is more than often not tested but practised widely in clinical impaction bone grafting. This modelling framework demonstrated that impacting the bone grafts in a single layer, the applied stresses do not impact the bone grafts evenly to the distal end of the graft bed. Sequentially impacting bone grafts in multiple layers help achieve a better accumulation of permanent strain than single layer impaction for similar stresses and are advisable to achieve a stable graft bed.

6.3. Future Work

This research was performed predominantly using ovine and bovine bone grafts due to the availability and ethical considerations required for the use of human bone grafts. Human bone grafts were not simulated in this research. The response of human bone grafts to impaction bone grafting should be investigated to use this study to help surgeons clinically.

The first order elements used in the computational model struggled to explain stress-strain fields accurately when subjected to large deformations (5.0 MPa – 9.0 MPa), implementing a sequential remeshing technique during impaction to the model can help capture these deformations more accurately. Similarly, further experimental studies at higher stress levels (3.0 MPa – 9.0 MPa) can help reiterate the validity of the computational results on par with experimental testing.

This thesis examined the use of bone grafts as cubes which is not used in clinical practices. Using a computational model, it is easy to model any geometry of bone grafts and fill it to study the influence of shape in impaction. Exploring the influence of size, shape, and distribution will help establish a global standard combination of bone grafts needed to achieve a stable graft bed. Further studies using different types of bone grafts such as cortical bones, bio glass, xenografts, polymers, hydroxyapatite, tricalcium phosphate, or bone morphogenic proteins can help map the difference between different materials.

Existing literature on computational models in revision knee replacements only uses healthy bone models where defects and impactions are added to the model for testing (Hanspeter et al., 2005; Phillips et al., 2006; Kaku et al., 2015; Totoribe et al., 2018). Using enhanced imaging techniques like CT and Micro-CT, it is possible to obtain a clear image of real defects in knees and hips which could be constructed into a 3D model. Using this modelling technique, it's possible to simulate impaction grafting into these defects and then use the results to explore the fixation of revision implants. Similarly, Micro-CT can be used in replicating the experimental test to capture the

deformation of the particles sequentially during the impaction process to compare and further tune the computational model in capturing the behaviour of the bone grafts more accurately.

Currently, this technique is comprised of a rigid system and does not account for energy lost in realistic clinical scenarios. The study doesn't account for energy lost in the movement of the patient during impaction, or the strength and force exerted by the surgeon onto the impactor. The results achieved in this study and that achieved in the operating table are not on the same scale. The development of a more complicated realistic defect model with a representation of the human body on the operation table will show the consequences of a wobbly mass and what's realistically achievable in impaction.

Finally, this thesis focused on simulating impaction bone grafting using a rigid system and not on a defective knee. Using this technique and taking this technique beyond an idealised model of an experimental setup but using it to simulate impaction bone grafting of type 3 defected knee. This would help understand the change in behaviour of the bone graft when impacted into a defected bone as compared to a rigid pot. Further simulations can be performed by virtually implanting the bone graft, and the behaviour of the bone-implant construct can then be explored.

References

Aglietti, P., Buzzi, R., & Scrobe, F. (1991). Autologous bone grafting for medial tibial defects in total knee arthroplasty. *Journal of Arthroplasty*, *6*(4), 287–294. https://doi.org/10.1016/S0883-5403(06)80178-6

Albert, A. I. (2009). Mechanical characteristics in impaction allografting, the role of graft densitiy and cement penetration profile, (October).

Albert, C., Masri, B., Duncan, C., Oxland, T., & Fernlund, G. (2008a). Impaction allografting-The effect of impaction force and alternative compaction methods on the mechanical characteristics of the graft. *Journal of Biomedical Materials Research Part B: Applied Biomaterials*, *87B*(2), 395–405. https://doi.org/10.1002/jbm.b.31117

Albert, C., Masri, B., Duncan, C., Oxland, T., & Fernlund, G. (2008b). Impaction allografting - The effect of impaction force and alternative compaction methods on the mechanical characteristics of the graft. *Journal of Biomedical Materials Research - Part B Applied Biomaterials*, *87*(2), 395–405. https://doi.org/10.1002/jbm.b.31117

Allogo JJ, F. L. G. G. M. P. F. M. C. N. M. A. (1995). [Analysis of restraint of the femur head. Experimental study of allograft of cold bone and autoclaved bone to kill the HIV virus] - PubMed. Retrieved September 29, 2020, from https://pubmed.ncbi.nlm.nih.gov/7640406/

Anderson, M. J., Keyak, J. H., & Skinner, H. B. (1992). Compressive mechanical properties of human cancellous bone after gamma irradiation. *The Journal of Bone and Joint Surgery*, *74*(5), 747–752. Retrieved from http://dx.doi.org/

Austin MS, Sharkey PF, Hozack WJ, R. R. (2004). Knee failure mechanisms after total knee arthroplasty. *Tech Knee Surg.*, *3*, 55–59.

Australian Orthopaedic Association. (2019). *Australian Orthopaedic Association National Joint Replacement Registry*. Retrieved from www.aoa.org.au

Australian Orthopaedic Association National Joint Replacement Registry. (2016). Annual Report.

Awadalla, M., Al-Dirini, R. M. A., O'Rourke, D., Solomon, L. B., Heldreth, M., Rullkoetter, P., & Taylor, M. (2019). Influence of stems and metaphyseal sleeve on primary stability of cementless revision tibial trays used to reconstruct AORI IIB defects. *Journal of Orthopaedic Research*, *37*(5), 1033–1041. https://doi.org/10.1002/jor.24232

Ayers, M. P., Clift, S. E., & Gheduzzi, S. (2014). Morsellised sawbones is an acceptable experimental substitute for the in vitro elastic and viscoelastic mechanical characterisation of morsellised cancellous bone undergoing impaction grafting. *Medical Engineering and Physics*, *36*(1), 26–31. https://doi.org/10.1016/j.medengphy.2013.08.005

Backstein D, Safir O, G. A. (2006). Management of bone loss: Structural grafts in revision total knee arthroplasty. *Clin Orthop Relat Res*, *446*, 104–112.

Barbara Mittleman, M.D., and James Panagis, M.D., M.P.H., NIAMS/NIH; John H. Klippel, M.D., Arthritis Foundation, Atlanta, GA; Frank A. Pettrone, M.D., Arlington/Vienna, VA; Khaled J. Saleh, M.D., the University of Virginia, Charlottesville, VA; and W. No, N. (2016). knee problems. Retrieved from https://www.niams.nih.gov/health_info/knee_problems/

Barink, M., Meijerink, H., Verdonschot, N., Van Kampen, A., & De Waal Malefijt, M. (2007). Asymmetrical total knee arthroplasty does not improve patella tracking: A study without

patella resurfacing. *Knee Surgery, Sports Traumatology, Arthroscopy*, *15*(2), 184–191. https://doi.org/10.1007/s00167-006-0158-y

Bavadekar, A., Cornu, O., Godts, B., Delloye, C., Van Tomme, J., & Banse, X. (2001). Stiffness and compactness of morselized grafts during impaction: An in vitro study with human femoral heads. *Acta Orthopaedica Scandinavica*. https://doi.org/10.1080/000164701753532790

Bayraktar, H. H., Morgan, E. F., Niebur, G. L., Morris, G. E., Wong, E. K., & Keaveny, T. M. (2004). Comparison of the elastic and yield properties of human femoral trabecular and cortical bone tissue. *Journal of Biomechanics*, *37*(1), 27–35. https://doi.org/10.1016/S0021-9290(03)00257-4

Bergmann, G., Bender, A., Graichen, F., Dymke, J., Rohlmann, A., Trepczynski, A., … Kutzner, I. (2014). Standardized Loads Acting in Knee Implants. *PLoS ONE*, *9*(1), e86035. https://doi.org/10.1371/journal.pone.0086035

Biomechanical aspects of bone autografts and allografts., & Orthop Clin North Am 1987;18(2) :235—239. (1987). Biomechanical aspects of bone autografts and allografts - PubMed. Retrieved September 29, 2020, from https://pubmed.ncbi.nlm.nih.gov/3561975/

Biomechanical aspects of bone autografts and allografts - PubMed. (n.d.). Retrieved September 28, 2020, from https://pubmed.ncbi.nlm.nih.gov/3561975/

Bisschop R, Brouwer RW, V. R. J. (2010). Total knee arthroplasty in younger patients: a 13-year follow-up study. *Orthopedics.*, *33(12)*(Dec), 876. Retrieved from https://www.ncbi.nlm.nih.gov/pubmed/21162506/

Boettner, F., Bechler, U., Springer, B., Faschingbauer, M., & Jungwirth-Weinberger, A. (2020). Impaction Bone Grafting in Revision Total Knee Arthroplasty—Using Mesh and Cone to Contain the Defect: A Report of 3 Cases. *Arthroplasty Today*, *6*(3), 578–584. https://doi.org/10.1016/j.artd.2020.07.001

Bolder, S., Schreurs, B., Verdonschot, N., van Unen, J., Gardeniers, J., & Slooff, T. (2003). Particle size of bone graft and method of impaction affect initial stability of cemented cups: human cadaveric and synthetic pelvic specimen studies. *Acta Orthopaedica Scandinavica*, *74*(6), 652–657. https://doi.org/10.1080/00016470310018144

Bow, A., Anderson, D. E., & Dhar, M. (2019, October 2). Commercially available bone graft substitutes: the impact of origin and processing on graft functionality. *Drug Metabolism Reviews*. Taylor and Francis Ltd. https://doi.org/10.1080/03602532.2019.1671860

Brekelmans, W. A. M., Poort, H. W., & Slooff, T. J. J. H. (1972). A new method to analyse the mechanical behaviour of skeletal parts. *Acta Orthopaedica*, *43*(5), 301–317. https://doi.org/10.3109/17453677208998949

Brewster, N. T., Gillespie, W. J., Howie, C. R., Madabhushi, S. P. G., Usmani, A. S., & Fairbairn, D. R. (1999). Mechanical considerations in impaction bone grafting. *Journal of Bone and Joint Surgery - Series B*, *81*(1), 118–124. https://doi.org/10.1302/0301-620X.81B1.8480

Brewster, N T, Gillespie, W. J., Howie, C. R., Madabhushi, S. P., Usmani, A. S., & Fairbairn, D. R. (1999). Mechanical considerations in impaction bone grafting. *The Journal of Bone and Joint Surgery. British Volume*, *81*(1), 118–124. Retrieved from http://www.ncbi.nlm.nih.gov/pubmed/10068018

Brewster, Nigel T., Madabhushi, S. P. G., Pankaj, P., Howie, C. R., Dunlop, D. G., & Usmani, A. S. (2016). Techniques To Improve the Shear Strength of Impacted Bone Graft. *The Journal of*

Bone and Joint Surgery-American Volume, *85*(4), 639–646. https://doi.org/10.2106/00004623-200304000-00009

Brodt, M. D., Swan, C. C., & Brown, T. D. (1998). Mechanical behavior of human morselized cancellous bone in triaxial compression testing. *Journal of Orthopaedic Research*, *16*(1), 43–49. https://doi.org/10.1002/jor.1100160108

Campana, V., Milano, G., Pagano, E., Barba, M., Cicione, C., Salonna, G., … Logroscino, G. (2014). Bone substitutes in orthopaedic surgery: from basic science to clinical practice. *Journal of Materials Science: Materials in Medicine*, *25*(10), 2445–2461. https://doi.org/10.1007/s10856-014-5240-2

Campbell, A. W., Bain, W. E., McRae, A. F., Broad, T. E., Johnstone, P. D., Dodds, K. G., … McEwan, J. C. (2003). Bone density in sheep: Genetic variation and quantitative trait loci localisation. *Bone*, *33*(4), 540–548. https://doi.org/10.1016/S8756-3282(03)00228-X

Chandler, H. P. (1992). Structural Bone Grafting Technique in Total Knee Replacement Surgery. In *Bone Implant Grafting* (pp. 175–187). Springer London. https://doi.org/10.1007/978-1-4471-1934-0_23

Cornu, O., Bavadekar, A., Godts, B., Van Tomme, J., Delloye, C., & Banse, X. (2003a). Impaction bone grafting with freeze-dried irradiated bone. Part I. Femoral implant stability: Cadaver experiments in a hip simulator. *Acta Orthopaedica Scandinavica*, *74*(5), 547–552. https://doi.org/10.1080/00016470310017938

Cornu, O., Bavadekar, A., Godts, B., Van Tomme, J., Delloye, C., & Banse, X. (2003b). Impaction bone grafting with freeze-dried irradiated bone. Part II. Changes in stiffness and compactness of morselized grafts: Experiments in cadavers. *Acta Orthopaedica Scandinavica*, *74*(5), 553–558. https://doi.org/10.1080/00016470310017947

Cornu, O., Libouton, X., Naets, B., Godts, B., Tomme, J. Van, Delloye, C., … Van Tomme, J. (2004). Acta Orthopaedica Scandinavica Freeze-dried irradiated bone brittleness improves compactness in an impaction bone grafting model Freeze-dried irradiated bone brittleness improves compactness in an impaction bone grafting model. *Acta Orthop Scand*, *75*(3), 309–314. https://doi.org/10.1080/00016470410001240

Cornu, O., Schubert, T., Libouton, X., Manil, O., Godts, B., Tomme, J. Van, … Delloye, C. (2009). Particle size influence in an impaction bone grafting model. Comparison of fresh-frozen and freeze-dried allografts. *Journal of Biomechanics*, *42*(14), 2238–2242. https://doi.org/10.1016/j.jbiomech.2009.06.045

Cundall, P. A., & Strack, O. D. L. (1979). A discrete numerical model for granular assemblies. *Géotechnique*, *29*(1), 47–65. https://doi.org/10.1680/geot.1979.29.1.47

Daines BK, D. D. (2013). Management of bone defects in revision total knee arthroplasty. *Instr Course Lect*, *62*, 341–348. Retrieved from https://www.ncbi.nlm.nih.gov/pubmed/23395039

Dalstra, M., & Huiskes, R. (1995). Load transfer across the pelvic bone. *Journal of Biomechanics*, *28*(6), 715–724. https://doi.org/10.1016/0021-9290(94)00125-N

De Thomasson, E., Williams, J. B., Marmorat, J. L., Guigand, O., & Mazel, C. (2005). Modified Exeter technique in revision hip surgery: Does distal fixation of the stem affect allograft transformation? *Journal of Arthroplasty*, *20*(4), 473–480. https://doi.org/10.1016/j.arth.2004.09.037

De Waal Malefijt MC, van Kampen A, S. T. (1995). Bone grafting in cemented knee replacement.

45 primary and secondary cases followed for 2-5 years. *Acta Orthop Scand*, *66*(325–8).

DEM Solutions Ltd. (2017). WHAT IS (DEM), Theoretical background behind the Discrete Element Method.

Dooley, G. (2021). Investment Casting Strength - Part 2: The parameters - REMET. Retrieved June 24, 2021, from https://www.remet.com/en/insights/investment-casting-strength-part-2/

Dunlop, D. G., Brewster, N. T., Gopal Madabhushi, S. P., Usmani, A. S., Pankaj, P., & Howie, C. R. (2003). Techniques to improve the shear strength of impacted bone graft: The effect of particle size and washing of the graft. *Journal of Bone and Joint Surgery - Series A*, *85*(4), 639–646. https://doi.org/10.2106/00004623-200304000-00009

Eckart EngelbrechtElmar NiederDietrich Klüber. (1996). *Ten to Twenty Years of Knee Arthroplasty at the Endo-Klinik: A Report on the Long-term Follow-up of the St. Georg Hinge and the Medium-term Follow-up of the Rotating Knee ENDO Model | SpringerLink*. Retrieved from https://link.springer.com/chapter/10.1007/978-4-431-68464-0_25

Elia Eugene A. M.D.; Lotke, P. A. M. D. (1991, October). Results of Revision Total Knee Arthroplasty Associated With... : Clinical Orthopaedics and Related Research (1976-2007). Retrieved October 6, 2020, from https://journals.lww.com/corr/Abstract/1991/10000/Results_of_Revision_Total_Knee_Arthroplasty.16.aspx

Engh GA, A. D. (2007). Use of structural allograft in revision total knee arthroplasty in knees with severe tibial bone loss. *J Bone Joint Surg Am*, *89*(12), 2640–2647.

Fetzer, G. B., Callaghan, J. J., Templeton, J. E., Goetz, D. D., Sullivan, P. M., & Johnston, R. C. (2001). Impaction Allografting With Cement for Extensive Femoral Bone Loss in Revision Hip Surgery A 4-to 8-Year Follow-Up Study. https://doi.org/10.1054/arth.2001.29136

Fideler, B. M., Vangsness, C. T., Bin lu, Orlando, C., & Moore, T. (1995). Gamma Irradiation: Effects on Biomechanical Properties of Human Bone-Patellar Tendon-Bone Allografts. *The American Journal of Sports Medicine*, *23*(5), 643–646. https://doi.org/10.1177/036354659502300521

Flannery, O. M., Britton, J. R., O'reilly, P., Mahony, N., Prendergast, P. J., & Kenny, P. J. (2010). The threshold force required for femoral impaction grafting in revision hip surgery: A preliminary study in sow femurs. *Acta Orthopaedica*, *81*(3), 303–307. https://doi.org/10.3109/17453674.2010.480936

Foran, J. R. H., & Stuart J. Fischer. (2020). Total Knee Replacement. Retrieved January 12, 2021, from https://orthoinfo.aaos.org/en/treatment/total-knee-replacement/

Fosse, L., Rønningen, H., Lund-Larsen, J., Benum, P., & Grande, L. (2004). Impacted bone stiffness measured during construction of morsellised bone samples. *Journal of Biomechanics*, *37*(11), 1757–1766. https://doi.org/10.1016/j.jbiomech.2004.01.022

Fosse, Lars, Rønningen, H., Benum, P., & Sandven, R. B. (2006). Influence of water and fat content on compressive stiffness properties of impacted morsellized bone: An experimental ex vivo study on bone pellets. *Acta Orthopaedica*, *77*(1), 15–22. https://doi.org/10.1080/17453670610045641

Fosse, Lars, Se´bastien Muller, S., Rønningen, H., Irgens, F., & Benum, P. (2006). Viscoelastic modelling of impacted morsellised bone accurately describes unloading behaviour: An

experimental study of stiffness moduli and recoil properties. *Journal of Biomechanics*, *39*, 2295–2302. https://doi.org/10.1016/j.jbiomech.2005.07.014

Frei, H, Mitchell, P., Masri, B. A., Duncan, C. P., & Oxland, T. R. (2004). Allograft impaction and cement penetration after revision hip replacement a histomorphometric analysis in the cadaver femur. *J Bone Joint Surg [Br]*, *86*(5), 771–777. https://doi.org/10.1302/0301-620X.86B5

Frei, Hanspeter, Gadala, M. S., Masri, B. A., Duncan, C. P., & Oxland, T. R. (2006). Cement flow during impaction allografting: A finite element analysis. *Journal of Biomechanics*, *39*(3), 493–502. https://doi.org/10.1016/j.jbiomech.2004.12.010

Frei, Hanspeter, Mitchell, P., Masri, B. A., Duncan, C. P., & Oxland, T. R. (2005). Mechanical characteristics of the bone–graft–cement interface after impaction allografting. *Journal of Orthopaedic Research*, *23*(1), 9–17. https://doi.org/10.1016/j.orthres.2004.05.012

G A Engh, D. J. A. (1999). Bone loss with revision total knee arthroplasty: defect classification and alternatives for reconstruction. *Instr Course Lect*, *48*, 167–175.

García-Rojo, R., Herrmann, H. J., McNamara, S., & Association pour l'Etude de la Micromécanique des Milieux Granulaires. (2005). *Powders and grains 2005. Volume 1 : proceedings of the 5th International Conference on Micromechanics of Granular Media, Stuttgart, Germany, 18-22 July, 2005*. A.A. Balkema. Retrieved from https://books.google.com.au/books?id=I0_vBQAAQBAJ&pg=PA279&lpg=PA279&dq=Kishino+Y.+(ed.),+Powders+%26+Grains+2001,+Balkema,+Rotterdam,+2001.&source=bl&ots=nZ5-6tRVMi&sig=ACfU3U1KKYSOhzUG4qvrw-1xBeE5mGl2lw&hl=en&sa=X&ved=2ahUKEwjW3MaogPXjAhUGf30KHYf3DKYQ6A

Garino, J. P. (2002). The use of impaction grafting in revision total knee arthroplasty. *J Arthroplasty*, *17*(4 Suppl 1), 94–97. https://doi.org/10.1054/arth.2002.32457

Gie, G. A., Linder, L., Ling, R. S. M., Simon, J. P., Slooff, T. J. J. H., & Timperley, A. J. (1993a). Impacted cancellous allografts and cement for revision total hip arthroplasty. *Journal of Bone and Joint Surgery - Series B*, *75*(1), 14–21. https://doi.org/10.1302/0301-620x.75b1.8421012

Gie, G. A., Linder, L., Ling, R. S. M., Simon, J. P., Slooff, T. J., & Timperley, A. J. (1993b, October 1). Contained morselized allograft in revision total hip arthroplasty: Surgical technique. *Orthopedic Clinics of North America*. Retrieved from http://europepmc.org/article/med/8414437

Giesen, E. B., Lamerigts, N. M., Verdonschot, N., Buma, P., Schreurs, B. W., & Huiskes, R. (1999). Mechanical characteristics of impacted morsellised bone grafts used in revision of total hip arthroplasty. *The Journal of Bone and Joint Surgery. British Volume*, *81*(6), 1052–1057. https://doi.org/10.1302/0301-620X.81B6.8742

Glyn-Jones, S., Gill, H. S., McLardy-Smith, P., & Murray, D. W. (2004). Roentgen stereophotogrammetric analysis of the Birmingham hip resurfacing arthroplasty. *Journal of Bone and Joint Surgery - Series B*, *86*(2), 172–176. https://doi.org/10.1302/0301-620X.86B2.14371

Grimm, B., Blom, A. W., Miles, A. W., & Turner, I. G. (2002). In-vitro endurance testing of bone graft materials for Impaction Grafting. Retrieved from https://researchportal.bath.ac.uk/en/publications/in-vitro-endurance-testing-of-bone-graft-materials-for-impaction-

Grimm, B., Miles, A. W., & Turner, I. G. (2001). Optimizing a hydroxyapatite/tricalcium-

phosphate ceramic as a bone graft for impaction grafting. In *Journal of Materials Science: Materials in Medicine* (Vol. 12, pp. 929–934). https://doi.org/10.1023/A:1012840527774

Haas, S. B., Insall, J. N., Montgomery, W., & Windsor, R. E. (2009). Revision total knee arthroplasty with use of modular components with stems inserted without cement Revision Total Modular Components Knee Arthroplasty with Use with Stems Inserted without of Cement. *J. Bone Jt. Surg. - AM.*, *77*(11), 1700–1707.

Haddad, F. S. (2016). The epidemiology of failure in total knee arthroplasty, *98*(1), 105–112. https://doi.org/10.1302/0301-620X.98B1.36293

Heiner, A. D., & Brown, T. D. (2001). A physical model for simulating fusion of impaction-grafted morselized cancellous bone. *Journal of Biomechanics*, *34*(6), 811–814. https://doi.org/10.1016/S0021-9290(01)00032-X

Heiner, A. D., Callaghan, J. J., & Brown, T. D. (2005). A laboratory simulation for morselized bone graft fusion: Apparent modulus under operatively based femoral impaction kinetics. *Journal of Biomechanics*, *38*(4), 811–818. https://doi.org/10.1016/j.jbiomech.2004.05.005

Hernigou, P. (2000). Allograft sterility as exemplified by human immunodeficiency virus and sterilization by irradiation. *Journal of Arthroplasty*, *15*(8), 1051–1058. https://doi.org/10.1054/arth.2000.4343

Heyse TJ, Ries MD, Bellemans J, Goodman SB, Scott RD, Wright TM, Lipman JD, Schwarzkopf R, F. M. (2014). Total knee arthroplasty in patients with juvenile idiopathic arthritis. *Clin Orthop Relat Res.*, *472*(1), 147–154. Retrieved from https://www.ncbi.nlm.nih.gov/pubmed/23761173/

Hilgen, V., Citak, M., Vettorazzi, E., Haasper, C., Day, K., Amling, M., … Gebauer, M. (2013). 10-year results following impaction bone grafting of major bone defects in 29 rotational and hinged knee revision arthroplasties. *Acta Orthopaedica*, *84*(4), 387–391. https://doi.org/10.3109/17453674.2013.814012

Hills, D. A., Nowell, D., & Barber, J. R. (2017). KL Johnson and contact mechanics. *Proceedings of the Institution of Mechanical Engineers, Part C: Journal of Mechanical Engineering Science*, *231*(13), 2451–2458. https://doi.org/10.1177/0954406216634121

Hooten, J. P., Engh, C. A., Heekin, R. D., & Vinh, T. N. (1996). Structural bulk allografts in acetabular reconstruction: Analysis of two grafts retrieved at post-mortem. *Journal of Bone and Joint Surgery - Series B*, *78*(2), 270–275. https://doi.org/10.1302/0301-620X.78B2.0780270

Hotz, M. A., Speirs, A. D., Oxland, T., Müller, M., Hämmerle, C., & Häusler, R. (1999). Radiologic and Mechanical Properties of Inactivated Ossicle Homografts. *The Laryngoscope*, *109*(1), 65–69. https://doi.org/10.1097/00005537-199901000-00014

Huang, C.-H., Liau, J.-J., & Cheng, C.-K. (2007). Fixed or mobile-bearing total knee arthroplasty. *Journal of Orthopaedic Surgery and Research 2007,*. https://doi.org/10.1186/1749-799X-2-1

Huff, T. W., & Sculco, T. P. (2007). Management of bone loss in revision total knee arthroplasty. *The Journal of Arthroplasty*, *22*(7), 32–36. https://doi.org/10.1016/j.arth.2007.05.022

Jiang, M., & Yu, H.-S. (2006). Application of Discrete Element Method to Geomechanics (pp. 241–269). Springer, Berlin, Heidelberg. https://doi.org/10.1007/978-3-540-35724-7_15

Johnson, K. L. (1985). *Contact Mechanics*. Cambridge: Cambridge University Press. https://doi.org/10.1017/CBO9781139171731

Johnson, K. L. (Kenneth L. K. K. A. D. R. (1971). *Surface energy and the contact of elastic solids* (Vol. 324).

Julin J, Jämsen E, Puolakka T, Konttinen YT, M. T. (2010). Younger age increases the risk of early prosthesis failure following primary total knee replacement for osteoarthritis. A follow-up study of 32,019 total knee replacements in the Finnish Arthroplasty Register. *Acta Orthop Scand*, *81*(4), 413–419. Retrieved from https://www.ncbi.nlm.nih.gov/pubmed/20809740/

K M Samuelson. (1988, January). Bone grafting and noncemented revision arthroplasty of the knee - PubMed. Retrieved October 6, 2020, from https://pubmed.ncbi.nlm.nih.gov/3275518/

Kaku, N., Hara, K., Tabata, T., & Tsumura, H. (2015). Influence of the volume of bone defect, bone grafting methods, and hook fixation on stress on the Kerboull-type plate and screw in total hip arthroplasty: three-dimensional finite element analysis. *European Journal of Orthopaedic Surgery and Traumatology*, *25*(2), 321–329. https://doi.org/10.1007/s00590-014-1497-x

Keeney JA, Eunice S, Pashos G, Wright RW, C. J. (2011). What is the evidence for total knee arthroplasty in young patients?: a systematic review of the literature. *Clin Orthop Relat Res*, *469*(2), 574–583. Retrieved from https://www.ncbi.nlm.nih.gov/pubmed/20814772/

Kelly, N., & McGarry, J. P. (2012). Experimental and numerical characterisation of the elasto-plastic properties of bovine trabecular bone and a trabecular bone analogue. *Journal of the Mechanical Behavior of Biomedical Materials*, *9*, 184–197. https://doi.org/10.1016/j.jmbbm.2011.11.013

Kuiper, J. H. (1997). Mathematical Optimization of Elastic Properties: Application to Cementless Hip Stem Design. *Journal of Biomechanical Engineering*, *119*(2), 166. https://doi.org/10.1115/1.2796076

Kurtz, S., Ong, K., Lau, E., Mowat, F., & Halpern, M. (2007). Projections of primary and revision hip and knee arthroplasty in the United States from 2005 to 2030. *The Journal of Bone and Joint Surgery. American Volume*, *89*, 780–785. https://doi.org/10.2106/JBJS.F.00222

L A Whiteside. (1993, January). Cementless revision total knee arthroplasty - PubMed. Retrieved October 6, 2020, from https://pubmed.ncbi.nlm.nih.gov/8425339/

Lee, D.-H., Lee, S.-H., Song, E.-K., Seon, J.-K., Lim, H.-A., & Yang, H.-Y. (2017). Causes and Clinical Outcomes of Revision Total Knee Arthroplasty. *Knee Surgery & Related Research*, *29*(2), 104–109. https://doi.org/10.5792/ksrr.16.035

Lindstrand, A., Hansson, U., Toksvig-Larsen, S., & Ryd, L. (1999). Major bone transplantation in total knee arthroplasty. *The Journal of Arthroplasty*, *14*(2), 144–148. https://doi.org/10.1016/S0883-5403(99)90117-1

Lotke, P. A., Carolan, G. F., & Puri, N. (2006). Technique for Impaction Bone Grafting of Large Bone Defects in Revision Total Knee Arthroplasty. *Journal of Arthroplasty*, *21*(4 SUPPL.), 57–60. https://doi.org/10.1016/j.arth.2006.01.019

Luding, S. (2008). *Introduction to Discrete Element Methods Basics of Contact Force Models and how to perform the Micro-Macro Transition to Continuum Theory*. Retrieved from https://pdfs.semanticscholar.org/ec8b/26e2d20b7d8a09d15f0e10660f0d02b4458d.pdf

Lunde, K. B., Foss, O. A., Fosse, L., & Skallerud, B. (2008). Constitutive Models for Constrained Compression of Unimpacted and Impacted Human Morselized Bone Grafts. *Journal of Biomechanical Engineering*, *130*(6), 061014. https://doi.org/10.1115/1.2979878

Malkani, A. L., Voor, M. J., Fee, K. A., & Bates, C. S. (1996). Femoral component revision using

impacted morsellised cancellous graft. *The Journal of Bone and Joint Surgery. British Volume*, *78-B*(6), 973–978. https://doi.org/10.1302/0301-620x.78b6.0780973

McKeen, L. W. (2016). Introduction to Fatigue of Plastics and Elastomers. In *Fatigue and Tribological Properties of Plastics and Elastomers* (pp. 1–26). Elsevier. https://doi.org/10.1016/b978-0-323-44201-5.00001-0

McNamara, I., Howard, J., Rayment, A., Schalk, R., Brooks, R., Best, S., & Rushton, N. (2014). Mechanical properties of morcellised bone graft with the addition of hydroxyapatite. *Journal of Materials Science: Materials in Medicine*, *25*(2), 321–327. https://doi.org/10.1007/s10856-013-5085-0

McNamara, L. M., Ederveen, A. G. H., Lyons, C. G., Price, C., Schaffler, M. B., Weinans, H., & Prendergast, P. J. (2006). Strength of cancellous bone trabecular tissue from normal, ovariectomized and drug-treated rats over the course of ageing. *Bone*, *39*(2), 392–400. https://doi.org/10.1016/j.bone.2006.02.070

Meneghini, R. M., Pierson, J. L., Bagsby, D., Berend, M. E., Ritter, M. A., & Meding, J. B. (2007). The Effect of Retropatellar Fat Pad Excision on Patellar Tendon Contracture and Functional Outcomes after Total Knee Arthroplasty. *Journal of Arthroplasty*, *22*(6 SUPPL.), 47–50. https://doi.org/10.1016/j.arth.2007.03.031

Meneghini RM, Lewallen DG, H., & AD. (2009). Use of porous tantalum metaphyseal cones for severe tibial bone loss during revision total knee replacement: Surgical technique. *J Bone Joint Surg Am*, *91*, 131–138.

Mittra, E., & Qin, Y. X. (2003). Material properties of sheep trabecular bone determined by nanomechanical testing. In *Proceedings of the IEEE Annual Northeast Bioengineering Conference, NEBEC* (Vol. 2003-Janua, pp. 229–230). Institute of Electrical and Electronics Engineers Inc. https://doi.org/10.1109/NEBC.2003.1216077

Nafei, A., Danielsen, C. C., Linde, F., & Hvid, I. (2000). Properties of growing trabecular ovine bone. *The Journal of Bone and Joint Surgery. British Volume*, *82-B*(6), 910–920. https://doi.org/10.1302/0301-620X.82B6.0820910

Nafei, A., Fellow, R., Danielsen, C. C., Linde, F., & Hvid, I. (2000). *THE JOURNAL OF BONE AND JOINT SURGERY Properties of growing trabecular ovine bone PART I: MECHANICAL AND PHYSICAL PROPERTIES*. *J Bone Joint Surg [Br]* (Vol. 82).

Naim, S., & Toms, D. (2013). *Impaction bone grafting for tibial defects in knee replacement surgery. Results at two years*.

National Joint Registry for England Wales and Northern Ireland. (2016). 13th Annual Report. *13th Annulary Report*, (December 2015).

Nelson CL, Vanushkina M, I. K., & Strohecker K, B. T. (2015). Stemmed femoral implants show lower failure rates in revision total knee arthroplasty. *Knee*, *22*(5), 429–434.

Niebur, G. L., Feldstein, M. J., Yuen, J. C., Chen, T. J., & Keaveny, T. M. (2000). High-resolution finite element models with tissue strength asymmetry accurately predict failure of trabecular bone. *Journal of Biomechanics*, *33*(12), 1575–1583. https://doi.org/10.1016/S0021-9290(00)00149-4

Niebur, G. L., Yuen, J. C., Burghardt, A. J., & Keaveny, T. M. (2001). Sensitivity of damage predictions to tissue level yield properties and apparent loading conditions. *Journal of Biomechanics*, *34*(5), 699–706. https://doi.org/10.1016/S0021-9290(01)00003-3

Oftadeh, R., Perez-Viloria, M., Villa-Camacho, J. C., Vaziri, A., & Nazarian, A. (2015). Biomechanics and mechanobiology of trabecular bone: a review. *Journal of Biomechanical Engineering*, *137*(1), 0108021. https://doi.org/10.1115/1.4029176

Ostendorf, M., Johnell, O., Malchau, H., Dhert, W. J. A., Schrijvers, A. J. P., & Verbout, A. J. (2002). The epidemiology of total hip replacement in the Present status and future needs, *73*(3), 282–286.

Otto Robertsson et al. (2019, December). Sweedish Knee registry. Retrieved September 23, 2020, from http://www.myknee.se/pdf/SVK_2019_1.0_Eng.pdf

P. Noble, E. Foley, J. Simpson, J. Gold, J. Choi, S. Ismaily, K. Mathis, S. I. (2018). Inter-surgeon variability in the Assembly of modular head-neck tapers in tha via the posterior approach. *Orthopaedic Proceedings*, *99*(B:SUPP_5), 59–65.

Pagnano MW. (2006). Management of bone defects, in Insall JN, Scott WN. *Surgery of the Knee*, *4*, 1799–1813.

Pasha, M., Dogbe, S., Hare, C., Hassanpour, A., & Ghadiri, M. (2014). A linear model of elasto-plastic and adhesive contact deformation. *Granular Matter*, *16*(1), 151–162. https://doi.org/10.1007/s10035-013-0476-y

Phillips, A. T. M., Pankaj, P., Howie, C. R., Usmani, A. S., & Simpson, A. H. R. W. (2006). 3D non-linear analysis of the acetabular construct following impaction grafting. *Computer Methods in Biomechanics and Biomedical Engineering*, *9*(3), 125–133. https://doi.org/10.1080/10255840600732226

Phillips, A., Pankaj, P., May, F., Taylor, K., Howie, C., & Usmani, A. (2006a). Constitutive models for impacted morsellised cortico-cancellous bone. *Biomaterials*, *27*(9), 2162–2170. https://doi.org/10.1016/j.biomaterials.2005.10.034

Phillips, A., Pankaj, P., May, F., Taylor, K., Howie, C., & Usmani, A. (2006b). Constitutive models for impacted morsellised cortico-cancellous bone. *Biomaterials*, *27*(9), 2162–2170. https://doi.org/10.1016/j.biomaterials.2005.10.034

Phillips, A. T. M., Pankaj, Brown, D. T., Oram, T. Z., Howie, C. R., & Usmani, A. S. (2006). The elastic properties of morsellised cortico-cancellous bone graft are dependent on its prior loading. *Journal of Biomechanics*, *39*(8), 1517–1526. https://doi.org/10.1016/j.jbiomech.2005.03.032

Phillips, A. T. M., Pankaj, P., Howie, C. R., Usmani, A. S., & Simpson, A. H. R. W. (2007). Finite element modelling of the pelvis: Inclusion of muscular and ligamentous boundary conditions. *Medical Engineering and Physics*, *29*(7), 739–748. https://doi.org/10.1016/j.medengphy.2006.08.010

Poelert, S., Valstar, E., Weinans, H., & Zadpoor, A. A. (2013). Patient-specific finite element modeling of bones. *Proceedings of the Institution of Mechanical Engineers, Part H: Journal of Engineering in Medicine*, *227*(4), 464–478. https://doi.org/10.1177/0954411912467884

Putzer, D., Ammann, C. G., Coraça-Huber, D., Lechner, R., Schmölz, W., & Nogler, M. (2017). The Influence of Liquids on the Mechanical Properties of Allografts in Bone Impaction Grafting. *Biopreservation and Biobanking*, *15*(5), 410–416. https://doi.org/10.1089/bio.2017.0003

Ranawat, A. S., & Ranawat, C. S. (2012). The history of total knee arthroplasty. In *The Knee Joint: Surgical Techniques and Strategies* (pp. 699–707). Paris: Springer Paris.

https://doi.org/10.1007/978-2-287-99353-4_63

Rho, J. Y., Zioupos, P., Currey, J. D., & Pharr, G. M. (1999). Variations in the individual thick lamellar properties within osteons by nanoindentation. *Bone*, *25*(3), 295–300. https://doi.org/10.1016/S8756-3282(99)00163-5

Rocky DEM. (2018). DEM Technical Manual 4.2.

Roidis, N., & Athanasios Pollalis. (2014). Bone graft and implant graft interface in total hip arthroplasty. *Springer Verlag - London*. https://doi.org/10.1007/978-1-4471-5409-9_15

Schimmel, J. W., Buma, P., Versleyen, D., Huiskes, R., & Slooff, T. J. J. H. (1998). Acetabular reconstruction with impacted morselized cancellous allografts in cemented hip arthroplasty: A histological and biomechanical study on the goat. *Journal of Arthroplasty*, *13*(4), 438–448. https://doi.org/10.1016/S0883-5403(98)90010-9

Scholl, L., Schmidig, G., Faizan, A., Tenhuisen, K., & Nevelos, J. (2016). Evaluation of surgical impaction technique and how it affects locking strength of the head-stem taper junction. *J Engineering in Medicine*, *230*(7), 661–667. https://doi.org/10.1177/0954411916644477

Schreurs, B. Willem, Buma, P., Huiskes, R., Mark Slagter, J. L., & Slooff, T. J. J. (1994). Morsellized allografts for fixation of the hip prosthesis femoral component: A mechanical and histological study in the goat. *Acta Orthopaedica*, *65*(3), 267–275. https://doi.org/10.3109/17453679408995452

Schreurs, B W, Surgeon, O., Slooff, T. J. J. H., Buma, O. P., Gardeniers, B. J. W. M., Huiskes, R., … Gardeniers, J. W. M. (1998). Acetabular reconstruction with impacted morsellised cancellous bone graft and cement. *J Bone Joint Surg [Br]*, *8080*(3), 391–395. https://doi.org/10.1302/0301-620X.80B3.8534

Schreurs, B W, van Tienen, T. G., Buma, P., Verdonschot, N., Gardeniers, J. W., & Slooff, T. J. (2001). Favorable results of acetabular reconstruction with impacted morsellized bone grafts in patients younger than 50 years: a 10- to 18-year follow-up study of 34 cemented total hip arthroplasties. *Acta Orthopaedica Scandinavica*, *72*(2), 120–126. https://doi.org/10.1080/000164701317323354

Schwager, T., & Pöschel, T. (2007). Coefficient of restitution and linear-dashpot model revisited. *Granular Matter*, *9*(6), 465–469. https://doi.org/10.1007/s10035-007-0065-z

Slooff, T. J. J. H., Huiskes, R., van Horn, J., & Lemmens, A. J. (1984). Bone grafting in total hip replacement for acetabular protrusion. *Acta Orthopaedica*, *55*(6), 593–596. https://doi.org/10.3109/17453678408992402

Smuts, E. M., Deglon, D. a, & Meyer, C. J. (2012). *Methodology for Coupled CFD-DEM Modelling of Particulate Suspension Rheology*. *9th International Conference on CFD in the Minerals and Process Industries*. Retrieved from http://www.cfd.com.au/cfd_conf12/PDFs/107SMU.pdf

Speirs, A. ., Hotz, M. ., Oxland, T. ., Häusler, R., & Nolte, L.-P. (1999). Biomechanical properties of sterilized human auditory ossicles. *Journal of Biomechanics*, *32*(5), 485–491. https://doi.org/10.1016/S0021-9290(99)00012-3

Stulberg, S. D. (2000). Impaction grafting: The science and clinical reality. *Orthopedics*, *23*(9), 945–947. https://doi.org/10.3928/0147-7447-20000901-21

Stulberg, S. David. (2002). Impaction grafting: Doing it right. In *Journal of Arthroplasty* (Vol. 17, pp. 147–152). Churchill Livingstone Inc. https://doi.org/10.1054/arth.2002.33267

Suárez-Suárez MA, Murcia A, M. A. (2002). Filling of segmental bone defects in revision knee arthroplasty using morsellized bone grafts contained within a metal mesh. *Acta Orthop Belg*, *68*(2), 163–167.

Te Stroet, M. A. J., Bronsema, E., Rijnen, W. H. C., Gardeniers, J. W. M., Schreurs, B. W., Te Stroet, □ M A J, … Schreurs, □ B W. (2014). The use of a long stem cemented femoral component in revision total hip replacement A FOLLOW-UP STUDY OF FIVE TO 16 YEARS. *Bone Joint J*, *96*(9), 1207–1220. https://doi.org/10.1302/0301-620X.96B9

Theuerkauf, J., Dhodapkar, S., & Jacob, K. (2007). Modeling granular flow: using discrete element method--from theory to practice: this emerging simulation technique is changing the face of solids processing. *Chemical Engineering*, *114*(4), 39–47. Retrieved from https://go.gale.com/ps/i.do?id=GALE%7CA162695891&v=2.1&u=flinders&it=r&p=AONE&sw=w

Totoribe, K., Chosa, E., Yamako, G., Hamada, H., Ouchi, K., Yamashita, S., & Deng, G. (2018). Finite element analysis of the tibial bone graft in cementless total knee arthroplasty. *Journal of Orthopaedic Surgery and Research*, *13*(1), 113. https://doi.org/10.1186/s13018-018-0830-1

Trutna, P. T. L. (2012). *e-Handbook of Statistical Methods*. (N. arroll Croarkin - Statistical Engineering Division, Information Technology Laboratory & S. Paul Tobias - Statistical Methods Group, Eds.). Retrieved from https://www.itl.nist.gov/div898/handbook/pri/section3/pri3362.htm

Tsuji, Y., Tanaka, T., & Ishida, T. (1992). Lagrangian numerical simulation of plug flow of cohesionless particles in a horizontal pipe. *Powder Technology*, *71*(3), 239–250. https://doi.org/10.1016/0032-5910(92)88030-L

Tsumura, H., Kaku, N., Ikeda, S., & Torisu, T. (2005). A computer simulation of rotational acetabular osteotomy for dysplastic hip joint: Does the optimal transposition of the acetabular fragment exist? *Journal of Orthopaedic Science*, *10*(2), 145–151. https://doi.org/10.1007/s00776-004-0866-4

Ullmark, G. (2000). Bigger size and defatting of bone chips will increase cup stability. *Archives of Orthopaedic and Trauma Surgery*, *120*(7–8), 445–447. https://doi.org/10.1007/s004029900122

Ullmark, G., & Hovelius, L. (1996). Impacted morsellized allograft and cement for revision total knee arthroplasty: A preliminary report of 3 cases. *Acta Orthopaedica*, *67*(1), 10–12. https://doi.org/10.3109/17453679608995600

Van Der Donk, S., Buma, P., Verdonschot, N., & Schreurs, B. W. (2002). Effect of load on the early incorporation of impacted morsellized allografts. *Biomaterials*, *23*(1), 297–303. https://doi.org/10.1016/S0142-9612(01)00108-9

Vasso, M., Beaufils, P., Cerciello, S., & Panni, A. S. (2014). Bone loss following knee arthroplasty: potential treatment options. *Arch Orthop Trauma Surg*, *134*, 543–553. https://doi.org/10.1007/s00402-014-1941-8

Verdonschot, N., Van Hal, C. T. H., Schreurs, B. W., Buma, P., Huiskes, R., & Slooff, T. J. J. H. (2001). Time-dependent mechanical properties of HA/TCP particles in relation to morsellized bone grafts for use in impaction grafting. *Journal of Biomedical Materials Research*, *58*(5), 599–604. https://doi.org/10.1002/jbm.1058

Vessely MB, Whaley AL, Harmsen WS, Schleck CD, B. D. (2006). The Chitranjan Ranawat Award: Long-term survivorship and failure modes of 1000 cemented condylar total knee arthroplasties. *Clin Orthop Relat Res.*, *452*, 28–34. Retrieved from

https://www.ncbi.nlm.nih.gov/pubmed/16936585/

Voor, M. J., Nawab, A., Malkani, A. L., & Ullrich, C. R. (2000a). *Mechanical properties of compacted morselized cancellous bone graft using one-dimensional consolidation testing. Journal of Biomechanics* (Vol. 33). Retrieved from https://ac.els-cdn.com/S0021929000001561/1-s2.0-S0021929000001561-main.pdf?_tid=3178af3f-ee10-4d1f-a406-d9fc71341509&acdnat=1552890644_d0ffae802cd82f46a1b59cc6a3c1ab1b

Voor, M. J., Nawab, A., Malkani, A. L., & Ullrich, C. R. (2000b). Mechanical properties of compacted morselized cancellous bone graft using one-dimensional consolidation testing. *Journal of Biomechanics*, *33*(12), 1683–1688. https://doi.org/10.1016/S0021-9290(00)00156-1

Voor, M. J., White, J. E., Grieshaber, J. E., Malkani, A. L., & Ullrich, C. R. (2004). Impacted morselized cancellous bone: Mechanical effects of defatting and augmentation with fine hydroxyapatite particles. *Journal of Biomechanics*, *37*(8), 1233–1239. https://doi.org/10.1016/j.jbiomech.2003.12.002

Wang, W., & Yeung, K. W. K. (2017, December 1). Bone grafts and biomaterials substitutes for bone defect repair: A review. *Bioactive Materials*. KeAi Communications Co. https://doi.org/10.1016/j.bioactmat.2017.05.007

Wangerin, K., Ewers, R., Wottge, H. U., & Randzio, G. (1986). The autoclaved autogenous bone graft as a re-implant. Results of animal experiments. *Journal of Maxillofacial Surgery*, *14*(C), 132–137. https://doi.org/10.1016/S0301-0503(86)80278-8

Welten, M. L., Schreurs, B. W., Buma, P., Verdonschot, N., & Slooff, T. J. (2000). Acetabular reconstruction with impacted morcellized cancellous bone autograft and cemented primary total hip arthroplasty: a 10- to 17-year follow-up study. *The Journal of Arthroplasty*, *15*(7), 819–824. https://doi.org/10.1054/arth.2000.7110

Whittaker, J. P., Dharmarajan, R., & Toms, A. D. (2008). The management of bone loss in revision total knee replacement, *90*(8). https://doi.org/10.1302/0301-620X.90B8

William DC. (2001). *(PDF) Callister - Fundamentals of Materials Science and Engineering 5e HQ | AKINJO OLORUNTOBI - Academia.edu*. (John Wiley and Sons, Ed.). Retrieved from https://www.academia.edu/35598279/Callister_Fundamentals_of_Materials_Science_and_Engineering_5e_HQ

Xu, Z. J., Chen, L. Y., Zhong, C., Tan, Y. Bin, & He, R. X. (2011). Mechanical properties of 7-10 mm bone grafts and small slurry grafts in impaction bone grafting. *Journal of Orthopaedic Research*, *29*(10), 1491–1495. https://doi.org/10.1002/jor.21357

Zhang, Yongde, Ahn, P. B., Fitzpatrick, D. C., Heiner, A. D., Poggie, R. A., & Brown, T. D. (1999). Interfacial frictional behavior: Cancellous bone, cortical bone, and a novel porous tantalum. *Journal of Musculoskeletal Research*, *03*(04), 245–251. https://doi.org/10.1142/S0218957799000269

Zhang, Yongxing, Homsi, D., Gates, K., Oakes, K., Sutherland, V., & Wolfinbarger, L. (1994). A Comprehensive Study of Physical Parameters, Biomechanical Properties, and Statistical Correlations of Iliac Crest Bone Wedges Used in Spinal Fusion Surgery. *Spine*, *19*(3), 304–308. https://doi.org/10.1097/00007632-199402000-00008

Zhao, Stacey & Wiebe, S & Morrison, Jason & Burnell, C & Turgeon, Thomas & Petrak, M. (2012). (PDF) Measuring impact loads by surgical hammers: A study involving insertion of smooth pins into polyurethane. Retrieved September 1, 2020, from https://www.researchgate.net/publication/305700967_Measuring_impact_loads_by_surgic

al_hammers_A_study_involving_insertion_of_smooth_pins_into_polyurethane

Appendix

Approach – 1: Discrete Element Analysis

A discrete element method is an approach used for modelling and understanding macroscopic particulate material behaviour (García-Rojo et al., 2005). Discrete element modelling has been extensively used in civil engineering applications to model soils concerning the foundation of structures and buildings. For this reason, the discrete element model was explored as a way to model and simulate bone grafts

The foundation of DEM techniques for modelling particulate mechanics was created by Cundall and Stack (Cundall et al 1979). There have been studies published on the application of DEM to a variety of problems from geo-mechanical to chemical engineering and DEM has been a common method of modelling in rock and soil mechanics (Jiang et al 2006). However, DEM has not been used for modelling problems in biomechanical particles or bone mechanics. The underlying mechanisms for force transmission are difficult to visualise and measure, therefore a continuum approach that assumes bulk solids have been widely used (Theuerkauf et al 2007).

Understanding the discrete element modelling method

Discrete modelling is generally made up of two categories, the hard-sphere approach and the soft sphere approach.

The hard-sphere approach

In a hard-sphere or quasi rigid model, the interaction forces between particles are impulsive. It's an event-driven method where the particle collisions are assumed to be binary and instantaneous. The particles are assumed to move undisturbed until a collision occurs, and the collisions are assumed to be the only means for exchanging momentum. Impulse/momentum transfer is used to calculate the post-collision velocities. Though energy dissipation is introduced with a coefficient

of restitution, it doesn't account for any deformation or overlapping of the contacting interfaces. The particles are completely rigid and that creates a challenge in the application of this modelling method to impaction bone grafting. Thus, the hard-sphere approach was not deemed as a suitable method for simulations.

Soft-sphere approach

DEM's in the soft sphere approach is based on Newton's second law of motion rather than Hooke's law which is used in implicit finite element analyses. Multiple particle contacts and their resulting equilibrium conditions can be handled by soft sphere models which are important for modelling dense and quasi-static systems. Using this approach dense granular flow with unusual geometries and large deformation can be simulated. Particle accelerations are double integrated to determine the position of each particle. A Hertzian contact model acting at each contact point generates the forces acting between particles and particle to wall interactions.

This image has been removed due to copyright restriction. Available online from "(DEM solutions 2017) "

A.Figure 1: Soft sphere particles which allow for small overlaps/overclosure (DEM solutions 2017)

The model assumes velocities and accelerations to be constant during each time step (t). DEM is a time stepped simulation and assumes the velocities and accelerations to be constant during each step. The solution scheme assumes that the disturbance cannot propagate beyond the neighbouring particles during the step time which allows for an explicit analysis. This solution is identical to that used for continuum analysis by the explicit finite-difference method (Cundall & Strack, 1979). Particles are assumed to be spherical rigid bodies with finite mass, either as separate individual entities or as clusters of particles bonded to each other A.Figure 2.

This image has been removed due to copyright restriction. Available online from "(DEM solutions 2017) "

A.Figure 2: Possible variety of shapes that can be created using DEM by bonding, glueing spheres (DEM solutions 2017)

Particles have contact points on their surface and can only interact at those contact points with each contact point assumed to involve either surface or walls. Overlaps of particles are assumed to be small and particle deformations are mimicked by overlapping adjacent particles. Collisions between particles are not considered instantaneous

DEM models use a dynamic process to describe the interaction between particles and particle clusters. The movement of individual particles are traced, and the contact forces and displacements of the particles are calculated. The movement of particles is calculated through rotational and translational motions. The movement of each particle describes the mechanical behaviour of the system, the moment and force acting at each contact.

The magnitude of the forces acting on the particles is calculated using this approach to determine the load at which the particles start deforming and break. These particles have 6 degrees of freedom and hence have two types of motion namely translational and rotational. Newton's second law is used to calculate the acceleration of both the translation and rotational degrees of freedom which is then numerically integrated over time step definition to update each particle position and velocities.

The translational motion is calculated based on equation (6.1**Error! Reference source not found.**)

$$m_i \frac{d^2}{dt^2} r_i = f_i + m_i g \qquad 6.1$$

Where m_i is the mass of the particle, r_i the position, $f_i = \sum_c f_i^c$ acting on the particle as a result of contacts with other particles, g the acceleration due to gravity

The rotational motion is calculated based on equation (6.2**Error! Reference source not found.**)

$$I_i \frac{d}{dt}\omega_i = t_i \qquad 6.2$$

Where I_i the spherical moment of inertia, ω_i the angular velocity and $t_i = \sum_c (l_i^c \times f_i^c + q_i^c)$, where q_i^c is the resulting contact torque acting on the particle.

The movement of all particles are independent of the other particles and they are assumed to interact only at the contact points. Soft-sphere particles can overlap each other. A Hertzian type of model is used to represent the force-displacements laws at the contacts. The contact model compares the amount of overlap between two objects and determines the magnitudes of forces.

The contact between two particles was calculated using the following formulas (Luding, 2008)

The radius of the contact area is calculated by equation (6.3**Error! Reference source not found.**)

$$a = \sqrt[3]{\frac{3F\left[\frac{1-v_1^2}{E_1} + \frac{1-v_2^2}{E_2}\right]}{4(\frac{1}{R_1} + \frac{1}{R_2})}} \qquad 6.3$$

Where E_1 and E_2 are the elastic modulus, v_1 and v_2 the Poisson's ratio of sphere's 1 and 2 respectively.

The maximum contact pressure at the centre of the circular contact area is given by equation (6.4**Error! Reference source not found.**)

$$P_{max} = \frac{3F}{2\pi a^2} \quad 6.4$$

The depth of indentation d is calculated from equation (6.5**Error! Reference source not found.**)

$$d = \frac{a^2}{R} = \sqrt[3]{\frac{9F^2}{16RE^{*2}}} \quad 6.5$$

Where R is the effective radius defined as $\frac{1}{R} = \frac{1}{R_1} + \frac{1}{R_2}$

An overall concept of DEM modelling is shown below (A.Figure 3). Input parameters vary based on the contact model selected. The output calculated is an estimate of the particle position, velocities and the forces in the system acting on the particles and walls.

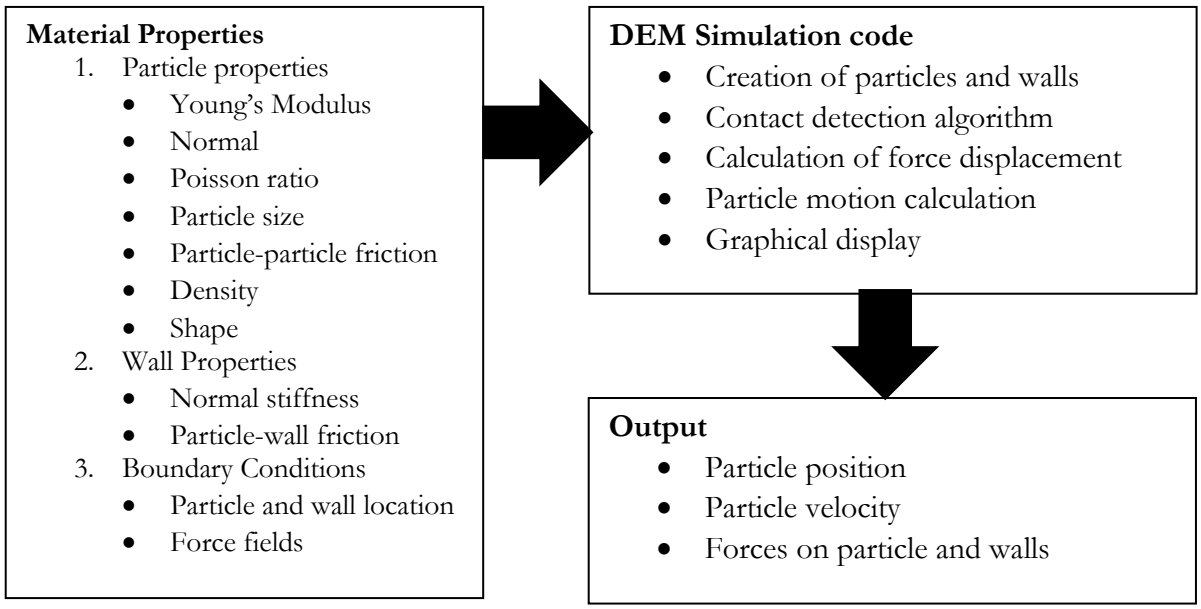

A.Figure 3: Typical input parameters of DEM program and the outputs of a typical simulation

Discrete element model

The DEM model was created using Abaqus 2017 where the Discrete Element method was embedded in the software. Accurate specifications of properties of particles are important to ensure that the behaviour of the simulated particle is on a realistic scale. To limit the computational

size of the problem, a two-particle geometry was created to understand the mechanics of the system and calibrate the particles and their overlap for the problem.

Depth of indentation was calculated and plotted as a table for the surface behaviour of the DEM particles. The surface definition of the particles were defined based on the pressure over indentation depth.

Though there are alternate force-displacement models proposed in the literature, the selection of an appropriate model depends on the problem and the type and the properties of the particles being simulated. In this model, the particles were created as spheres.

To ensure numerical stability, the collision time in a DEM simulation has to be determined. This critical time step is chosen to be 10 to 100 times smaller than implicit analysis to prevent excessive overlaps, unrealistic high forces and to avoid effects of disturbance waves. The time step is calculated using Rayleigh criteria, similar to the approach used to calculate time steps in explicit finite element analysis. Rayleigh time is the time taken by a surface wave to propagate through a solid particle (Smuts et al 2012). The time step was selected as a fraction of the Rayleigh time, typically using equation (6.6**Error! Reference source not found.**)

$$T = \frac{\pi R \sqrt{\frac{\rho}{G}}}{0.1631v + 0.8766} \qquad 6.6$$

Where T is the Rayleigh time step, R particle radius, ρ is the density, G the shear modulus and v the Poisson's ratio of the particle.

Two particle DEM numerical model

Methods

Two particles were created with one node and one element each. The nodes were named a base node and a top node. A discrete section for both the top element and base element was created with a density of $1.5e-05\ kg/mm^3$ (Campbell et al., 2003). The radius of the particles was chosen to be 3mm, 4mm and 5mm as they were found to be in the range of cancellous bone grafts used in impaction bone grafting. Particles with a discrete elastic modulus of 0.5 GPa, 1 GPa, 2 GPa were calibrated as they were found to be in the range of cancellous bones from literature (Nafei et al 2000). The discrete elasticity of both particles was chosen to be identical for all simulations**.** The base was assigned a boundary condition and encastered to stop it from moving in any direction. Gravity load was assigned to the top particle in the first step followed by a concentrated load in the second step in the direction of gravity. The concentrated load was applied with a smooth step amplitude with a constant linear increase of 100N every 0.1s of simulation time. Surface interaction was assigned through surface behaviour, pressure overclosure tabular. The overclosure/depth of indentation was calculated using the Hertzian contact theorem equation. The displacement and deformation of the top particle on the base for applied force was compared with the theoretical displacement and deformation achieved from numerical calculations for the same force.

The loading profile of these initial simulations was run with a reduced number of loading cycles to reduce the run time and post-processing time. The resultant stress and strain values were compared with the experimental results from Figure 3.11. The full analysis of compression testing was only done on the models which exhibited a response similar to the experimental results.

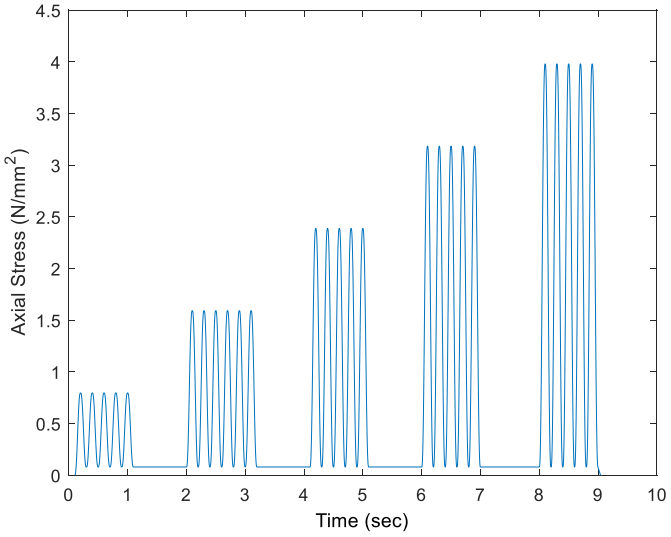

A.Figure 4: (a) Loading profile of computational model (b)

Evaluation of stress-strain and comparison with experimental studies

Python scripting was used to pull out load and displacement data of the impactor. Stress applied to the DEM were calculated using a bulk stress equation given by equation (6.7**Error! Reference source not found.**)

$$\sigma_a = \frac{F}{A} \tag{6.7}$$

Where F is the Force and A the Area.

The initial position of the load applicator was determined to be the position of the load applicator in the Z direction at the end of Step 2. The strain on the DEM's were calculated from the displacement of the impactor inside the cylinder and was given by equation (6.8**Error! Reference source not found.**)

$$\varepsilon_a = \frac{dl}{l_0} \qquad 6.8$$

Where dl was the change in height and l_o- the initial height of the impactor once it has come to rest over the particles.

Results of calibration

A.Figure 5**Error! Reference source not found.**(a) shows that the displacement of the particle increases with an increase in force. The rate of increase of displacement from the numerical model was around 1.8% lower than the displacement calculated using hertz theory at 50N increasing to a 6% deficit at a force of 380N. Calibrating the model reduced the difference between the observed displacement and the calculated displacement to 0.6% at the 50N and 3% at a force of 380N. As the method shows that the error between the theory and the results were less than 3% the DEM method was deemed to be performing as expected.

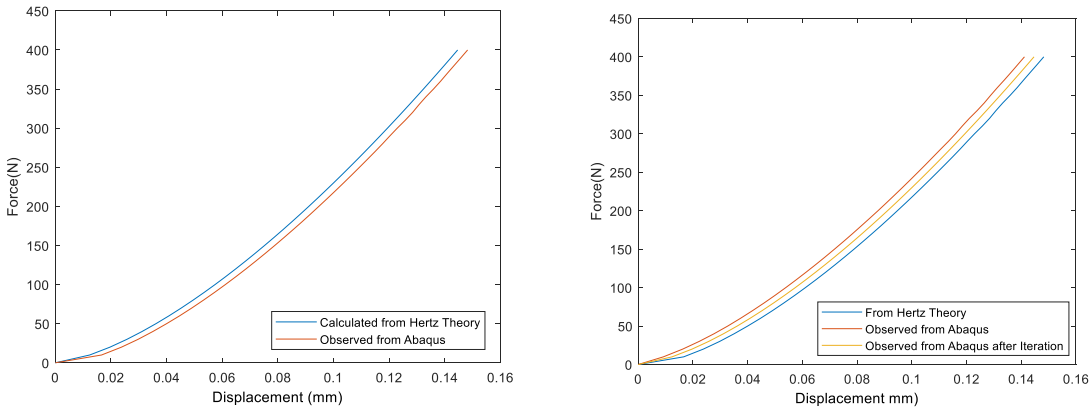

A.Figure 5: Force displacement curve for 3mm DEM particles at 1GPa elastic modulus: (a) before iteration (b) after iteration

Replicating a confined compression experiment using DEM

The numerical model with identical specification as the experimental model was used as described in A.Figure 6. The material definition of this numerical model consists of spheres of 5 mm

diameter set to 1.0 GPa as Young's modulus (Rho, Zioupos, Currey, & Pharr, 1999) and 0.4 Poisson ratio (Brodt et al., 1998). The DEM particles were created using a particle generator tool within Abaqus Explicit and positioned on top of the cylinder's open end. The particles created were allowed to fill the chamber under gravity load applied to the particle once created. The surface interaction between the particles and the chamber were set to surface-to-surface hard contacts. The impactor was positioned behind the particle generator. The simulation was emulated in a three-step process with the particle generating the particles to fill the chamber in the first step, gravity acceleration of 9.81 m/s² was applied to the impactor to let the impactor settle on top of the particles imitating a preconditioning process in step two. The impaction test was carried out with 25 force-controlled impaction cycles at the rate of 5 impaction per second with impact stress in the range of 0.5 MPa to 4.0 MPa in step three.

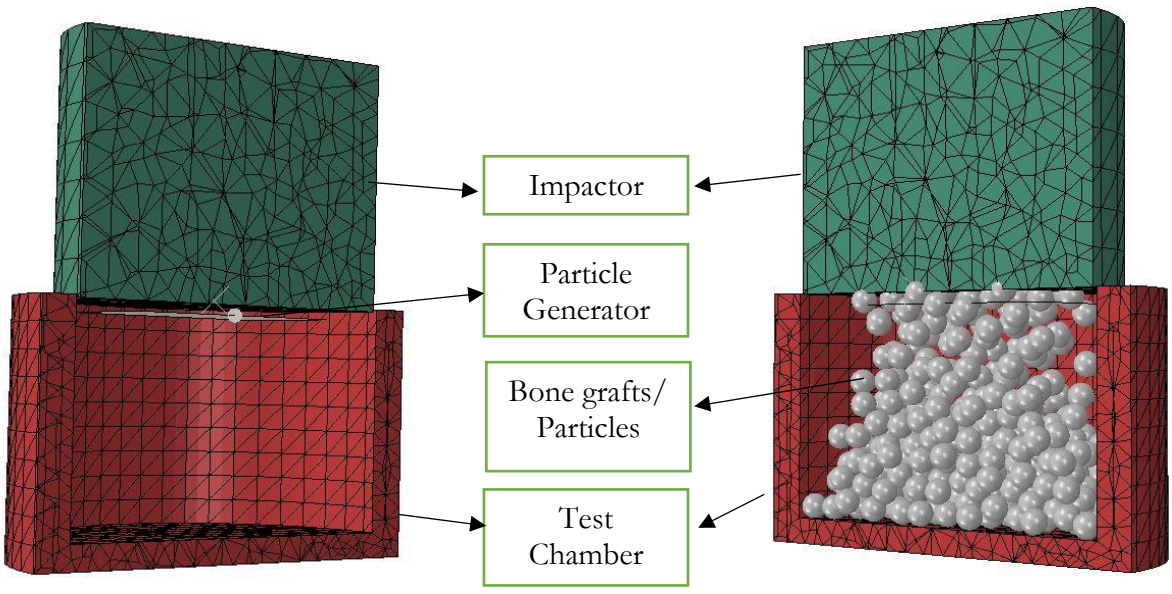

A.Figure 6: Computational model with particle generator without particles (left) and with particles (right)

The stress and strain of each simulation were compared with the experimental results. The results from the computational analysis were used to tune the input assumptions, which have a significant impact on the outputs. Factors that influence the results were determined to be damping between

the particles, size of particles, friction and the elastic modulus. The size of the particles and the elastic modulus being a known controllable variable, the rest of the factors were used to design a full factorial experiment with 25 computational simulations to try tune the particles to act as bone graft particles under impaction. The combinations of which can be seen below.

Elastic modulus in MPA	Size in mm	Friction coefficient					Damping ratio		
500	5	0.6	1.2	1.8	2.4	3.0	1.0	2.0	3.0
1000							2.0		
2000		1.0	1.5	2.0	2.5	3.0	1.0		

A.Table 1: Full factorial combinations of numerical experiments simulated and tested

Results

The initial results from the computational simulations were plotted on a stress-strain curve plot with a damping coefficient of 1.0 and friction coefficient ratio of 0.6 in the lowest factorial point and then adjusted in further simulations to see how close the results were to the experimental results obtained from Chapter 3 as seen from A.Figure 8.

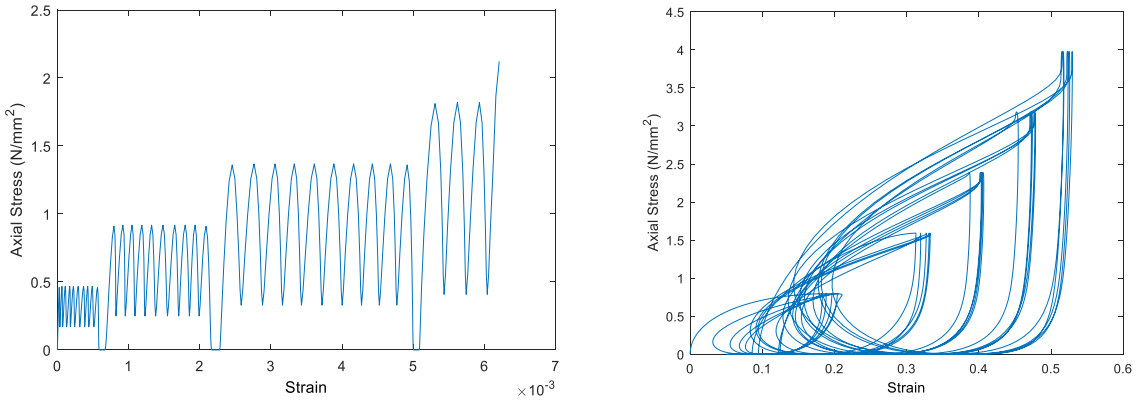

A.Figure 7: Computational model results (a) Elastic modulus of 1GPa, a damping ratio of 1.0 and friction coefficients of 0.6, (b) Elastic modulus of 2GPa a damping ratio of 2.0 and a friction coefficient of 1.2

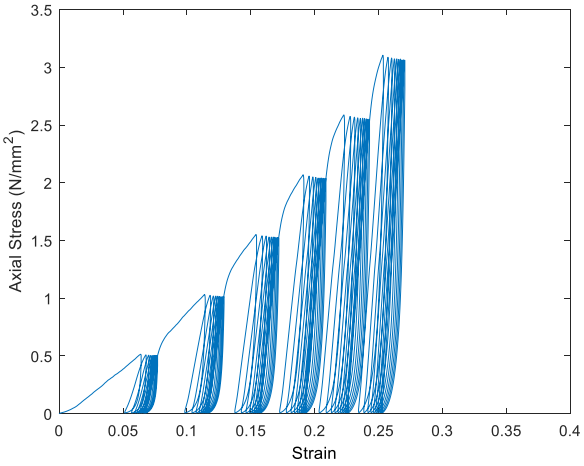

A.Figure 8: Representative sample of the stress-strain curve obtained from experimental results (chapter 2)

A.Figure 7 (a) shows that upon loading at the first stress level of 0.5 MPa the figure does not match the measured behaviour of the graft. It can be observed from A.Figure 7(b) that doubling the damping ratio and friction changes the output significantly. A cycling loading and unloading trend can be seen on all 25 loading cycles. At the stress level of 0.5 MPa, there is an increase in strain to 0.2%. During the unloading phase, the strain starts to decrease slower than the previous run and by the end of the first loading cycle, the accumulated strain from the bone grafts is 0.1%. However, as the stress level increases from 1.5 MPa to 3.0 MPa the accumulated strain is stored in the particles till the applied stress reaches 0.5 MPa after which the strain decreases drastically.

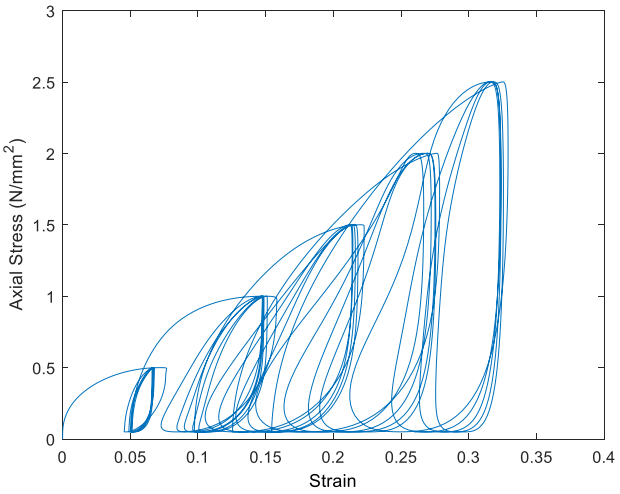

A.Figure 9: Computational model result with a modulus of 3.0MPa, high damping co-efficient of 2.4 and friction coefficient ratio of 3.0

A.Figure 9 shows the result from the computational model by increasing the friction ratio to 3.0 and the damping coefficient to 2.4. At a stress level of 0.5 MPa, the average strain accumulated from the model is 0.07%. As the stress level is increased from 1.5 MPa to 3.0 MPa the accumulated strain is stored in the particles till the applied stress reaches a value ranging from 0.08 - 0.12 at the end of stress level 1.0 MPa, 0.1 - 0.18 at 1.5 MPa, 0.13 - 0.27 at 2.0 MPa and 0.15 - 0.32 at 3.0 MPa respectively.

Discussion

It can be observed from the initial set of results as seen in A.Figure 7(a) that, they behave as completely elastic. Bone grafts in the actual form are not completely elastic, they exhibit elastic and plastic properties which clearly cannot be seen from the results from A.Figure 7(a).

In addition to the elastic modulus, damping, and friction were the only parameter variables that could be controlled using DEM within Abaqus. Although varying levels of damping and friction have a significant influence on how the graft behaved, the values of friction and damping coefficient to achieve the response does not coincide with the research findings on the friction coefficient values of cancellous bone grafts.

Research suggests that cancellous bone has an average friction coefficient of 0.98 to 1.10 (Yongde Zhang et al., 1999). Applying these to a computational simulation doesn't give results similar to the experimental data. This is due to the particles permanently deforming in the experiment and hence exhibiting an elastoplastic behaviour that cannot be obtained without introducing plasticity into the computational analysis. DEM's created in Abaqus explicit are rigid bodies and Abaqus only provides minimal options to try to induce/spoof plasticity into the DEM through the contacts or by changing the other parameters like damping and friction. Increasing damping decreases the critical time step and the simulation becomes less stable. An increase in friction does have a significant influence by allowing the DEM's to remain compacted for a longer period during the unloading phase but the value of friction necessary to make the DEM's behave in that manner is beyond the average friction range as stated in the literature. Hence using DEM's within Abaqus to model bone grafts is not suitable. As such the second approach on modelling DEM's were attempted using a ROCKY DEM solver.

Approach – II: Rocky DEM

Rocky DEM is a software package developed by ESSS Rocky, S.L. The software package is used to create a DEM model to predict the behaviour of bulk solids. Rocky uses a mesh-free method and does not solve for the continuum equations of motion. However, a stress-strain relationship can be obtained as an output from the DEM model. This method was used to try overcoming the downfalls in Abaqus of having minimal parameters to tune.

Rocky calculates the equation of motion for every individual particle by numerically integrating the displacement with time. The DEM program uses the particle position, velocity and time step information to move the particle location. This is done using an elastic-plastic normal contact model that allows simulation of plastic energy dissipation on contact without introducing the

overhead of long simulations. The forces in the simulations are calculated using two parts namely normal forces and tangent forces to the contact plane.

Normal contact force models in Rocky

Rocky DEM offers two different contacts models namely Hysteretic linear spring model and Hertzian spring model which are described as follows.

Hysteretic linear spring model

This model in Rocky is calculated incrementally, as described by equation (6.9& 6.10)

$$F_n^t = \begin{cases} \min(F_n^{t-\Delta t} + K_{nu}\Delta s_n, K_{nl}s_n^t) & if\ \Delta s_n \geq 0 \\ \max(F_n^{t-\Delta t} + K_{nu}\Delta s_n, 0.001\,K_{nl}s_n^t) & if\ \Delta s_n < 0 \end{cases} \quad 6.9$$

$$\Delta s_n = s_n^t - s_n^{t-\Delta t} \quad 6.10$$

Where Δt the time step F_n^t the normal elastic-plastic contact force at the current time Δs_n the change in contact overlap at the current time K_{nl} and K_{nu} the values of loading and unloading contact stiffness respectively (Rocky DEM, 2018).

This provides an additional parameter of stiffness which can be controlled by using Rocky, the loading and unloading stiffness which is defined by the restitution coefficient ε of contacting materials as a separate input. The coefficient of restitution (Schwager & Pöschel, 2007) measures the energy dissipation for the contacting pair 1 & 2 defined by equation (6.11 & 6.12)

$$\frac{1}{K_{nl}} = \frac{1}{K_{npl_1}} + \frac{1}{K_{npl_2}} \quad 6.11$$

$$K_{nu} = \frac{K_{nl}}{\varepsilon^2} \quad 6.12$$

Where, K_{nl} is the contact pair loading contact stiffness, K_{npl_1} the loading contact stiffness of particle 1, K_{npl_2} the loading contact stiffness of particle, 2, K_{nu} the unloading contact stiffness of the contact pair.

The tangential forces were given by a model referred to the elastic coulomb model where the tangential force is modelled as an elasto-frictional force. This was calculated using equation (6.13)

$$F_{t,e}^{t} = F_{t}^{t-\Delta t} + K_t \Delta s_t \tag{6.13}$$

Where $F_t^{t-\Delta t}$ the value of tangential force at the last time step, Δs_t tangential relative displacement and K_t the tangential stiffness which in turn is defined by: $K_t = r_K K_{nl}$ where r_K the tangential stiffness ratio (Johnson et al 1985).

The Timestep for the hysteretic linear spring model was calculated considering the two different values of stiffness k_{nl} & k_{nu}. The expression used can be summarised by the equation (6.14)

$$\Delta t = \min\left(\frac{\pi}{2N_{\Delta t}^{l}}\sqrt{\frac{m^*}{K_{nl}}}, \frac{\pi}{8}\sqrt{\frac{m^*}{K_{nu}}}\right) \tag{6.14}$$

Where m^* the effective mass, and $N_{\Delta t}^{l}$ the minimum number of time steps per loading cycle.

Hertzian spring dashpot model

In the Hertzian spring model, the contact normal force is modelled as a sum of damping and elastic force. The elastic force is based on the contact theory developed by Hertz. The expression was given by the equation (6.15)

$$F_n = \frac{4}{3}E^*\sqrt{R^*}s_n^{\frac{3}{2}} + \eta_n\left(\frac{4}{3}\, m^* E^* \sqrt{R^* s_n}\right)^{\frac{1}{2}} \dot{s_n} \tag{6.15}$$

Where:

E^* - The young's modulus, defined by the expression from equation (6.16)

$$\frac{1}{E^*} = \frac{1 - v_1^2}{E_1} + \frac{1 - v_2^2}{E_2} \qquad 6.17$$

In which E_1 and E_2 are the young's modulus of particle 1 and 2, $v_1$and v_2 are the Poisson's ratio respectively.

m^*- The effective mass, η_n- the normal damping ratio for the Hertzian model based on the equation (6.18)

$$\eta_n = -\ln \varepsilon \sqrt{\frac{5}{\ln^2 \varepsilon + \pi^2}} \qquad 6.18$$

(Tsuji et al 1992)

Where ε is the restitution coefficient, for particle-particle interaction to be defined by the user.

The Hertzian model is non-linear needed the contact stiffness to be calculated as a function of the overlap distance. This is done using the following expression from the equation (6.19)

$$K_H = \frac{4}{3} E^* \sqrt{R^*} s_n^{\frac{3}{2}} \qquad 6.19$$

Where, s_n is the time derivative of the contact normal overlap, $E*$ is the reduced Youngs modulus defined by the expression from the equation (6.20)

$$\frac{1}{E*} = \frac{1 - v_1^2}{E_1} + \frac{1 - v_2^2}{E_2} \qquad 6.20$$

In which E_1 and E_2 are the Youngs modulus of the two particles andv_1 and v_2 are their respective Poisson's ratio.

K_H is the Hertzian contact stiffness estimated considering that the magnitude of overlap is 10% of the effective radius R^*, defined by the expression from equation (6.21)

$$\frac{1}{R*} = \begin{cases} \frac{2}{L_1} + \frac{2}{L_2} \ for\ particle\ -\ particle\ contact, \\ \frac{2}{L}\ for\ particle\ -\ boundary\ contact, \end{cases} \quad 6.21$$

The time step for the Hertzian spring dashpot model was calculated using the following expression from equation (6.22)

$$\Delta t = \frac{\pi}{2N_{\Delta t}^{t}} min\left(\sqrt{\frac{m^*}{K_H}}\right) \quad 6.22$$

Where, m^* is the effective mass

$$\frac{1}{m*} = \begin{cases} \frac{1}{m_1} + \frac{1}{m_2} \ for\ particle\ -\ particle\ contact, \\ \frac{1}{m}\ for\ particle\ -\ boundary\ contact, \end{cases} \quad 6.23$$

Adhesive force models

While the normal force models capture the repulsive forces, granular materials can have various moisture content that can cause the particles to adhere to themselves or surfaces they are in contact with, this adhesion of bulk solid is a function of the stress. The adhesive forces model in rocky capture the physical phenomenon by scaling the adhesion with the force of contact. There are three different types of Adhesive force models in rocky namely, constant adhesive force model, Leeds adhesive force model and the JKR adhesive force model

Constant adhesive force model

This is the simplest default adhesive model available in rocky, the adhesive force in this model is measure using two parameters namely, the minimum distance between particles when the force is

activated and the force fraction value. As a result, if the force fraction is 1, the adhesive force of the particle will be the gravity force applied. If the particles have different masses, gravity force calculations are based on the smallest mass.

This constant adhesive force is described from the equation (6.24)

$$F_{n,adh=}\begin{cases}0 & if-s_n \geq \delta_{adh'} \\ f_{adh}\, g \min(m_1, m_2) & if-s_n < \delta_{adh}\end{cases} \quad 6.24$$

Where $F_{n,adh}$- normal adhesive contact force, s_n the contact overlap, m_1, m_2 the mass of the particles g the gravity, and $\delta_{adh'}$ adhesive distance as given by the user.

Leeds adhesive force model

Leeds adhesive model is used to stimulate elastoplastic-adhesive behaviour based upon the model developed by Pasha et al (Pasha, Dogbe, Hare, Hassanpour, & Ghadiri, 2014). The force overlap equation for this force model is given by the equation (6.25)

$$F_n = \begin{cases} -K_{nu}s_n + \dfrac{10}{9}F_{ce} \\ K_{nu}s_n + \dfrac{8}{9}F_{ce} \\ K_{nl}(s_n - s_0) \\ K_{nu}(s_n - s_p) \\ -K_{nu}(s_n + s_p - 2s_{cp}) \end{cases} \quad 6.25$$

Where, loading and unloading stiffness is defined by the equations $K_{nl}\ and\ K_{nu}$ and the values for F_{ce} is given from the equation $F_{ce} = \frac{3}{2}\pi R^* T$ with R^* being the particle radius and T the surface energy. The overlap values are s_0, s_p & s_{cp} are calculated from the following equations (6.26 – 6.28)

$$s_0 = -\frac{8}{9}\left(\frac{F_{ce}}{K_{nu}}\right) \quad 6.26$$

$$s_p = s_{max} - \frac{K_{nl}}{K_{nu}}(s_{max} - s_0) \quad 6.27$$

$$s_0 = s_p - \sqrt{\frac{162}{137}\frac{\pi T}{K_{nu}}(s_p - s_0)(2R^* - s_p + s_0)} \quad 6.28$$

Where, s_{max} gives the maximum overlap as defined from the Hertzian contact model.

JKR adhesive force model

Johnson-Kendall-Roberts (JKR)(Johnson et al 1971) adhesive force model is used to introduce the adhesion effect into a Hertzian contact model. In this model, surface-energy is added to the total energy of the system similar to the Leeds model. However, the JKR model can only be used with the Hertzian dashpot model and not with the hysteretic linear spring model.

The normal adhesive force in this model is given by (Hills et al 2017)

$$F_{n,adh} = \sqrt{8\pi T E^* a^3} \quad 6.29$$

Where T gives the surface energy, E* the Young's modulus and a gives the radius between the boundary and particle or between two particles.

The normal overlap is calculated using the following expression (6.30)

$$s_n = \frac{a^2}{R^*} - \left(\frac{2\pi T a}{E^*}\right)^{1/2} \quad 6.30$$

Where R^* gives the effective particle radius, T the surface energy, a the radius of contact between particles or the boundary.

Methods

Rocky being an add on software for ANSYS, the software does not have a Pre-processor component built in it, so the finite element model of a test apparatus was created in ANSYS and imported as an STL file for use in the Rocky simulations. Upon importing the STL file into Rocky DEM, A circular particle generator inlet was created and positioned on top of the test chamber and below the impactor.

The bone-grafts were set to 5mm spheres and modelled using either Hysteretic linear spring or Hertzian spring dashpot normal force for contacts. The material properties used in the simulations were the same as defined in page **Error! Bookmark not defined.**. The surface interaction between the chamber and the particles were set to either constant or linear adhesive force for interaction between particles and hard contact for the walls of the cylinder and the impactor.

The computational simulation was done in a three-step process, Step 1: The particle generator generates the specified number of particles required to fill the chamber. Step 2: Gravity acceleration of 9.81 m/s^2 was applied to the impactor to let the impactor settle on the particles. Step 3: The impaction test was carried out with 30 force-controlled loading and unloading cycles. With 5 loading cycles and unloading cycles per stress level from 0.5 MPa to 3.0 MPa.

Results

The stress-strain behaviour predicted using a hysteretic linear spring as a normal force, a constant adhesive force under a tangential force derived from the coulomb limit and an adhesive distance of 0.1mm and a restitution coefficient of 0.1 is shown in A.Figure 10.

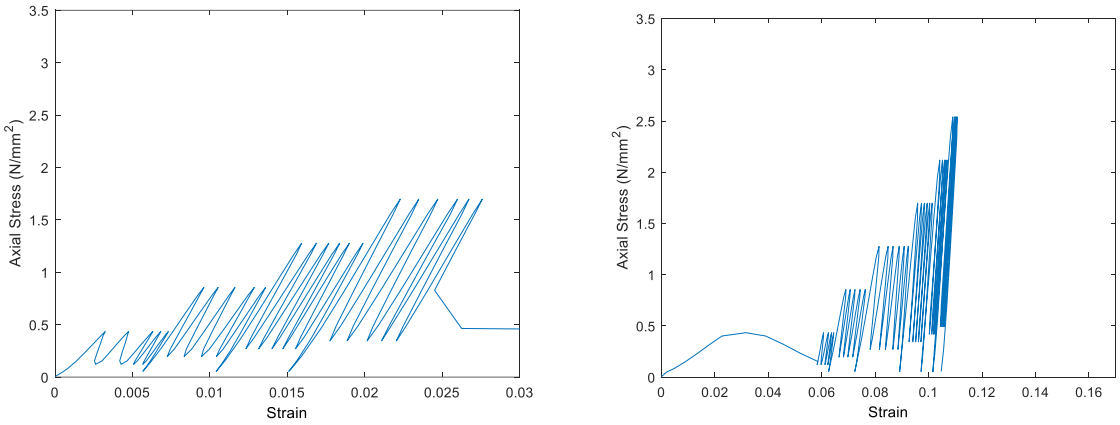

A.Figure 10: Computational Stress-strain curve Rocky DEM results (a) Hysteretic linear spring model (b) Hysteretic linear spring model with Leeds adhesive force

Upon loading at the first stress level of 0.5 MPa the particles compress and there is an increase in stress on each impaction force, during the unloading phase there is an immediate decrease in stress observed from the graph with an increase in strain. However, loading and the unloading forces do not create a cycling hysteresis as seen from Abaqus DEM or experimental results as the model is behaving completely elastic without exhibiting plastic properties.

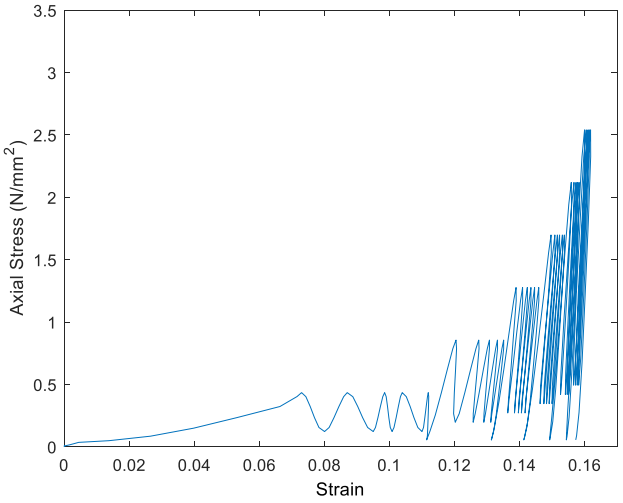

A.Figure 11: Computational Rocky DEM Hertzian dashpot model with adhesive force derived from JKR theory.

Implementing the Hertzian spring dashpot model with the adhesive force defined by Johnson-Kendall-Roberts (JKR) (A.Figure 11) shows that during the first loading cycle the strain increases gradually to 0.07% and during the unloading phase there is no elastic recovery and an increase in strain to 0.08% by the end of the first loading cycle. The rate of increase in strain is identical with the strain increasing to 0.16% by the end of the second load cycle at 0.5 MPa stress level. Beyond the second loading cycle, the rate of increase in strain decreases with the final 5^{th} loading cycle in the stress level accumulating a strain of 0.16%. The result from Rocky shows an initial high accumulation of strain that slows with the number of loading cycles and stress amplitude. The grafts get stiffer as applied stress gets higher. However, this approach doesn't appear to capture the hysteresis seen from the experimental tests as the particles behave completely elastic.

Discussion

It can be observed from that results of A.Figure 10(a) that while using the hysteretic linear spring dashpot model as the stress increases the particles start to compress and the strain increases. During the first two loading cycles, the strain continued to increase even on the removal of the stress. Upon subsequent load cycles, the stress relaxation curve tightens and the rate of increase in strain decreases. It can be observed from the graph that there is no hysteresis with the particles behaving completely elastic. The particles did not capture the cyclic motion exhibited through the experimental analysis from Figure 3.11. A second simulation was run with the same loading conditions and by changing adhesive force from linear constant adhesive to Leeds adhesive force (A.Figure 10 (b)) and though the increase in strain is considerably higher than the previous simulation, no cyclic loading and unloading hysteresis was observed and the range of strain obtained from this simulation was still lower than the experimental results or even from the results obtained from Abaqus DEM's. A third simulation as seen (A.Figure 11) was run with the Hertzian spring model, the change is strain follows a similar pattern to previous simulations after the second loading and unloading cycle. Elastic deformation is seen through the loading and unloading cycles

at each stress level. However, the difference in results is that the strain achieved is still lower than the Abaqus DEM simulations with most of the impaction happening during the first three stress levels. The particles behave elastically with no hysteresis observed. Varying levels of normal contact forces (1-10) and change in the coefficient of restitution (0-1) influenced how the simulated graft behaved, however, the hysteresis achieved was still not on a comparable scale to the experimental data.

Rocky DEM's results fail to achieve a response close to the experimental results, this is because the experimental results exhibit a visco-plastic behaviour which is although included through the contacts in Rocky simulations, it's not sufficient. DEM's created in Rocky DEM's are rigid bodies and only provides minimal options to try inducing plasticity into the DEM through the contacts or by changing the other parameters like contact force models, adhesion model and the coefficient of restitution. Increases in the coefficient of restitution do not have a significant influence (A.Figure 10) but allowed the DEM's to remain compacted for a longer period during the unloading phase but they are not enough to allow for cycling loading and unloading curves.

Realistic simulation of granular material is a huge challenge in research, the above two approaches were capable of modelling particulate material as a distinct entity efficiently. Modelling to simulate calculate and trace individual particles were possible using DEM's but analysing their behaviour was not possible with the DEM's predominantly being treated as a rigid body allowing for an overlap of only 10% of the size of each particle. Modelling large deformations were not possible with this limited overlap. DEM's also doesn't allow for the inclusion of plasticity and as such a plastic response as seen from the experimental study from A.Figure 8 will never be achievable. The advantage of DEM models is that they are easy to implement, but they may not be appropriate or at best provide an approximation similar to experimental results. DEM's in these simulations struggle to capture the mechanical behaviour due to the inability to account for large deformations of the particles.

Abaqus on the other hand has several options for plasticity models which can be used to model the inelastic behaviour of materials in deformable analyses. This can be done by using a constitutive approach to model the bone grafts as separate FEM bodies and using explicit computational mechanics for each bone graft particle.